Mechanisms of Mechanotransduction in the Pacinian Corpuscle

Submitted by Svetlana Pitts-Yushchenko to the University of Exeter as a thesis for the degree of Doctor of Philosophy in Physics, July 2013

I certify that all material in this thesis which is not my own work has been identified and that no material has previously been submitted and approved for the award of a degree by this or any other University.

(Signature) ……

Abstract

Touch perception is important in most living organisms and extremely sensitive detection systems have evolved to meet this need. Pacinian corpuscles (PCs) are primary mechanoreceptors. In the human, they are found in the skin (where they act as touch receptors), in the joints, in muscles and in many organs (where they act as motion sensors). The purpose of the work described in this thesis is to investigate how the performance of the PC is achieved, with reference to structure, mechanical properties and possible transduction mechanisms.

PCs were obtained from the equine hoof and their distribution and clustering were investigated. Corpuscles were located in the frog area of the hoof (the digital cushion); they were found to be surrounded by adipose tissue and often closely associated with blood vessels. The physiological implications of these observations are discussed.

The structure and composition of corpuscles was investigated using confocal microscopy with histological stains for collagen, proteoglycans and lipids. Nonlinear microscopy was also used to investigate the distribution of collagen (by second-harmonic generation), elastin (by intrinsic two-photon fluorescence) and membrane

lipids (by coherent Raman imaging). These techniques provided novel insights into the three-dimensional structure of the intact corpuscle, demonstrating: (i) three clearly distinguishable zones – the outer zone, the inner zone, and the core; (ii) blood vessels running through the outer lamellae and the core; (iii) the presence of proteoglycans – less in the outer zone than in the inner zone; (iv) two types of collagen fibres (one type associated with the lamellae and the other forming a complex fibre network through the inter-lamellar spaces); (v) occasional elastic fibres; (vi) a sheath of adipose tissue closely associated with the corpuscle's outer surface.

Mechanical testing by micro indentation, micropipette aspiration and osmotic challenge showed that the outer zone was stiff and able to quickly restore its original shape after distortion.

Dynamic mechanical properties were investigated over a range 50 to 400 Hz. Observations of lamellar displacement (amplitude and phase) were consistent with the predictions of the Loewenstein-Skalak model. This model includes 30 lamellae; however, the same overall frequency response could be replicated in a single-lamella model with suitably chosen parameters. The benefits of a lamellar structure for transduction of mechanical signals therefore remain unresolved.

The permeability of the corpuscle to water and solutes was investigated using osmotic swelling and fluorescence tracer techniques. Both revealed unexpected complexity in the pathways of uptake to the inner core and demonstrated the presence of an impermeable boundary between the inner and outer zones, whose implications for mechanotransduction and nutrition in the corpuscle remain to be determined.

Acknowledgments

Firstly, I would like to thank my supervisors, Professor Peter Winlove and Doctor Ian Summers, who helped and encouraged me over three and a half years of this project.

I am grateful to Doctor Ellen Green for her technical support and for guiding me through the laboratory work.

Special thanks to Doctor Jessica Mansfield who helped me with nonlinear microscopy. Financial support was provided by the Leverhulme Trust.

Sincere thanks to my family and friends who were great sources of inspiration throughout this multidisciplinary project.

Finally, I dedicate this thesis to anyone who finds it useful.

List of contents

List of figures

Chapter 1

Literature review

Introduction

This study investigates the lamellar structure of the Pacinian corpuscle (PC). Three main objectives are pursued: (i) using a range of microscopy techniques to obtain an improved understanding of the structure and composition of the PC; (ii) developing and then using appropriate measurement techniques to determine the mechanical properties of the lamellae and the dynamics of the interlamellar fluid in response to deformation of the capsule; (iii) testing the predictions of current theoretical models of mechanotranduction in the corpuscle.

This chapter continues with an introduction to touch perception and mechanoreceptors, leading, in section 1.2, to a description of the Pacinian corpuscle, a most sensitive mechanoreceptor which is the subject of this thesis. Section 1.3 provides an overview of the literature on the PC, which broadly covers experimental and theoretical work on anatomy, physiology, biomechanics, electrophysiology, biophysics and neuroscience; this provides a starting point for the present work, which is outlined in the final section of the chapter.

1.1 Touch perception

There are four main mechanoreceptors in mammals: Ruffini cells, Pacinian Corpuscles, Merkel's cells and Meissner`s corpuscles. In hairy skin, Meissner`s corpuscles are absent, and hair movement is detected by lanceolate endings. The receptors respond to mechanical deformation and distortion by firing nerve impulses, i.e., generating an action potential. Mechanoreceptors located in different skin layers and in other areas such as joints and organs have different receptive fields, morphology, and adaptation to stimuli, as expressed in the relationship

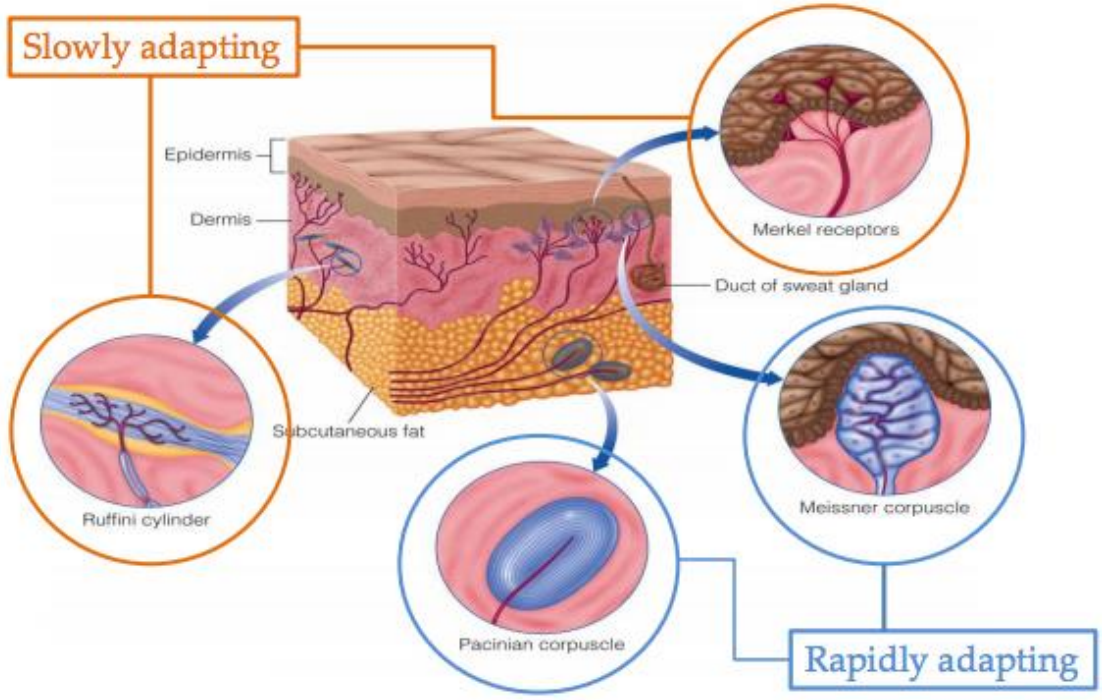

Figure 1.1. Rapidly and slowly adapting receptors in the skin. The mechanoreceptors are embedded in the top two layers of skin: the epidermis and the dermis. Adapted from [2].

between impulse generation and the stimulus [1]. Mechanoreceptors (figs.1.1 and 1.2) can be divided into rapidly adapting (RA) receptors (whose firing rate in response to a sustained stimulus returns quickly to a resting rate) and slowly adapting (SA) receptors (whose firing rate in response to a sustained stimulus returns slowly to a resting rate) [2].

Meissner's corpuscles (in humans typically 30-140 μm in length and 40-60 μm in width [3]) are RA mechanoreceptors with small receptive fields. As shown in figure 1.1, they are distributed in different areas of the dermis (just beneath the epidermis), and highly concentrated at the most sensitive locations such as fingertips and lips. They can sense light touch or vibration < 50 Hz. Interestingly, in humans the number of Meissner's corpuscles decreases between the ages of 12 and 50 [4, 5]. The other RA receptor is the PC (in humans typically 1 mm in length [6]) which has a large receptive field. PCs are located in the lower dermis, and are also found in joints and internal organs. They respond to a wide range of vibrating stimuli from 20 to 1000 Hz. Merkel cells (typical diameter 10 μm in humans [7]) are SA mechanoreceptors with small receptive fields. They are widely distributed in the superficial layers of the human skin and concentrated under the fingertip ridges that create the fingerprint. They are most sensitive to very low frequency vibration (5 to 15 Hz) and can detect finely detailed surface pattern [7]. The other SA receptors are the Ruffini cells, which have large receptive fields and are located in the dermis. They are sensitive to skin stretch and contribute to object manipulation [8, 9]. They are also found in joints where they respond to mechanical deformation

due to angle change in the joint. In skin they have an additional role as thermoreceptors [10, 11].

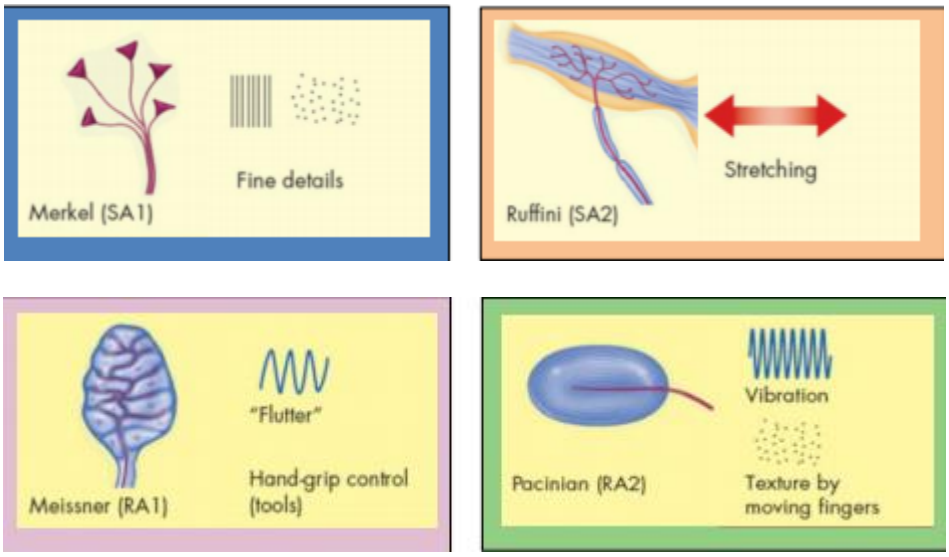

Figure 1.2. Merkel and Ruffini cells are SA receptors; their primary functions are, respectively, perception of fine detail and assisting object manipulation. Meissner's and Pacinian corpuscles are RA receptors; their primary functions relate, respectively, to detection of low and high frequency vibrations. Adapted from [2].

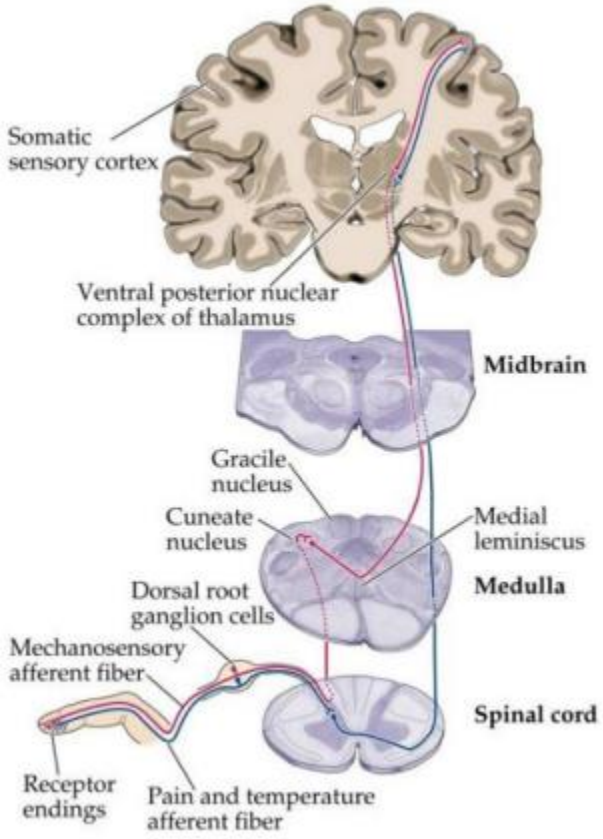

Figure 1.3. The pathway of signal transmission from a receptor. Adapted from [2].

Each mechanoreceptor transduces a signal from the environment into a signal that propagates through the nervous system via the dorsal column nuclei, through the thalamus, and eventually arrives at the somatosensory cortex (fig. 1.3).

1.2 The Pacinian Corpuscle

Specific structures at the distal terminals of nerves in human hands and feet were noticed by the German anatomist Abraham Vater in 1741. However in 1835 the Italian anatomist Filippo Pacini rediscovered them distributed throughout the body and gave an appropriate description. Since then, these mechanoreceptors have been named as Vater-Pacinian or Pacinian corpuscles [12]. In most medical literature these encapsulated receptors are called Pacinian corpuscles (PCs).

These receptors are larger than other receptors (see previous section) and sense vibrations and the onset and offset of static stimuli applied to the skin surface; in joints they are activated under compression through angle change in the joint capsule [1]. Because of their size and their significant role in haptic perception and the sense of balance, they have become a popular subject for research into touch perception [13].

This thesis is based on the *equine* hoof PC to because the *horse* hoof is anatomically equivalent to the end of the human finger. An interesting comparison between the anatomy of the *horse* hoof and the human finger is provided in the book *The Horse Conformation Handbook* by Heather Smith-Thomas [14].

The *horse* hoof consists of the long and short pastern bone together with the coffin bone which correspond with the phalanges in the human finger (fig. 1.4).There are no muscles within the horse hoof, it contains tendons, ligaments and blood vessels, which originate from the axillary artery and the digital nerves which arise from the median nerve and include sensory and autonomic fibres (fig. 1.5 a & b) [15, 16].

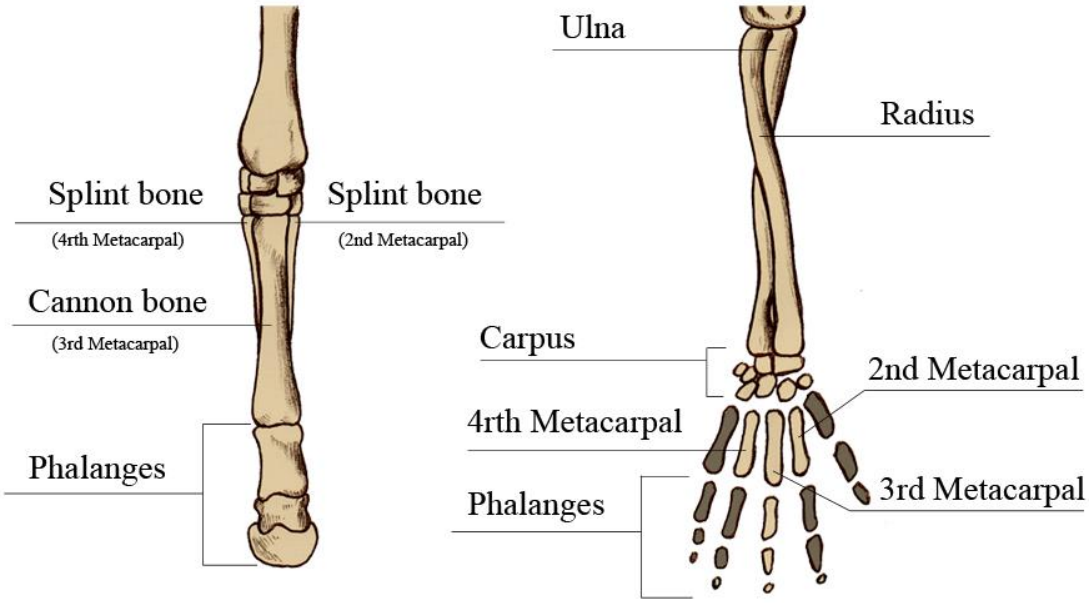

Figure 1.4.Comparison of the structure of the *equine* forelimb and human hand. Adapted from [14].

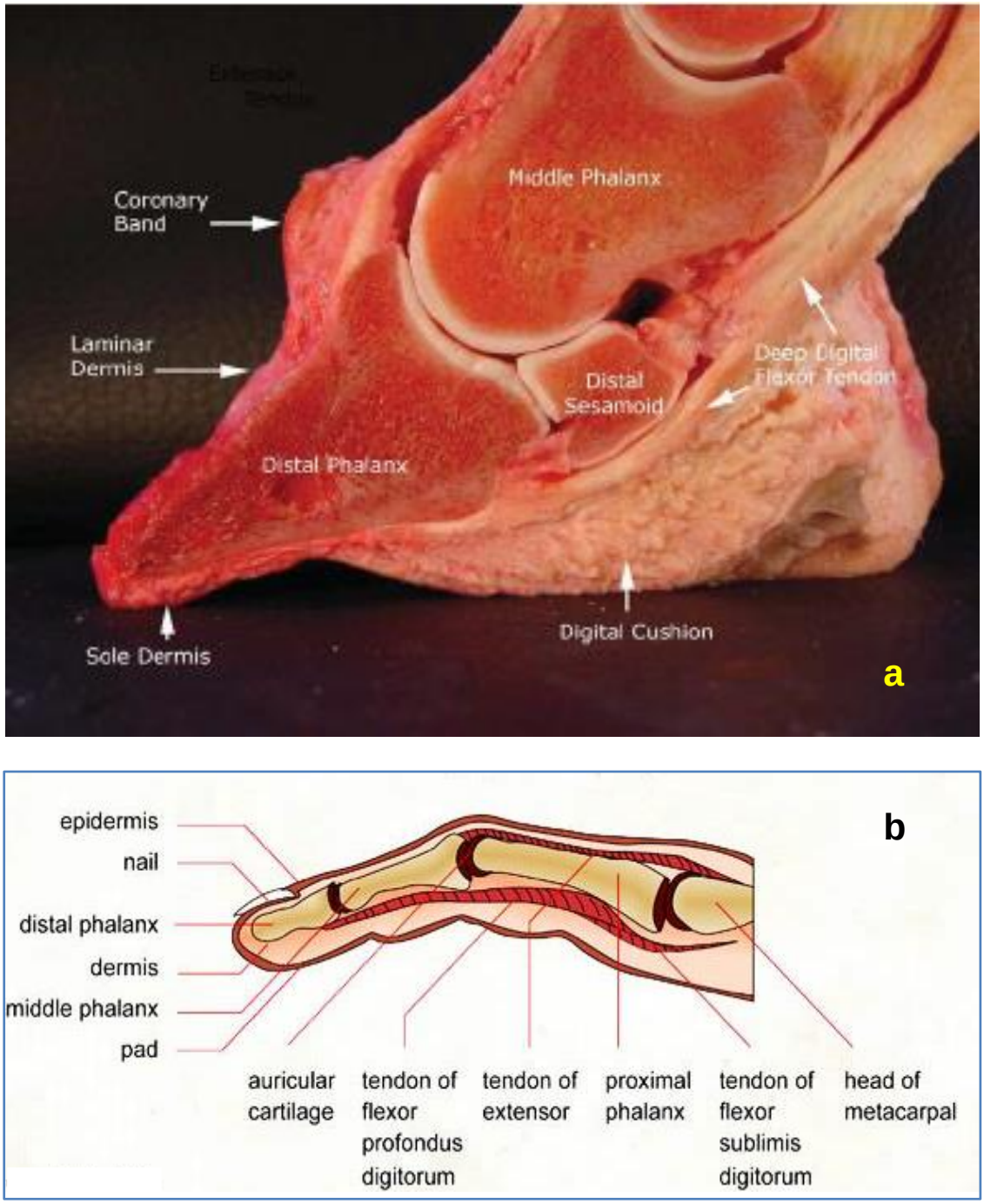

Figure 1.5. Comparison of (a) *equine* foot specimen (sagittal section with hoof capsule removed) and (b) schematic diagram of the human finger (sagittal section); adapted from [15], [16].

Two types of mechanoreceptors have been identified in *horse* hoof. The distribution of them through the hoof will be described in Section 1.2.1, together with the development, anatomy, neurophysiology and biomechanics of PCs obtained from numbers of studies on PCs during the last few decades.

1.2.1 The Distribution of Pacinian Corpuscles

In the study by Stark et al [17] up to 424 PCs were found in fresh human cadaver hands. 60% of them were located in the digital areas and rest of them in thenar and hypothenar regions. Most of the PCs were found close to large nerve bundles and blood vessels. Usually, they were found in groups of 5-8 surrounded by adipose tissue. They were generally surrounded by adipose tissue, as confirmed by later MRI investigations.

Cauna observed that human PCs tend to increase in size throughout life to age 75. However, in people above 75 years old, he found the PCs tended to shrink. These PCs were observed in the dermis and subcutaneous layers of the skin of human hand and were always attached to flexor tendon and short digital muscles [18].

Another study [19] of PCs distribution in the *cat* foot demonstrated that there was an average of 667 corpuscles in each fore foot. 80% of PCs were located in the toe areas and the rest were spread through the pad. PCs in the toe skin folds were

located next to the hairy follicles, however in the pad PCs were always found beside the metacarpal nerve. There was always a blood vessel closely neighbouring the PCs, in skin folds or the pad. The same group [20] also found 458 PCs in the right hand of the *monkey Macaque Fuscata*, and 416 PCs in the left hand. 405 were located in the digits and rest distributed through the palm areas. They suggested that the localization of those PCs may be associated with functions such as gripping as this is the main function of the primate hand (fig. 1.6). There was no difference in the structure of dermal and subcutaneous PCs. However, subcutaneous PCs were longer compared to those in the dermis and joints. The size of PCs in the fingers was smaller than in the palm area (left hand finger: length 470.5 ± 256.3 µm, width 229.5 ± 98.9 µm, left hand palm: length 703.3 ± 335.1 µm, width 376.9 ± 178.7 µm).

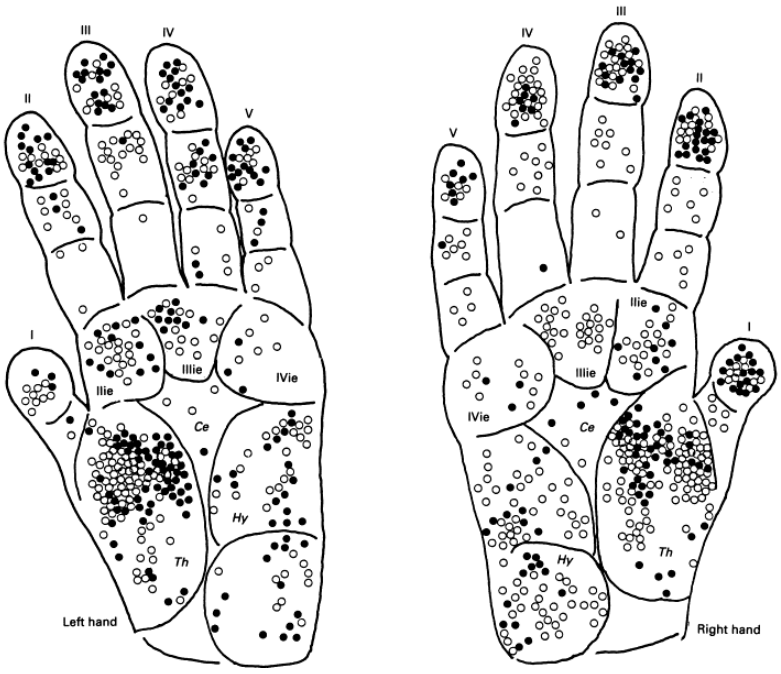

Figure 1.6. PC distribution in the monkey hand; solid circles represent PCs in the dermis and empty circles represent PCs in subcutaneous tissue. Adapted from [20].

Particularly relevant to the present work is the identification of PCs in the bulb area or “frog” of the *horse* hoof, a region involved with shock absorption, return of venous blood and control of balance (fig. 1.7) [21]. Lancaster et al [15] also identified PCs in the frog area (digital cushion), heel bulbs, in neighboring region to the lateral cartilages, and around the secondary tendon of the flexor tendon (close to the navicular bone) (fig. 1.7, fig.1.8 (a), (b), (c)). These corpuscles are used in the present work and so are discussed in more detail in Chapter 3.

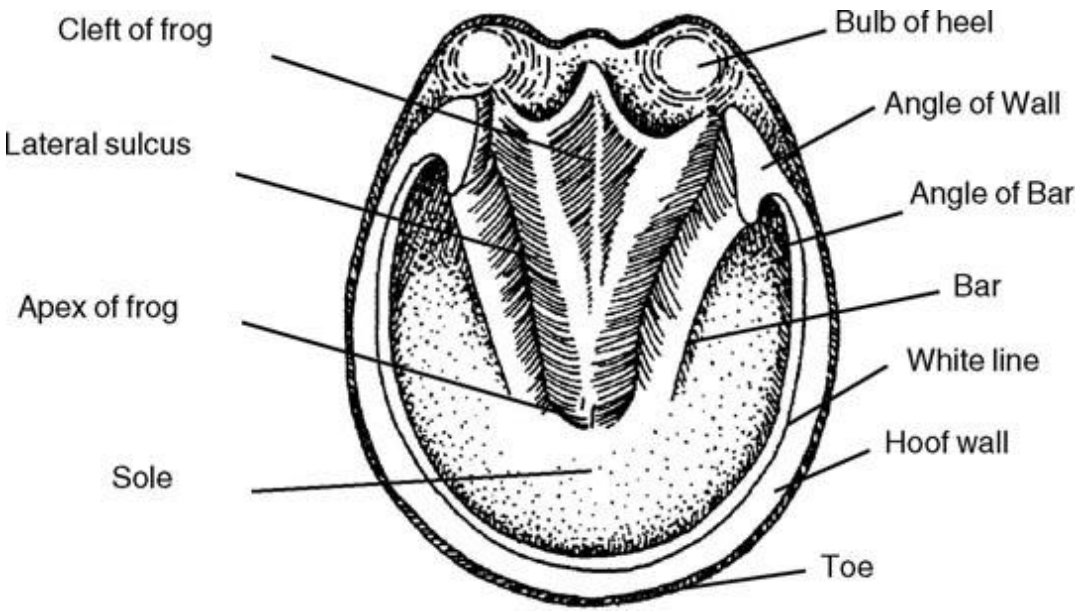

Figure 1.7. A scheme of the horse hoof in coronal plane shows localization of frog area and bulb of heels where most of PCs were identified. Adapted from [23].

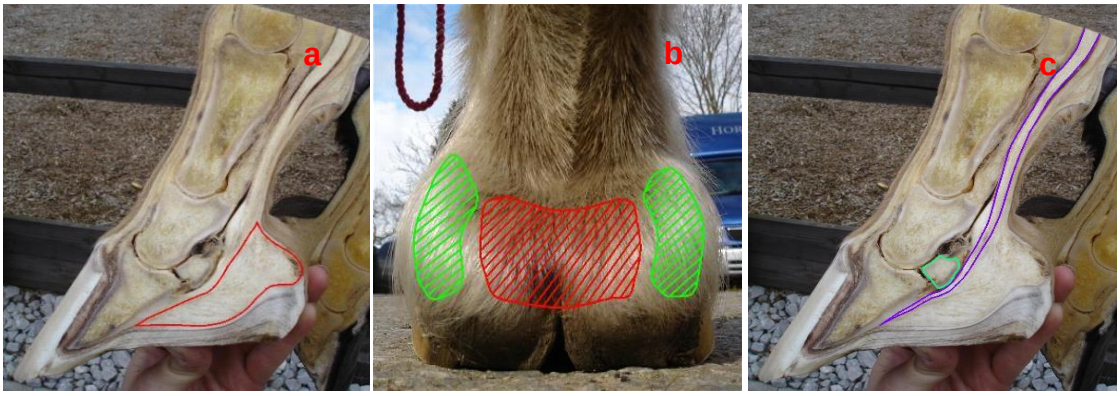

Figure 1.8. (a) a digital cushion (shown in red) located above the frog area and the lateral cartilages, the cushion acts as a shock absorber; (b) relative position of the digital cushion (shown in red) and the lateral cartilages (shown in green) which are incorporated in the shock absorption mechanism; (c) relation between navicular bone (shown in green) and digital flexor (shown in purple). Adapted from [24].

1.2.2 Development of Pacinian Corpuscles

Work by Cauna [22] with human PCs showed different stages of corpuscle development corresponding to the different prenatal periods; the first signs of corpuscles were evident in foetuses of 69-71mm length. The nerve endings become surrounded by cells, which later differentiate into outer and inner zones of the corpuscle. He concluded that once the outer lamellae become organized, this triggers further development in a growth zone between the outer lamellar and the inner zone.

Throughout development the corpuscle maintains an elongated shape with an aspect ratio of approximately 1:3. However, different shapes often occur in the same group of corpuscles due to uneven growth (fig.1.9).

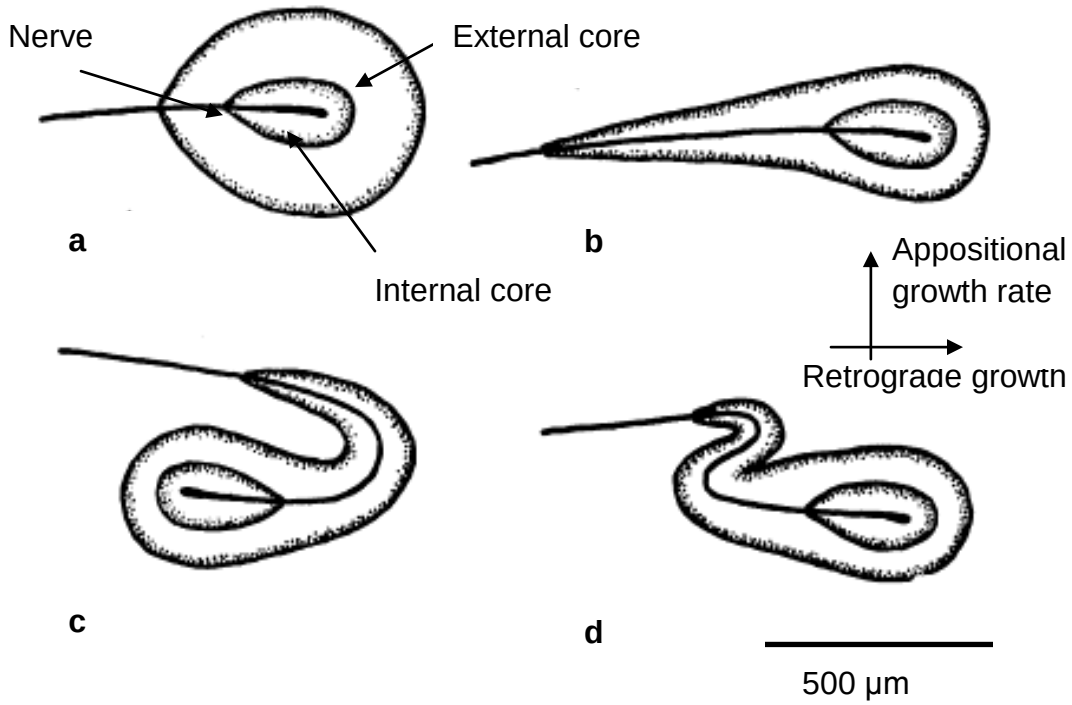

Figure 1.9. Diagram of changes in the external shape of PCs from human foetal tissue due to variations in appositional and retrograde growth rates; (a) both rates equal, leading to development of a spherical shape for the PC; (b) retrograde rate greater than appositional rate, resulting in elongation of the PC; (c &d) growth rates and external shape of the PC are determined by the course of the nerve that the PC grows along. Adapted from [22].

1.2.3 Vascularisation and Innervation

PCs are encapsulated end organs of peripheral nerves; for example, PCs in the human hand are innervated by single afferent nerve fibres [3]. Usually, each corpuscle has it is own axon running though the core.

Chalisova et al [25] discovered that, after additional innervation of the *cat* mesentery with somatosensory nerves (existing PCs having been previously removed), new PCs were generated. These were sometimes in complicated arrangements where several corpuscles, joined at their outer zones, were connected to the same nerve fibre, with the nerve ending crossing from one capsule to another. The discovery of this phenomenon, called polycapsularity, indicates the presence of a process of budding of the sensory capsules which could be a part of the regeneration and formation process. Interestingly, morphological and functional properties of the new PCs were indistinguishable from the properties of the original (removed) PCs. This leads to the hypothesis that, in the general case, generation of encapsulated end organs from the somatosensory nerves is induced by external stimuli from the surrounding tissue.

PCs require a microcirculation to maintain their metabolism. As already noted, PCs are generally located close to blood vessels. Cauna [3] found a capillary network in human corpuscles forming arterio-venous anastomoses (AVs). The network (fig.1.10, fig.1.11) is such that if venous drainage is occluded there is an increase

of pressure inside the corpuscle which is transmitted into the inner core and the neurite. This suggests that PCs may have a role in monitoring changes in local blood circulation.

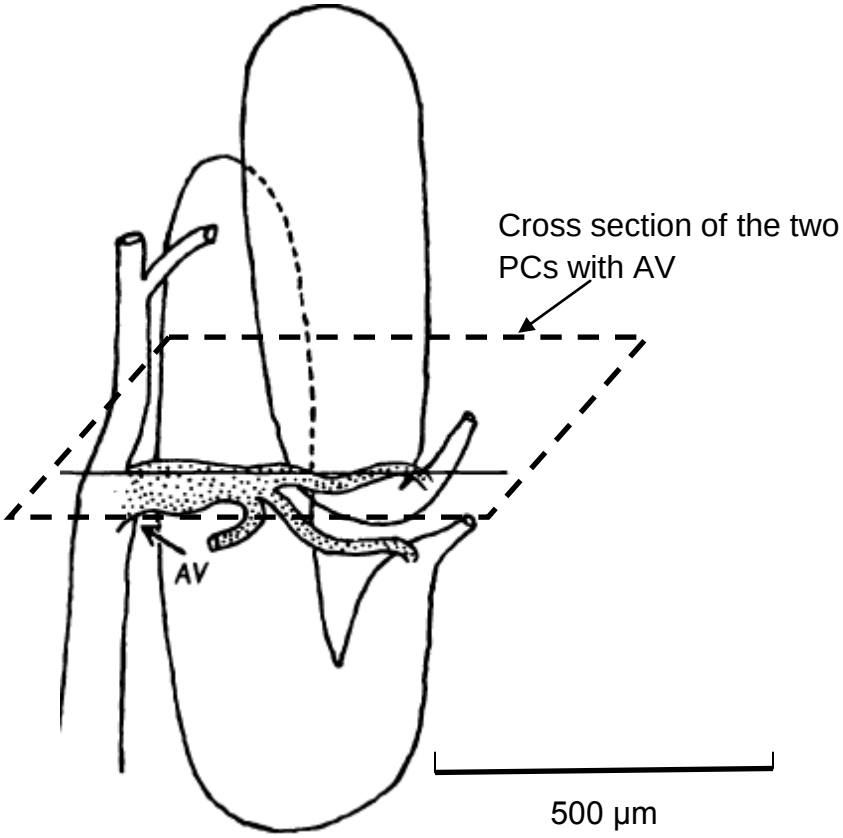

Figure 1.10. Diagram showing the plane (dotted line) of the cross section in Figure 1.11, through two PCs and an arterio-venous anastomosis (AV). Adapted from [3].

Winkelemenn and Osment found that the vessels within the corpuscle take an unusual loop around the area where the axon begins to lose its myelinated cells. This may provide specific pathways for metabolites between the outer connective tissue-growth zone and the nerve fiber (fig.1.12) [26]. Nishi et al [27] found blood vessels running through myelinated segments of PCs from the mesentery of the

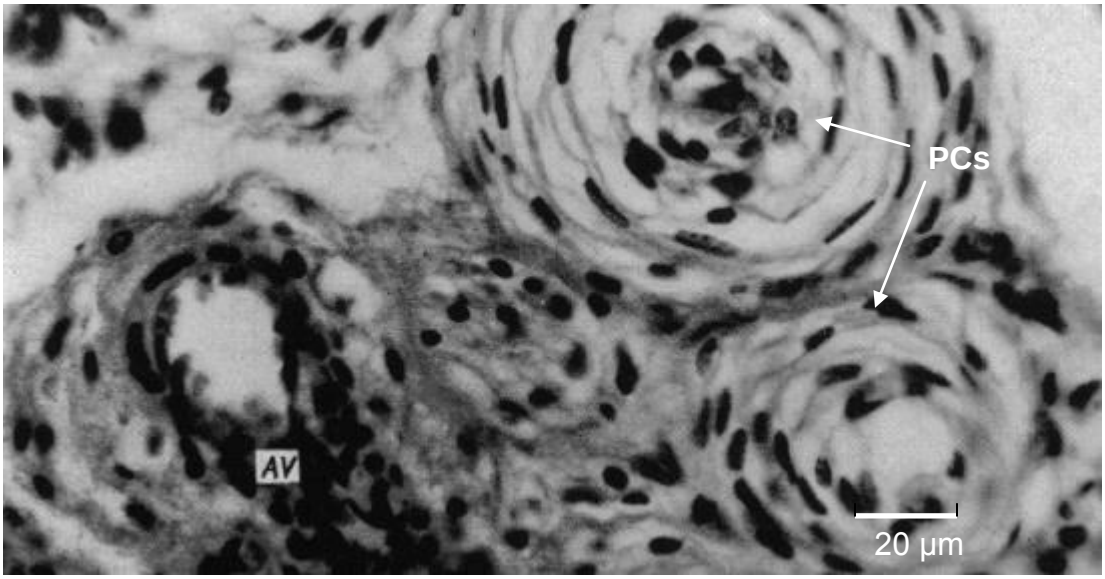

Figure 1.11. Two PCs from the index finger and a developing arteriovenous anastomosis (AV), the vein draining the corpuscles joins the venous end of the anastomosis. Adapted from [3].

cat, separated from the axon by collagen and a few lamellae. Michailow [28] injected dye into the circulation of PCs from *cat* mesentery, and observed a network of blood capillaries in the core. He did not observe blood vessels in the outer zone, suggesting that if they exist they arise from a different arterial supply.

Gamon and Bronk [29] reported that an accumulation of blood in the *cat*`s mesentery vessels increased arterial resistance, leading them to hypothesise a relationship between the response of PCs and vascular changes.

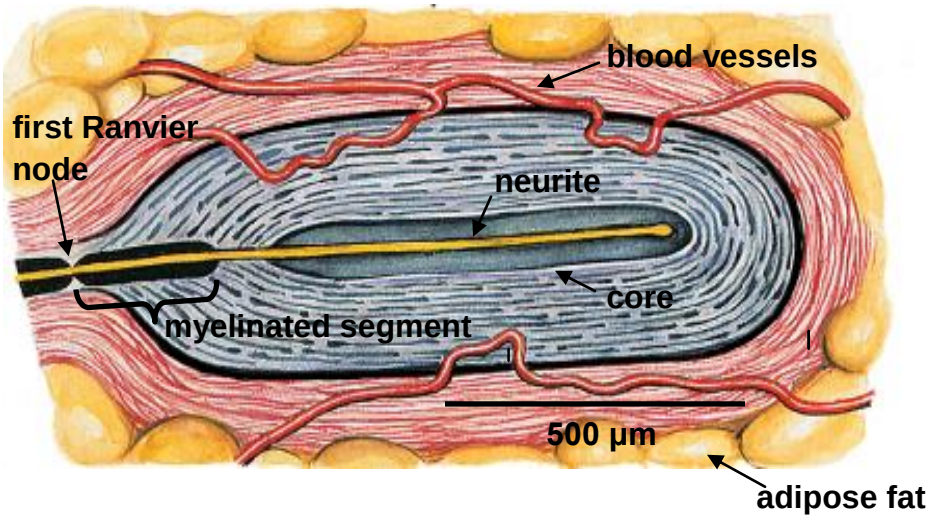

Figure 1.12. Schematic of the PC surrounding by adipose fat, showing, the core with the neurite (the end of the axon), the myelinated segment of the PC with blood vessels through. Adapted from [30].

As mentioned above, in addition to providing nutrition the blood vessels may also be involved in a PC function of maintaining circulatory control [31]. In *cat* 'mesentery PCs it was observed that the blood vessels share the same entrance into the PC as the nerve fibre and these blood vessels branch into capillary loops which supply the central core [32]. The nutritional pathways provided by these vessels will be investigated in Chapter 3 and 4.

1.2.4 Microscopic Structure

PCs in the mesentery of *cats* are thought to be uniquely involved in the sensation of ground vibration. They are sufficiently large to be visible by the naked eye and are thus most widely used by researchers on sensory structure [19, 25, 27, 29, 32-35, 39, 43, 46, 49, 55]. Consequently, the major sources of information in this review relate to PCs from the *cat*, but it is important to recognise that these may not be totally representative of corpuscles from other species.

Electron microscopy clearly indicates three main regions of *cat* PCs. There are around 30 lamellae in the outer zone and a number of tightly packed inner-zone lamellae. The inner region goes through the whole length of the capsule and links the major areas of the capsule including the neurite. Some cellular layers form a growth zone between the inner and outer lamellae. There are approximately 60-80 inner lamellae in *cat* mesentery PCs [33]. The number of lamella is significantly greater than that reported in other species, for example there are only 30-40 inner lamellae in PCs from human hands [34]. The number of lamellae changes during growth [36].

Outer zone lamellae are arranged concentrically and they are sufficiently widely spaced from each other that they can be distinguished by a light microscope. The lamellar cells, supported on a collagen matrix, are extremely flattened and the cytoplasm of neighbouring cells overlaps forming a continuous layer in which no

gap has been observed. The fluid space between the lamellae contains a sparse network of collagen fibrils (fig.1.13) [33].

Cauna [18] demonstrated histochemically the presence of fibroblasts in the lamellae, which are presumed to synthesise the collagen fibres. As seen in electron microscopy (fig.1.13) these fibroblasts are tightly attached to each other, suggesting that the lamellae are impermeable with no communication possible through them [33]. However, some fibroblasts show cytoplasmic protrusions into the interlamellar space, some of which connect neighbouring lamellae [40]. These connections are considered to be part of the transfer system within the sensory capsule [35], [36], [37]. More recently, electron micrographs of cat PCs reveal that the fibroblasts contain a large number of caveolae or vesicles which might be involved in cell-modulated trans-lamellar transport and may also be associated with the regulation of the metabolism of the whole lamellar structure [38].

Results from electron microscopy [33] also suggest that collagen fibrils between the outer lamellae are orientated orthogonally to collagen fibrils within the lamellae, with the latter tending to be perpendicular to the longitudinal axis of the corpuscle (fig.1.14). Interestingly the number of collagen fibrils increases with age [39], [40].

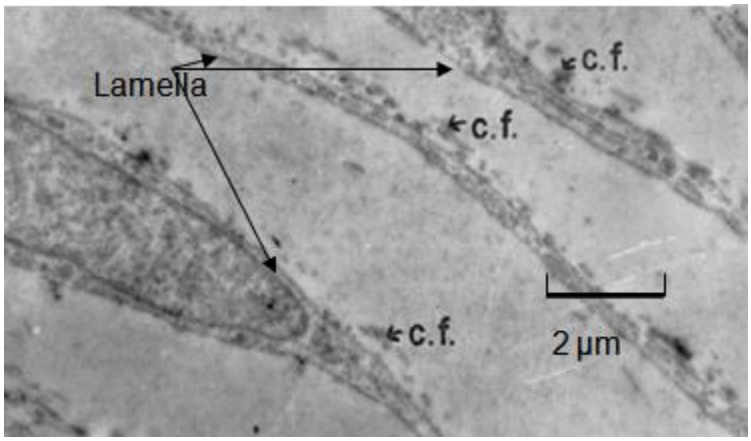

Figure 1.13. Electron micrograph of transverse section of the outer zone of the *cat* mesentery PC. Continuous cytoplasm sheets form the outer lamellae. Thickness of lamella approximately is 0.2µm. The collagen fibrils (c. f.) on the outer side of lamellae are most visible; however there are some faint collagen fibrils in the inter-lamellae space. Adapted from [33].

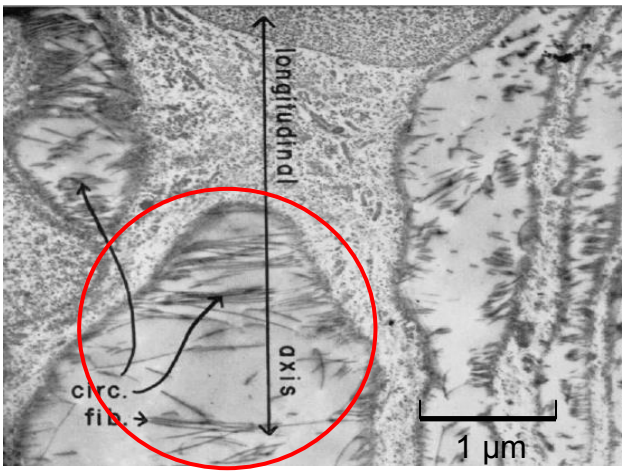

Figure 1.14. Electron micrograph of a PC in *cat* mesentery; the section is tangential to the surface of a lamella; the direction of the long axis of the corpuscle is indicated by the arrow; many collagenous fibres lie in the plane of the section (circled region), and most of these are oriented at right angles to the longitudinal axis. Adapted from [33].

The core fully encapsulates an unmyelinated axon. Extensions of the axon terminal incorporate radial clefts. These modified extensions progress into thin, bow-shaped hemi-lamellae which are separated from each other by longitudinally–orientated collagen fibrils creating a bulb around the neurite (fig.1.15). In the clefts there are small fibrils of elastin and a number of large fibrils of collagen [41].

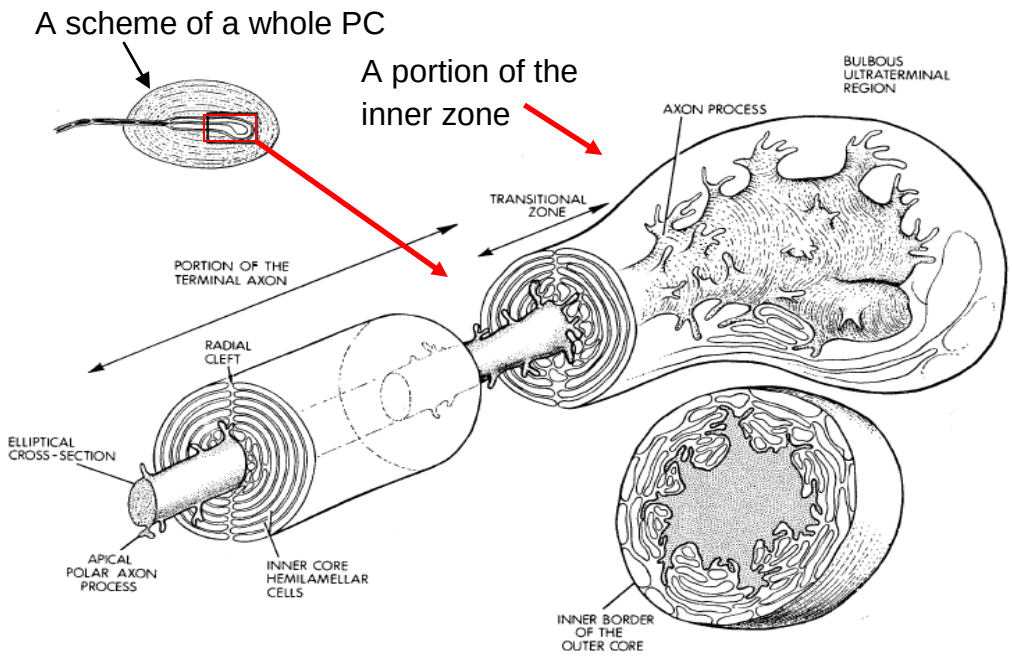

Figure 1.15. Schematic diagram of a portion of the inner zone demonstrating the morphological organisation of the inner core hemi-lamellar cells and axon processes within the bulbous ultra-terminal region. Adapted from [41].

The role of the radial clefts is still not clear. Some researchers suggested that these gaps are nutrition pathways via blood capillaries to regulate the environment around the neurite. Axon processes extending into the hemi-lamellae may relate to the detection of mechanical deformation from external stimuli transmitted through the lamellae [42].

1.2.5 Pacinian Corpuscle biochemistry

Analysis of mechanical properties of the corpuscle requires information on the extracellular matrix, which is determined by large volume of substances of fibrils with high binding capacity. In order to transmit pressure signal through the capsule, it is necessary for the PC to possess high viscoelasticity, which must impose considerable constraint on the tissue structure.

Histochemical studies on *cat* mesentery PCs by Sames [43] investigated the distribution of proteoglycans. One type of proteoglycan, decorin, which binds to and modulates the organisation of collagens type I and II, was found in the interlamellar spaces around the interconnections presumed to consist of collagen type II. Such complexes are found in cartilages subjected to compressive loads and thus might be responsible for the cartilage-like elasticity of the PC. Another proteoglycan, biglycan, which interacts with collagen type I and binds to collagen type V, was found in the lamellae of the growth zone. In this context, biglycan may play a role in corpuscular growth. Collagen IV (which forms the network structure of basement membranes which, in many tissues, couple cells into the surrounding matrix) was found in all components of *cat* mesentery PCs, except the axon.

From a biophysical point of view, one of the most important classes of proteoglycans are the large species such as aggrecan. These consist of a long protein core to which are attached a large number of glycosaminoglycans. These

molecules constitute the “space fillers” of the extracellular matrix and, through steric and electrostatic interactions, regulate the distribution and mobilities of water and solutes. Glycosaminoglycans were found in the interlamellar spaces of the outer core [43] and, together with collagen II, may also contribute to the cartilage-like elastic properties of the PC.

The presence of elastin within the PC from human hands was first documented in 1908-1909 [27], [44]. Michailow [29] observed an elastic capsule surrounding a PC from the human hand. An elastic fibril network was found around the core and in the blood vessels entering the corpuscle [29].

The differences in biochemistry between the different zones of the PC suggest that they have different biophysical properties and functions [45]. In the context of biomechanics the most important cellular structure is the cytoplasmic cytoskeleton. Actin has been detected in cytoplasmic extensions from the neurite through the clefts in the PC [45]. Similar structures in, for example, hair cells play an important part in mechanotransduction and the same may be true of the cytoplasmic extensions of the PC.

1.2.6 Functions of the Pacinian Corpuscle

There have been many discussions about the function of PCs in addition to tactile perception. Since 1865 a number of functions have been suggested, such as the measurement of the power of muscles or monitoring movement of joints. In this context they were generally thought to act as baroreceptors, but experimentally it has been difficult to establish relationships between specific stimuli and signals in the axon. (In two early studies, Gray and Malcolm [46] report measurements on nerve impulses from *cat* mesentery PCs in response to a wide range of mechanical signals of known displacement; Adrian and Umrath [47] report similar measurements in response to joint movement in the *cat* foot.) PCs have also been suggested to control tissue hydration, regulating the absorption of fluid from the microcirculation – this hypothesis implies that the corpuscles are osmosensitive. Both Adrian and Umrath [47] and Ramstrom [48] applied temperature stimuli directly to PCs (in the *cat* foot and the *human* parietal peritoneum, respectively). When mechanical stimulation was avoided, no response to temperature changes was found in either study.

Cauna [18] suggested that the PC has a blood supply for its own nutrition but may also respond to this supply and hence, together with other receptors in the skin, may contribute to a vascular reflex. PCs may have different primary functions depending on their size and location: some whose function is mainly sensory and others whose role is mainly related to regulation of the blood circulation. This

question of the function of the PC is addressed in a different context later, in chapter 3.

1.2.7 Mechanisms of Mechanotransduction

Mechanotransduction has been most extensively investigated in relation to tactile perception. When pressure or vibration is applied to the surface of the skin, a mechanical disturbance propagates through the neighbouring tissue, the receptor deforms and stress propagates through the lamellae resulting in the generation of a receptor potential at the nerve membrane (RP or GP-generator potential). When the signal reaches the threshold, an action potential (AP) is generated by opening stretch-activated ion channels (Na^+ and K^+) in the axon [49], [39]. The response of PCs is conveyed by a pattern of action potentials which depends on the stimulus type (e.g. dynamic or static loading); adaption to a stimulus is seen as a decrease in the firing rate [50]. It has been hypothesized that the mechanotransduction process is most effective when mechanical stimuli are applied in a direction orthogonal to the axon of the PCs [36].

Hubbard (see next section for experimental details) noted that the time course of mechanical disturbances in the corpuscle was similar to the adaptation of neural activation, and concluded that adaptation was the direct consequence of mechanical processes [55]. However, Loewenstein and Mendelson [39] studied

adaptation in *cat* mesentery PCs and suggested two components in adaptation: a mechanical component (acting as a high-pass filter in the form of the laminated capsule which prevents progression of slow stimuli to the neurite) and an electrochemical component relating to the neuronal mechanism. Interestingly, encapsulated and decapsulated PCs have different adaptation periods to sustained stimuli. The response of encapsulated PCs decreases to normal within 6 ms, while decapsulated PCs keep producing neural spikes for up to 70 ms [20].

Banker and Girvin found that vesicles at the end of the axon processes of PCs are similar to those in the sensory terminals of muscle spindles and believed them to contain neurotransmitters [37]. This gave rise to speculation that, during mechanical distortion of the PC, a substance is released from vesicles on the axon processes which is able to affect the ionic environment of the inner core, forming chemically-mediated synapses [41]. As mentioned above, Pawson et al [45] observed similarities in the composition of axon processes in the PC and stereocilia in the inner ear (known to be involved in auditory mechanotransduction), providing further evidence of the mechanotransduction role of axon processes in the PC.

The frequency response of the corpuscles is central to their function in perception. A variety of studies indicate that 250 Hz is the optimal frequency detected by PCs [35], although PCs are sensitive to a range of frequency from 10 to 1000 Hz [38]. The PC frequency response differs among species, perhaps in relation to different

functionality. It has been observed that PCs in the *cat* mesentery demonstrate polymorphism, which unusual structure may produce a broader overall frequency response [35]. However, such polymorphism has not been observed in *human* PCs.

Studies on human hands, e.g., [55], suggest that the PC is primarily responsible for perception at frequencies above 30 to 50 Hz, with other populations of receptors coming into play at lower frequencies. In a study on grasping of a vibrating cylinder, Brisben et al [53] report optimal sensitivity in the region 150-200Hz, with some subjects able to detect amplitudes < 0.01μm on the palm. Transition from the PC channel to perception via Meissner corpuscles was observed in the region 20-25 Hz (section 1.2.9 contains further discussion of the PC frequency response).

1.2.8 Experiments on Pacinian Corpuscles in Vitro

There have been a number of studies on PCs in vitro. However, there is significant concern about the viability of the corpuscles because morphological change in PCs can be observed after dissection. It was observed by light microscopy that the neurite and the core degenerate after 6-12 hours although the inner and outer zones can maintain their structure for up 27 hours [37]. Also freezing and thawing causes degeneration of the axon and the core after 3 days (fig. 1.16) [51].

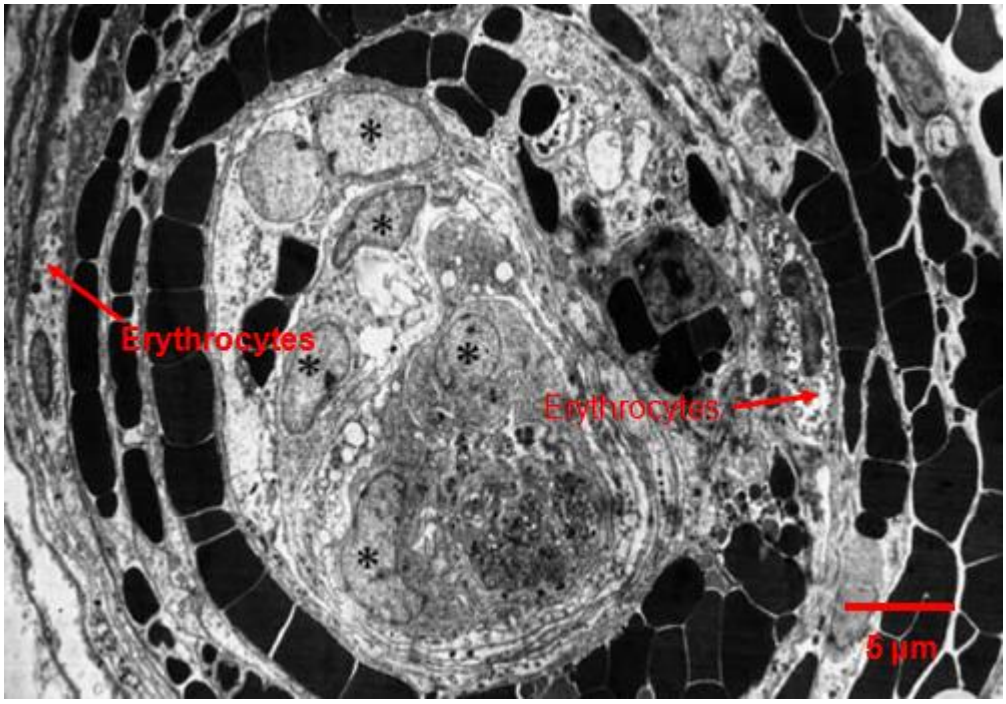

Figure1.16. A transverse ultrathin section of rat foot PC after 3 days of simultaneous freezing treatment and denervation. The space of the core is occupied by cells (asterisks) with cytoplasm of a moderate electron density; the growth zone contains a huge number of erythrocytes. Taken from [51].

The first studies on the mechanical properties of isolated corpuscles were performed by Hubbard [55] who used rapid mechanical compression of PCs from *cat* mesentery to study lamellae displacement under external compression. The experimental apparatus shown in figure 1.17 and the photographic apparatus used to image the corpuscles at different stages is shown in figure 1.18.

The corpuscle was squeezed between two microscope cover slides with total displacements (outer surface of PC) between 19 and 90 µm at rates in the range 2.5 to 40 µm ms^{-1}. Hubbard measured displacements within the corpuscle from

photographs taken at successive intervals, achieving a measurement error of around 1 μm. The displacement waveforms of three lamellae are shown in figure 1.19, together with “static” and “dynamic” components. This work was the stimulus for one of the investigations in the present study and a more detailed discussion of these results and a comparison with new data are given in Chapter 5.

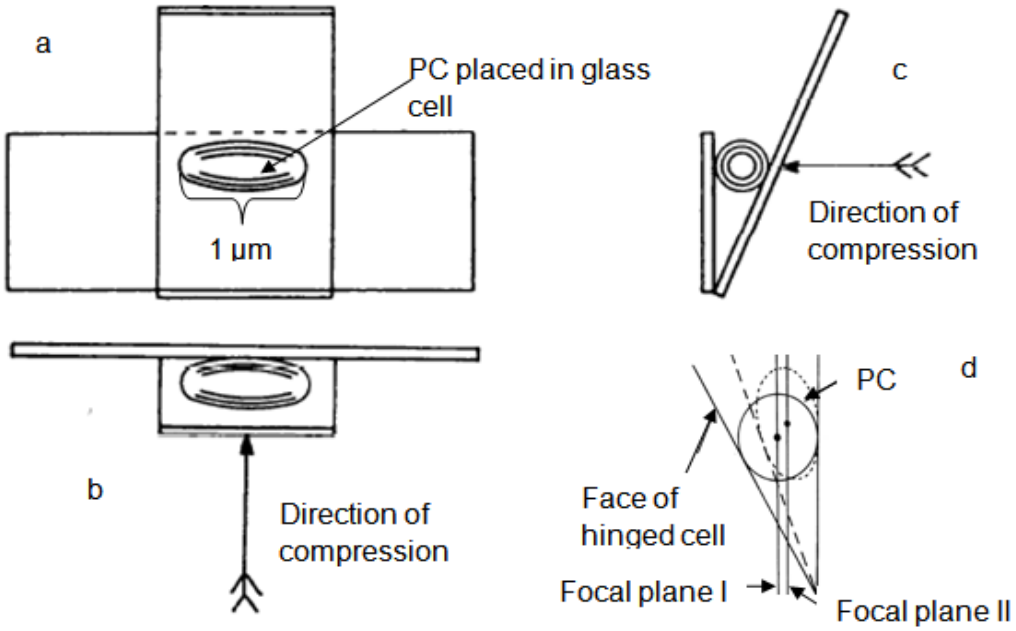

Figure 1.17. A schematic of the glass cell in which the PC was compressed. (a) Focal plane of the glass cell with the PC in; (b) a side view of the glass cell with the PC in, the arrow indicates the direction of compression; (c) a transverse plan of the glass cell with the PC in, the arrow indicates the direction of compression; (d) diagram showing change of position of the axis of the PC with compression. Dotted outline represent conditions at the peak of compression. Focal plane I and II show the amount of refocusing ideally required. Adapted from [55].

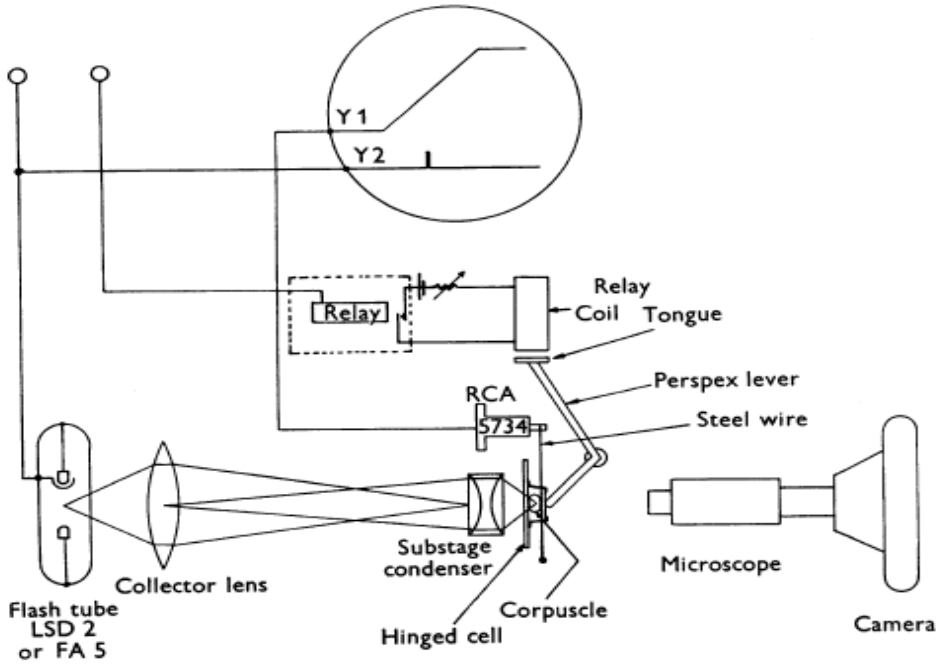

Figure 1.18. Diagram of the apparatus used for photography of the PC during and after an applied compression. Adapted from [55].

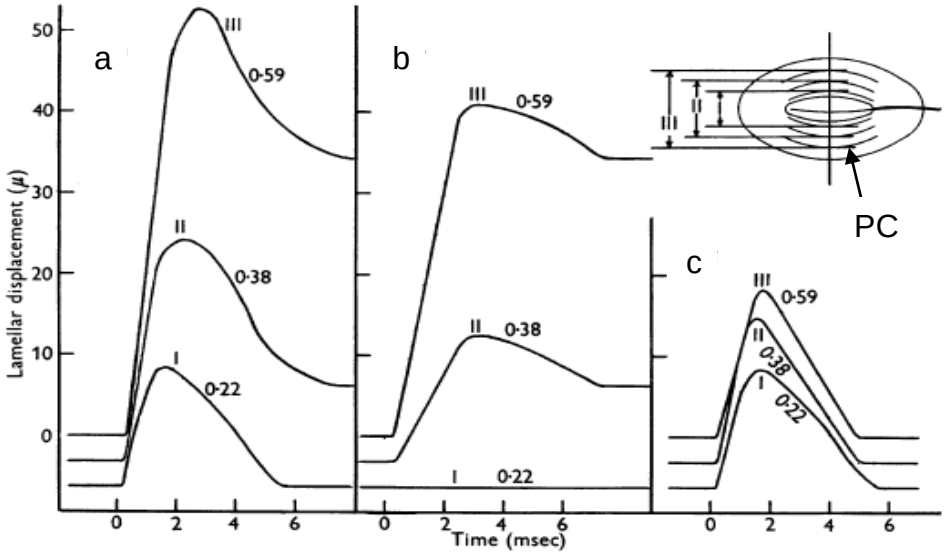

Figure 1.19. Lamellar displacements at three positions within a PC: (a) total displacement as recorded; (b) equivalent static displacement; (c) dynamic component of displacement. The numbers on the curves correspond to the ratio of the radius of the chosen lamella to the outer-capsule radius. Adapted from [55].

Sato [56] investigated the receptor potential in PCs from *cat* mesentery in response to sinusoidal stimulations of different frequencies and amplitudes. A part of the mesentery containing the PCs was exteriorised from the body of the *cat* and kept in Ringer`s solution [57], and a PC axon was dissected from its surroundings without disturbing the local blood supply. The axon output was connected to an amplifier and a stimulus generator producing a range of sinusoidal signals in the range 20-1000 Hz was directly applied on the surface of the PC. The experiments demonstrated an optimal frequency at around 150 and 300 Hz, respectively, with a fall-off in response at lower frequency which was steeper than that expected from the response of the nerve alone. Sato explains the fall-off in response above 300 Hz in term of the mechanism for generating receptor potential, which is depressed at high frequency. Interestingly, this study suggests the frequency of peak response is affected by temperature, moving from 300 Hz at 37º C to 150 Hz at 21ºC. It was suggested that this s due to the biochemistry of action potential generation. However, in another study Cauna and Mannan [18] observed no effect of temperature.

Study of the concentration of ions in the intra capsular fluid is important in order to understand the electrochemical responses of PCs at rest and under load. Sampling of the fluid exuded from punctured *cat* PCs revealed it to be viscous and transparent and containing particles of fat [42]. The concentration of potassium ions in fluid of PCs from cat mesentery was 6.19 ± 0.72 mEq/L, which is greater than in cats' blood plasma (2.78 ± 0.38 mEq/L), and the concentration of sodium ions was 114.4 ± 10.4 mEq/L, which is slightly lower than the concentration of

sodium ions in plasma. Cells normally contain a higher concentration of potassium than the extracellular fluid and a much lower concentration of sodium, an imbalance which is lost during the generation of an action potential and it is probable that the observed concentrations reflect depolarization processes within the neurite. Also, because there are nodes of Ranvier within the capsule, the higher concentration of potassium may decrease the excitation threshold for sensory responses of the PC [58]. In support of this hypothesis, Diamond [59] found that blood capillaries (fig. 1.20) around the first node ensure that the concentration of potassium ions is sufficient to originate a first nerve spike in the node and then generate an action potential.

A number of studies have investigated the effects of pharmacological agents on PC electrophysiology. Pawson et al [40] investigated the role of GABA (gamma-aminobutyric acid) on the response of *cat* PCs to a mechanical “ramp-and-hold” stimulus applied to the surface of the capsule. Under normal conditions, neural response to the static “hold” phase of the stimulus falls off rapidly as a consequence of the PC`s adaptation. However, in the presence of gabazine as a GABA receptor antagonist, many action potentials were observed during the “hold” phase. These results suggest that the normal adaptation response is not purely mechanical, as hypothesised by Hubbard [55] and others, but also has a chemical component, as suggested by Loewenstein and Mendelson [39].

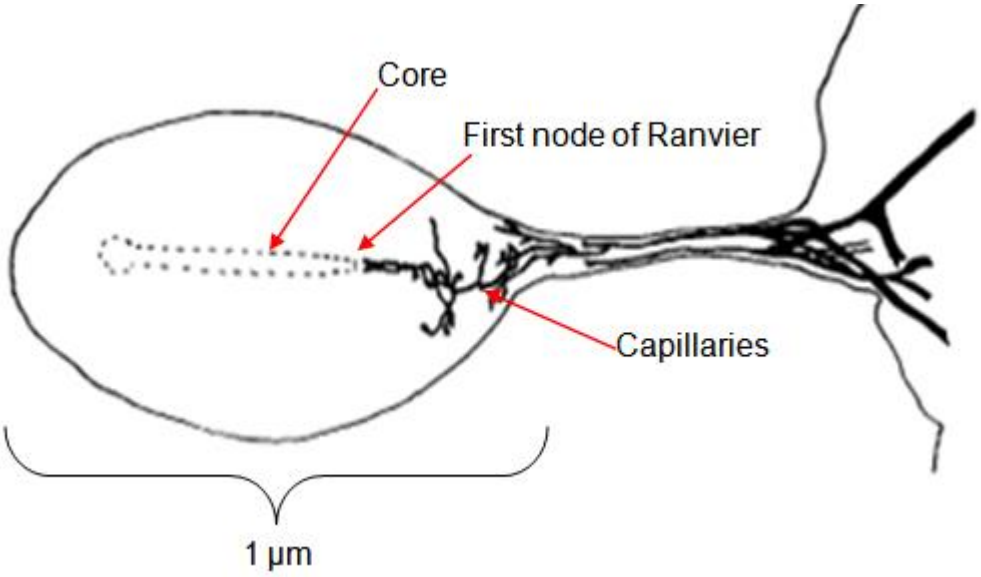

Figure 1.20. Schematic of the PC from cat mesentery; the corpuscle capillary bed was injected with Indian ink. The capillaries surround the first Ranvier node. Taken from [59].

It has been shown that PCs shrink in hypertonic solution and tend to expand in hypotonic solution [18]. The biomechanical implications of such experiments are discussed in more detail in the context of the present work in Chapter 4. An elecrophysiological study on the effects of sodium ion concentration on the receptor potential [59] demonstrated that, on replacing sodium by sucrose to maintain osmotic pressure, generation of the receptor potentials gradually declined, but returned to normal when the sodium concentration was restored, demonstrating the importance of sodium for the generation of electrical activity.

1.2.9 The frequency response of the Pacinian Corpuscle

In addition to the study by Brisben et al already discussed in 1.2.7, the literature includes many psychophysics studies of touch perception, notably numerous studies by Verrillo and colleagues, in which test subjects are required to respond to closely controlled stimuli at threshold levels or above-threshold levels, e.g., [60, 61, 62, 63]. Such studies typically involve vibratory stimuli in the form of displacement sine waves of known amplitude and frequency, delivered via a contactor with a surround to prevent spread of stimulation across the skin. The experimental results can be interpreted in terms of perception via four distinct channels (corresponding to receptor populations of four types – see section 1.1), including a PC channel. Figure 1.21 shows data fitted to a four-channel model.

The sensitivity of the PC channel varies with frequency; it is most sensitive at approximately 250 Hz and sensitivity falls off at around 10 dB per octave at lower and higher frequencies. A possible interpretation of this is that the PC response falls off at low frequencies due to the mechanical behaviour of the lamellar structure, and falls off at high frequencies due to the effect of a refractory period in the excitation of the nerve. (See previous section for a similar interpretation of Sato's in-vitro experiments.) In terms of the mechanical transmission from the outer surface of the PC to the core, this interpretation predicts a high-pass response with good transmission for frequencies $\geq$ 250 Hz but a fall off in transmission at lower frequencies.

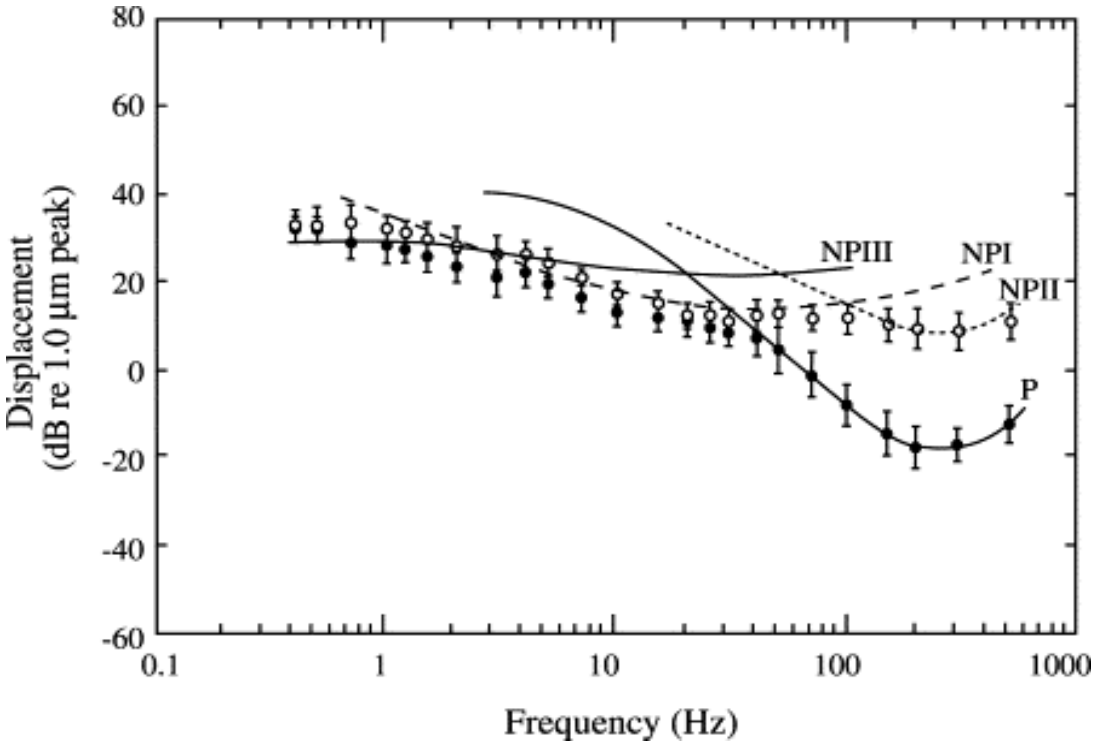

Figure 1.21. Threshold measurements for different populations of mechanoreceptors in the thenar eminence of the human hand; the thresholds from each of the four channels combine to give the overall threshold; the full line labelled P is the threshold for the PC channel, with a minimum in detection threshold (maximum sensitivity) at around 250 Hz; the NPI- channel corresponds to Meissner's corpuscles and contributes to the overall threshold in the range 3 – 30 Hz; the NPII-channel corresponds to Ruffini cells; the NPIII-channel corresponds to Merkel cells and contributes to the overall threshold below 3 Hz. The vertical scale is in decibels (logarithmic units) referenced to 1.0 µm peak. Adapted from [60].

1.3 Theoretical Modelling

Hubbard [54] was the first researcher to suggest a model of mechanotransduction in PCs based on his experimental studies. Hubbard's model proposed that the lamellar structure of PCs acts as a high-pass filter. Loewenstein and Skalak [36] took into account Hubbard`s experimental findings and morphological and mechanical properties such as membrane elasticity, viscosity of intercellular fluid, and interconnections between the lamellae; they constructed a model in which the part-spherical, part-cylindrical geometry of the PC was replaced by spherical or a complete cylindrical geometry. A model of the transmission of mechanical forces through the lamellae to the core was developed using a lumped parameter approach. The concept of the model was a series of concentric lamellae separated by incompressible fluid which recovers after deformation due to the elasticity of the lamellae. The lamellae were considered to be impermeable and the fluid, of specified viscosity was supposed to flow between the lamellae when the structure is deformed. Also, it was assumed that there were elastic interconnections between the lamellae, responsible for transmission of a static stimulus. Transmission of a mechanical stimulus was partly via these and partly via the interlamellar fluid. The entire corpuscle with a number of lamellae and the core was fully represented by the cylindrical model in figure 1.22.

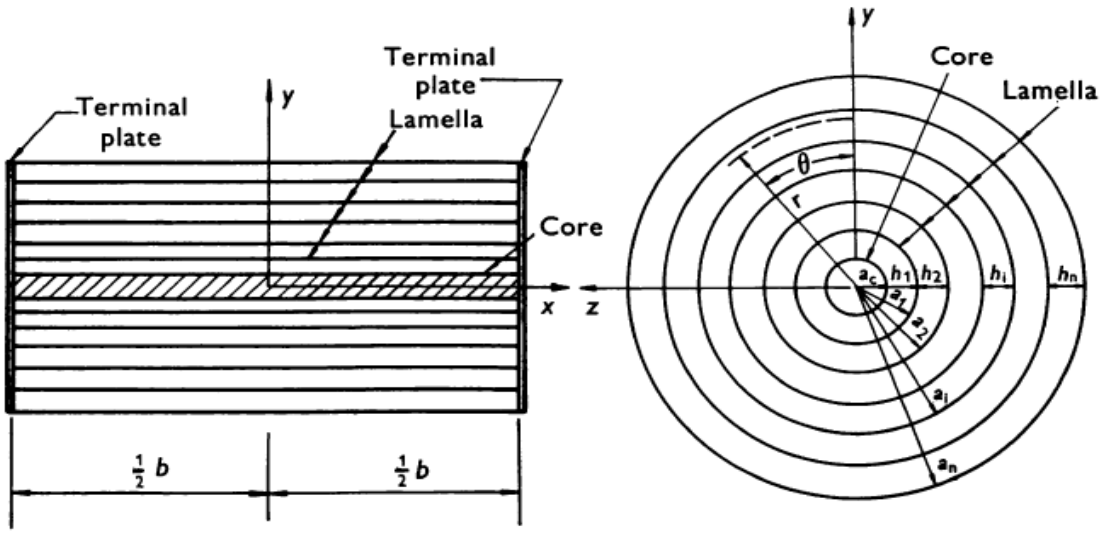

Figure 1.22. The cylindrical model of the PC. (a) Longitudinal plane along the axon, where b is the length of the corpuscle; (b) transverse plane, where h_i is the spacing of the i-th lamella and a_i is radius of the i-th lamella. Adapted from [36].

Pressure on the surface of the PC may distort the cylindrical geometry, but it is assumed that pressure distribution is symmetrical with respect to the *x*-plane (fig 1.22 (a)), and represented by a double Fourier series (equation (1)):

$$p = p_0 + \sum_k \sum_m A_{km} \cos(2\,k\theta)\, \cos(m\pi \frac{x}{b}) \qquad (1)$$

where p is pressure, with a static term p_0. The amplitude coefficients A_{km} have units of pressure. This relationship is applied to each lamella and related to displacement w_i by the equations:

$$p_i = A_i \cos(2\theta) \cos(\pi \frac{x}{b}) \quad (2)$$

$$w_i = B_i \cos(2\theta) \cos(\pi \frac{x}{b}) \quad (3)$$

$$B_i = A_i K_i, \qquad K_i = \frac{a_i^2}{E d_i} \left(1 + \frac{4b^2}{\pi^2 a_i^2}\right)^2 \quad (4)$$

Where K_i is the compliance of the i-th membrane; a_i is the radius of the i-th lamella; d_i is thickness of the i-th lamella; b is length of the PC; E is Young's modulus.

The stress σ developed in the radial springs due to the displacement of adjacent lamellae is expressed by (5), where the elastic modulus is taken to be αE and h_i is the spacing of the i–th lamella.

$$\sigma_i = \frac{w_i - w_{i-1}}{h_i} \alpha E \quad (5)$$

Or, in terms of the Fourier components:

$$\sigma_i = C_i \cos(2\theta) \cos(\pi \frac{x}{b}) \quad (6)$$

Combining the above equations gives the expression for the stress components:

$$C_i = \frac{B_i - B_{i-1}}{h_i} \alpha E \quad (7)$$

Lamellar deflection with relative velocity ($\dot{w_i}$-$\dot{w_{i-1}}$) of adjacent lamellae produces fluid motion; the resulting pressure in the viscous interlamellar fluid can be represented by the equation:

$$\bar{p_i} = D_i \cos(2\theta) \cos(\pi \frac{x}{b}) \quad (8)$$

Where the amplitude is given by:

$$D_i = R_i(\dot{B_i} - \dot{B}_{i-1}) \quad (9)$$

For a fluid of viscosity μ the resistance can be written as:

$$R_i = \frac{12\mu b^2}{h_i^3 \pi^2 \left(1+\frac{4b^2}{\pi^2 \alpha_i^2}\right)} \quad (10)$$

Ignoring inertial terms, the instantaneous load on the i-th lamella is given by the difference between viscous pressure and radial spring stress on both sides of the lamella:

$$p_i = \frac{w_i}{K_i} = \bar{p}_{i+1} + \sigma_{i+1} - \bar{p_i} - \sigma_i \quad (11)$$

and for any lamella except the first (outer lamella) and last (core):

$$\frac{B_i}{K_i} = R_{i+1}\left(\dot{B}_{i+1} - \dot{B}_i\right) + \frac{B_{i+1} - B_i}{h_{i+1}} \alpha E - R_i\left(\dot{B}_i - \dot{B}_{i-1}\right) - \frac{B_i - B_{i-1}}{h_i} \alpha E \quad (12)$$

This model can be solved either numerically or by the construction of a mechanical analogue (fig. 1.23) or an electrical analogue (fig 1.24). The latter is developed in Chapter 2.

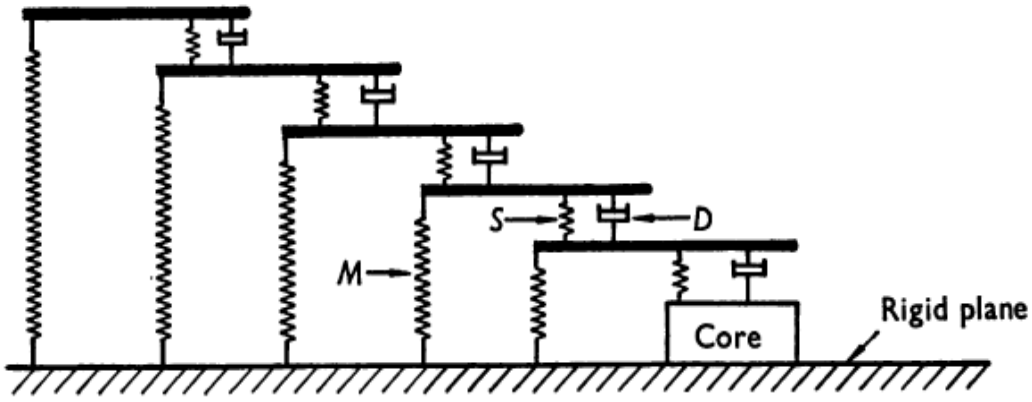

Figure 1.23. The model of the PC represented by a mechanical analogue; lamella compliance is associated with springs M; springs S represent radial spring compliance; fluid resistance is represented by dashpots D. Adapted from [36].

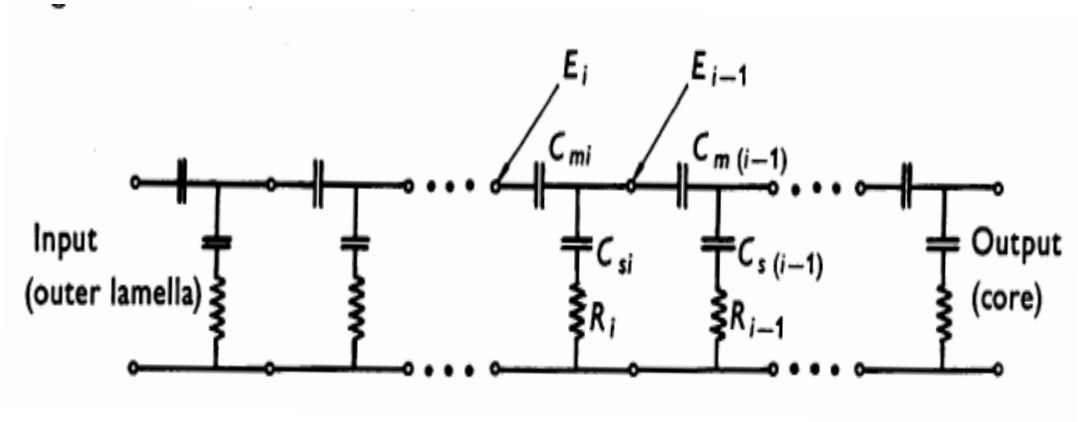

Figure 1.24. The model of the PC represented by an electrical analogue where all components of the mechanical model are converted into electrical equivalents; lamella compliance is represented by capacitance C_{mi}; fluid resistance is associated with resistance R_i; the radial spring compliance is represented by C_{si}. Adapted from [36].

This theoretical model predicted static lamellar displacements (fig. 1.25) which correlated with the experimental measurements by Hubbard [55]. For dynamic stimuli, the pressure transfer function of the lamellar structure was calculated to have the expected high-pass characteristic (fig.1.26) with a relatively flat response above 300 Hz. At frequency 300 Hz, 90 % of applied pressure was transmitted to the core due to the viscous properties of the interlamellar fluid. Only 3% of applied pressure transmitted to the core during zero frequency stimuli which corresponds to static stimuli.

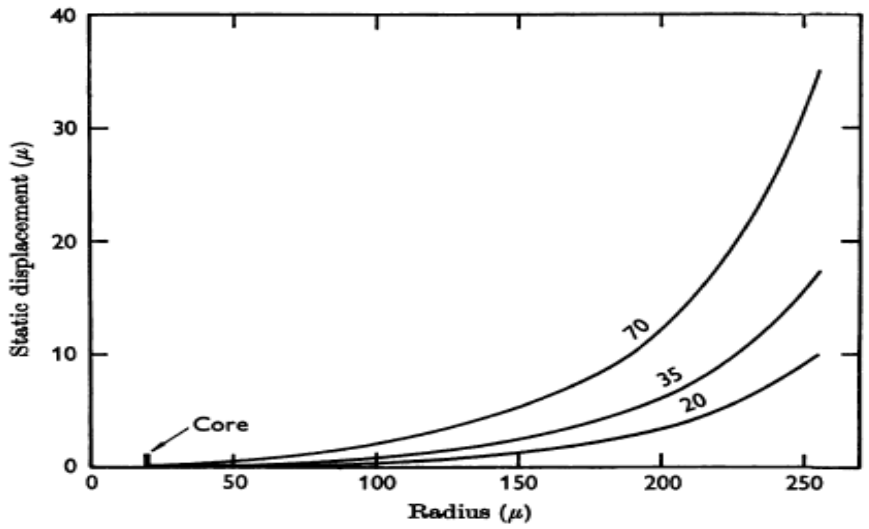

Figure 1.25. Lamellar displacement against position for static compression; the abscissa is the radius measured from the axis of the PC. The numbers on the curves represent the magnitude of the applied compression. Taken from [36].

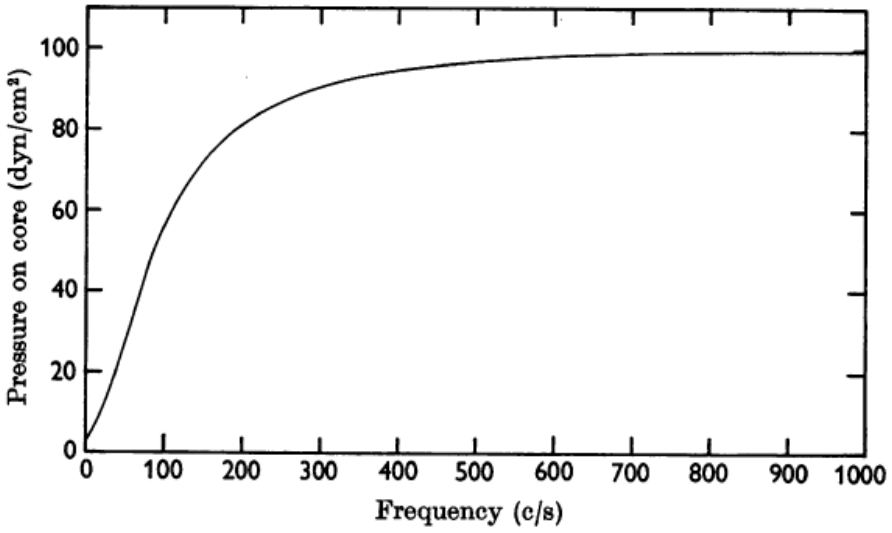

Figure 1.26. Core pressure in the PC against stimulus frequency for displacement of the outermost lamella at constant input pressure. The ordinate is the peak pressure exerted on the core for a peak pressure of $100 dyn/cm^2$ on the outermost lamella at the frequencies given by the abscissa. Taken from [36].

A comparison of the model with experimental data obtained in this project is described in Chapter 5.

Grandori and Pedotti [64] combined the Loewenstein and Skalak model of mechanotransmission with data on electrical transmission in unmyelinated nerves and a model of neural activation based on the statistical analysis of data of firing rates and interspike intervals collected by Bolanowski [50]. The model was found to be compatible with a large body of experimental data [27], [53], [36], [42], [49], [58], [65], [37], [55], [59]. Sinusoidal stimuli were encoded into the pattern of spikes in the nerve fibre.

Holmes and Bell [35] also developed a theoretical model of mechanotransduction in the PCs, again employing the Lowenstein-Skalak model of the mechanical component, which they coupled to another mechanism for neural excitation. They hypothesised the existence of stretch-activated ionic channels, which respond to mechanical pressures. However, the results were somewhat inconclusive due to the large number of free parameters in the model.

1.4 Discussion and Overview of Thesis

The literature review demonstrates that both experimental work and theoretical models have provided some understanding of the mechanism of mechanotransduction in the PC, but a number of questions still remain. The important point is that the structure and mechanical properties are still incompletely characterised and that more information is necessary before existing models can be fully tested or more elaborate ones developed. Most recent work on mechanotransduction in PCs has concerned the neurophysiology rather than the biomechanics.

The structure of the PC (fig. 1.27) can be summarised as follows: the lamellar structure has an inner zone and an outer zone, separated by a growth zone. The fluid spaces between the lamellae contain a complex collagen network [34]. Elastin is only found in the inner core, around the axon [41]. Lipids are present within the capsule [65]; proteoglycans are found in the inner lamellar spaces and may play an important role during compression [43]. Axon processes run from the neurite towards the growth zone and may reach the outer zone. It has been speculated that vesicles on the end of the axon processes behave as transmitters and are able to change the ionic environment after being triggered during compression [41], [37]. There are pathways between the hemilamellae and clefts of the inner core whose role is still unknown. However, some researchers associate them with nutrition pathways via capillaries [66], [42].

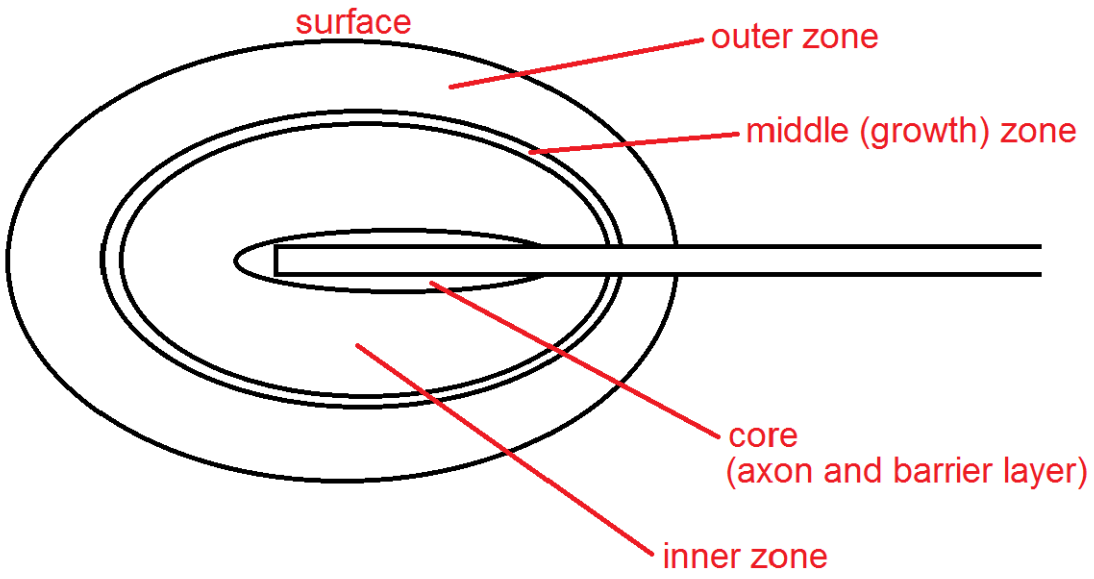

Figure 1.27. Schematic diagram of a PC, showing the core, surrounded by lamellae in inner, middle and outer zones.

Motivating the present work are important but still unanswered questions concerning connectivity of the fluid compartments which is crucial in determining the interlamellar fluid displacement under mechanical load. Daniel and Pease [33] raised an interesting question in relation to osmotic pressure: are the lamellae of the outer zone kept separate by hydrostatic pressure produced by osmotic forces? They proposed that colloidal material in the inter-lamellar solution generates an osmotic pressure which maintains the requisite pressure balance, and is oppose by stresses generated in the collagen fibre network. Intracapsular pressure is another important parameter, but previous attempts to measure it have encountered a problem of lamellar damaging during puncturing by a pressure probe [42], [67]. Also, there is very little information about corpuscle–tissue coupling; the

involvement of surrounding structures may be important for the transduction process.

The first stage of the present work is dissection of PCs from the *equine* hoof, providing an opportunity to investigate surrounding tissue and investigate corpuscle-tissue coupling.

Transmission, confocal and nonlinear microscopic techniques are combined in the present study to investigate the structure and biochemistry of the PC. Fluorescent tracer methods are used to study solute transport and provide data on fluid connectivity and lamellar permeability. Osmotic swelling measurements are undertaken further to explore the permeability and mechanics of the corpuscle. We also describe a number of direct mechanical measurements, including measurements of hydrostatic pressure and elastic properties of the capsule and lamellae. Finally, we undertake measurements of dynamic mechanical properties which we interpret using an electrical analogue of the Loewenstein-Skalak model.

Chapter 2

Methods

This chapter describes the experimental methods employed in this thesis, some of which were already established in the laboratory for measurements on other systems and others which were new or heavily modified. The method of dissection of the PC will be described in section 2.1, followed in section 2.2 by a description of the various microscopy techniques employed. Section 2.3 describes methods to investigate solute transport and osmotic swelling behaviour of the PC. The various methods of characterizing the mechanical properties of the corpuscle are described in sections 2.4, 2.5 and 2.6. The advantages and disadvantages of the methods and techniques used in the present study are discussed in the last section (2.7).

2.1 Dissection of Pacinian Corpuscles

It was initially intended to use PCs from *rat* and *mouse* limbs, which have been described by a number of authors [33], [45],[68], [69], [70] and snap frozen tissues were obtained from the School of Medicine, University of Bristol. However, pilot studies demonstrated that the overall shape and internal structure of PCs in defrosted *rat* limbs were seriously disrupted, presumably due to effects of the rapid

freezing, making the PCs difficult to recognise during dissection. Subsequently, fresh *horse* hooves (immediately after animal euthanasia) were obtained from animals of known age and health status at an abattoir (LJ Potters, Taunton) and transferred to the laboratory, allowing experiments to commence within one or two hours of euthanasia . Previous authors have described PCs in the frog area of the hoof [21], [71]. Their work aided the development of the dissection technique, and during the learning process other anatomical structures which may be associated with the functioning of PCs were also revealed and are discussed below.

Before dissections, hooves were cleaned with tap water. The dissection procedure was to make an incision of the back of the hoof; the scalpel (blade N22) was placed against the back of the heel and a wedge of tissue between the heel bulbs and frog apex was excised (fig. 2.1). Evans Blue (0.1% w/v in 0.15M NaCl) was applied to the surface of the extracted tissue to help in identifying blood vessels as landmarks for further investigation.

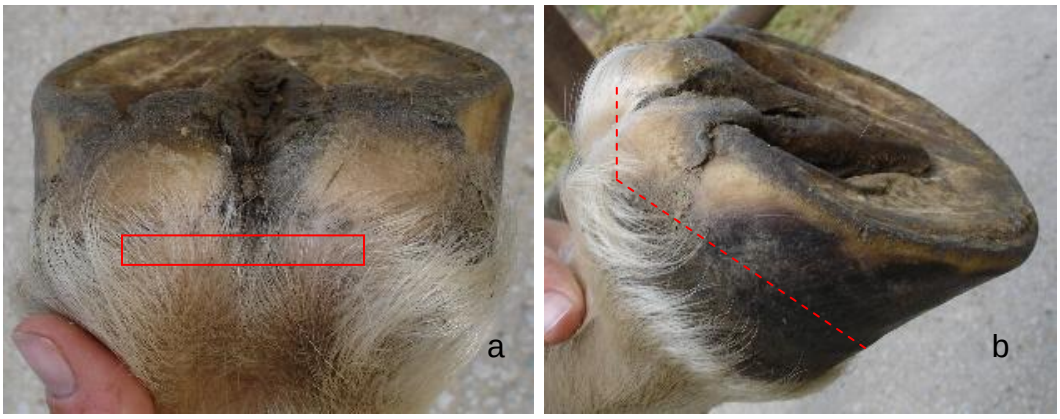

Figure 2.1. (a) coronal view of the hoof; the red box is the area of interest. (b) transverse view of the hoof; the dashed line is profile of excision. A wedge of tissue was cut from the hoof. Adapted from [21].

Two techniques were used to determine the distribution of corpuscles through the tissue. First, histological sections were prepared in order to study the relationship between surrounding structures such as blood vessels, glands and corpuscles. Cubes of the tissue of approximately 1cm x 1cm x 1cm were snapped frozen and 20 µm frozen sections were prepared (Leica Cryocut CM1800 Cryostat). The tissue sections were stained with Evans Blue (0.1% w/v in phosphate buffered saline) and observed under a dissection microscope (Wild Heerbrugg MS Stereomicroscope, total magnification 120x).

The second approach sought to dissect clusters of corpuscles. Tissue blocks were cut from regions identified from the histology as likely to contain PCs, and PCs were dissected with ocular scissors and a scalpel. Dissected groups of PCs, often tightly surrounded by a layer of adipose and loose connective tissue were stored in 0.15M NaCl at 4º C for up to 24hrs. For longer term storage of specimens for structural analysis, fixation of PCs in 4% formaldehyde was used. However, formaldehyde fixation can lead to tissue shrinkage and intercellular distortion, so results from such preparations were always confirmed on fresh tissue.

Isolated corpuscles and tissue sections containing corpuscles were taken for further microscopic investigation. Histological sections and intact corpuscles were stained with Alcian Blue, Van Gieson, for demonstration of, proteoglycans and collagen by standard procedures [72]. Blood vessels were also revealed by their uptake of fluorescein and rhodamine in the tracer studies described below. Some

specimens were and stained with di-8-anneps for visualisation and axon cell membranes, including the axon and lipid droplets [73]. Confocal and nonlinear microscopy were performed on intact corpuscles and a holding chamber was constructed by forming a 4-sided frame (1 cm x 1.5 cm x 1 mm) of Paraffin film (“M” Laboratory film, Bemis Flexible Packaging, Neenah, WI54956) and placing it on a microscope slide, which was placed on a hot plate (Gallenkamp, Magnetic Stirrer Hotplate 300) to melt the Paraffin and attach the frame to the slide. The tissue was placed in the chamber, 0.15M NaCl added and a cover slip was placed on the top of the frame and sealed with a brief touch of a soldering iron tip to melt the Paraffin. This chamber allowed good visualization whilst preventing the PCs from undergoing compression and dehydration. Other experiments (osmotic swelling, lamella displacement and cell aspiration) required a similar 3-sided chamber 1.5mm deep to allow the insertion of instruments or changes of bathing solution.

2. 2 Microscopy

2. 2. 1 Light microscopy

Transmitted light microscopy (Olympus U-TVO.5X with digital camera JVC, TK-C1381) was the main tool for morphological analyses, osmotic swelling and lamella displacement studies. Observations on whole corpuscles were generally made using 40×0.75 or 10×0.30 objectives, but 5×0.15 and 4×0.13 objectives were also available.

For experiments involving pressure measurements on the PC the rotation stage of the microscope (fig. 2.2 a) was modified as shown in figures 2.2 b and 2.3. The modified stage–plate contains a homemade micromanipulator, with two micrometers attached to it. A transparent plastic chamber with three access channels, inserted into a metal holder is also attached to the base plate. The chamber, diameter 4mm and depth 2.5mm, on the centre of the slide, has three access channels for different purposes, depending on the type of experiments. In general one channel was used to hold the PC in position using suction from a micropipette. Flexible glue (Word Precision Instrument Inc., Kit silicon Sealant) prevented saline leakage from the channels.

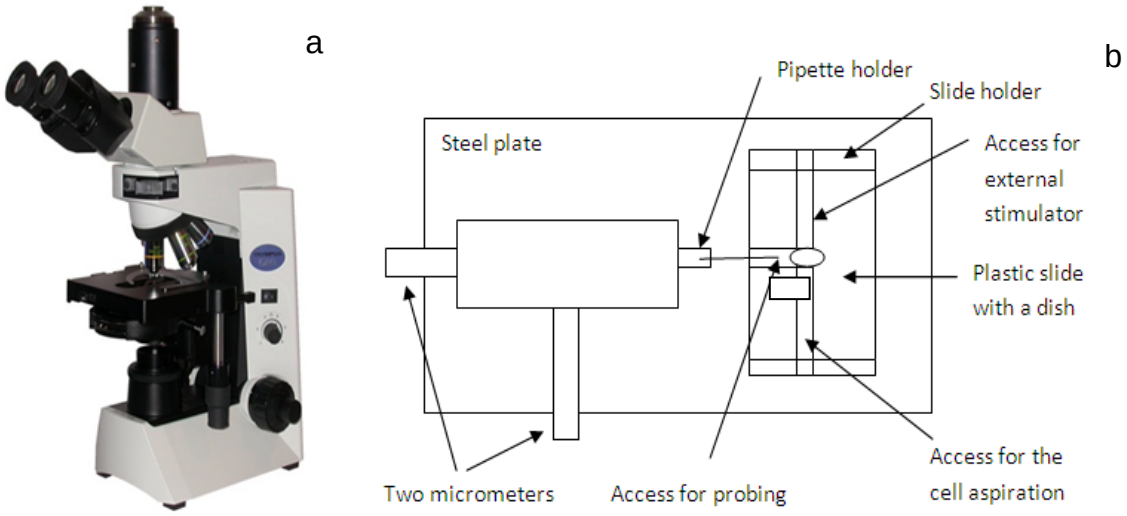

Figure 2.2. (a) The Olympus U-TVO.5X microscope. (b) The schematic on the right shows the micromanipulator and modified working plate.

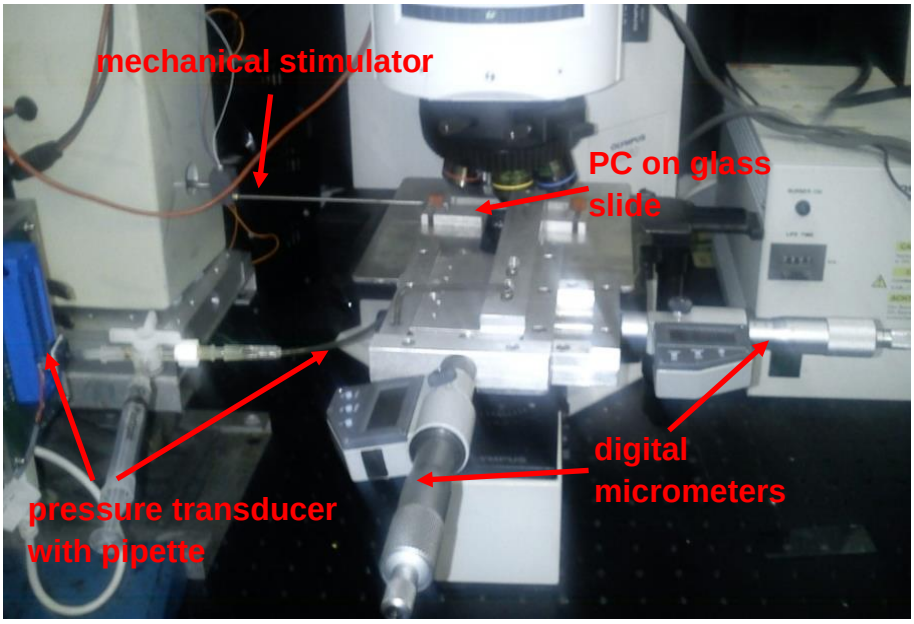

Figure 2.3. The experimental set–up with modified working plate for the light microscope. On the left is the mechanical stimulator (see section 2.5.3) and the pressure transducer with the micropipette attached.

2.2.2 Confocal microscopy

Confocal microscopy was used to determine the 3D structure of the intact PC and to investigate the uptake of fluorescent tracers. The basic mechanism of this microscope involves scanning a finely focused laser beam through a sample. The back scattered or transmitted light then passes through a pinhole, which rejects light which did not originate at the focal plane of the objective, before being directed to a photomultiplier tube. A series of consecutive two-dimensional scans taken at different depths can be reconstructed into three-dimensional images.

The present studies employed a TCS Leica LAS S5C inverted microscope equipped with four lasers (i) Ar^{+}, (ii) HeNe 543 nm, (iii) HeNe 594 nm, (iv) HeNe 633 nm, and a wide range of filters for fluorescence microscopy.

In the tracer uptake experiments fluorescein was stimulated at 490 nm and observed at 525 nm; for rhodamine B, stimulation was at 540 nm and observation at 625 nm.

2. 2. 3 Multiphoton microscopy

Multiphoton microscopy (MPM) allows confocal imaging based on intrinsic contrast mechanisms and therefore provides stain-free imaging of living tissue. Because excitation occurs at infrared wavelength it provides superior depth penetration to confocal microscopy. Three modalities were employed in this investigation: Second Harmonic Generation (SHG), Two–Photon Fluorescence (TPF) and Coherent Anti-Stoke Raman Scattering (CARS). Second harmonic generation was used to visualize fibrous collagen, TPF to visualize elastin and CARS, tuned to a vibrational frequency of the fatty acids of membrane phospholipids was used to visualize cell boundaries.

TPF is the simplest of the modalities. It uses two low-energy photons simultaneously to interact with the target molecule producing excitation of an electron to a higher energy level. For an appropriate molecule this is followed by

the emission of one photon of fluorescence as the electron returns to the ground state [74]. For fluorophores that are normally excited by ultraviolet light, TPF has the advantage of exciting the molecules using photons of longer wavelength which have better depth penetration and cause less photo-damage to the tissue. Because TPF is a weak effect a large number of photons must be delivered to the sample simultaneously in order to increase the probability of non-linear excitation. Constant illumination at this intensity would damage the sample, so a series of femto-second pulses is generated, resulting in high peak intensity whilst keeping the average power on the sample low [76]. The probability of a two-photon event occurring is dependent on intensity squared and, because intensity falls off rapidly outside the focal spot, TPF excitation only occurs in the focal volume and therefore the need for a pinhole, as occurs in confocal laser scanning microscopy, is removed. (Insertion of a pinhole can result in loss of the number of photons collected because even photons that were in the focal volume on excitation can become scattered on the exit path out of the sample.) Amongst the extracellular matrix macromolecules, only elastin displays TPF.

SHG is a second-order non-linear process in which two incoming photons are simultaneously scattered to emit a single photon with double the energy (half the wavelength) of those entering the sample [76]. Theoretical analysis of the scattering process reveals that it breaks symmetry and so can only occur when polarisation of the scatterer is itself antisymmetric. This happens at surfaces and in very asymmetric molecules or fibres. The principal source of SHG in tissues is collagen fibres [76].

CARS is a four-wave mixing process in which Raman vibrations are excited coherently by multiple photons. The process requires two incident laser beams, tuned to resonance with a particular vibrational mode of the target molecule, as shown in the energy-level diagram for this process (fig. 2.4) [77].

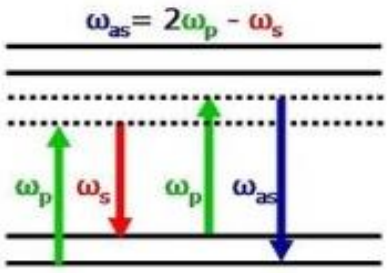

Figure 2.4. CARS levels. The two excitation beams (at ω_p and ω_s) form a beating field with angular frequency $\omega_p - \omega_s$. When $\omega_p - \omega_s$ matches a Raman frequency of the sample, the anti-Stokes signal at ω_{as} is enhanced. Adapted from [78].

The nonlinearity of the process means that the scattering intensity varies as the square of the number of bonds in the focal volume so it is particularly effective in visualising cell membranes when tuned to vibrational modes of the membrane phospholipids.

These modalities were implemented simultaneously using the purpose-made multimodal multiphoton microscope in the biophysical laboratory at Exeter (www.newton.ex.ac.uk/research/biomedical-old/multiphoton/).

SHG was generated in the forward direction, TPF in the epi-direction and CARS in both the forward and epi-directions. TPF and SHG were excited using a mode-locked femtosecond Ti:sapphire oscillator (Mira 900D; Coherent, USA) which resulted in the generation of 100-fs pulses at 76 MHz repetition rate and 800 nm wavelength. For CARS, the synchronised dual laser beams of differing wavelengths were provided by an optical parametric oscillator (Levante Emerald, APE, Berlin, Germany) pumped with a frequency-doubled Nd:vanadium picosecond oscillator (High-Q Laser Production GmbH). The signal beam was tuned to 924 nm and the idler beam to 1254 nm, stimulating phospholipid vibration at 2845 cm^{-1}.

2.3 Tracer Uptake Experiments

Two low molecular weight tracers differing in charge and lipid solubility, rhodamine B (molecular weight 479Da, 0.55nm hydrodynamics radius, $C_{28}H_{31}ClN_2O_3$, Sigma, UK) and fluorescein (molecular weight 332Da, 0.4nm hydrodynamic radius, $C_{20}H_{12}O_5$ Sigma, UK) were studied. Fluorophore distribution as a function of time was quantified using the confocal microscope.

These tracers were chosen because of their low molecular weights, so their rates of transport and transport pathways are likely to be similar to the nutrient and signal molecules important for the nutriton of the capsule and involved in its electrophysiology. The two tracers have different charges, rhodamine B is cationic

and fluorescein is anionic, allowing us to investigate the effects of charge on solute transport and distribution.

For these experiments the corpuscle was immersed in the microscopy chamber described above containing solutions of fluorescein (1mg /100ml) and rhodamine B (1mg /100ml) in 0.15M NaCl at room temperature for time periods varying from 5 minutes to 18 hours. Then the PC was briefly washed in 0.15M NaCl and transferred to another chamber containing 0.15M NaCl alone on the stage of the confocal microscope. Stacks of 60, 80 or 100 images with one micron interval between the images were obtained and saved in RAW format for image–processing using Image J software (www. imagej.nih.gov/ij/). Each Raw file was separately visualized in two sequences of images using the Image J plugin “Channel Separator”. Profiles of tracer distribution over selected regions were constructed and compared at different incubation period.

2.4 Osmotic Challenge Experiments

The response of PCs to changes in osmotic pressure in the surrounding medium provides information on the permeability to a particular osmolyte of the capsule and internal structure and, when swelling or shrinkage occurs, it provides insight into the mechanical properties of the restraining structure.

Four osmolytes were employed in these experiments. Sucrose, polyethylene glycol (mw 20,000) and bovine serum albumin (mw 67,000) (Sigma Chemicals, UK) were used to probe the permeability of the outer corpuscle and successive lamellae to neutral solutes of increasing size, and NaCl was used to probe permeability to ions which may be directly involved in the transduction process.

In each experiment the corpuscle was placed in a chamber on the stage of the transmission microscope and allowed to equilibrate with 0.15M saline solution (generally up to ½ hr), and then the solution was changed to the chosen solution (e.g. sucrose or saline in higher concentration). The time-course of structural change was determined from measurements made using Image J on still frames from a video recording. The principal measurements were: length of the corpuscle, maximum diameter and interlamellar spacing and width.

2.5 Mechanical Measurements

2.5.1 Measurement of Intracorpuscular Hydrostatic Pressure

A knowledge of intracorpuscular pressure and the ways in which it changes as static and dynamic loads are applied to the capsule are important to understand the structure of the PC and mechanisms of mechanotransduction. In the present study, the original intention was to measure hydrostatic pressure in PCs using a

servo-null pressure measurement system developed by Wierhieml [79] to measure pressure in the microcirculation. However, preliminary assessment suggested that it should be possible to make pipette pressure measurements without the servo feedback system in order to improve frequency response. It was therefore decided to construct a new system for direct pressure measurement.

The experimental system for combined pressure measurement and observation of lamella displacement comprised the standard microscopy chamber, open on one side (see 2.2.1) into which was inserted a sharpened glass micropipette connected directly to a sensitive pressure transducer and mounted on a micromanipulator (micrometer head 0-25 mm, 0.001 mm World Precision Instrument, the UK), the whole being positioned next to the stage of the microscope (fig. 2.5). In order to take measurements inside the PC, a micropipette with a sharp, fine tip was required to penetrate the capsule. The micropipette (boron glass, 2 mm o.d WPI) was pulled using an electrode puller (Harvard Apparatus Model) to a tip diameter of approximately 3.5 µm and ground to a tip angled at approximately 45° using a grinding wheel covered with 1000 grade abrasive paper. After cleaning in an ultrasonic cleaning bath (Sonic, Ultrawave, PH-5.5-6) it was then filled with 0.15 M NaCl solution and connected directly to a pressure transducer with internal amplifier (HDIM020GBZ8PS, Sensor Technics). A fresh PC was placed on the slide and positioned by aspirating it, under negative hydrostatic pressure, into a second, wider micropipette which had been soda-glass annealed to provide a non-penetrating tip. The corpuscle was centred under the microscope and the tip of the pressure probe micropipette was advanced into the PC.

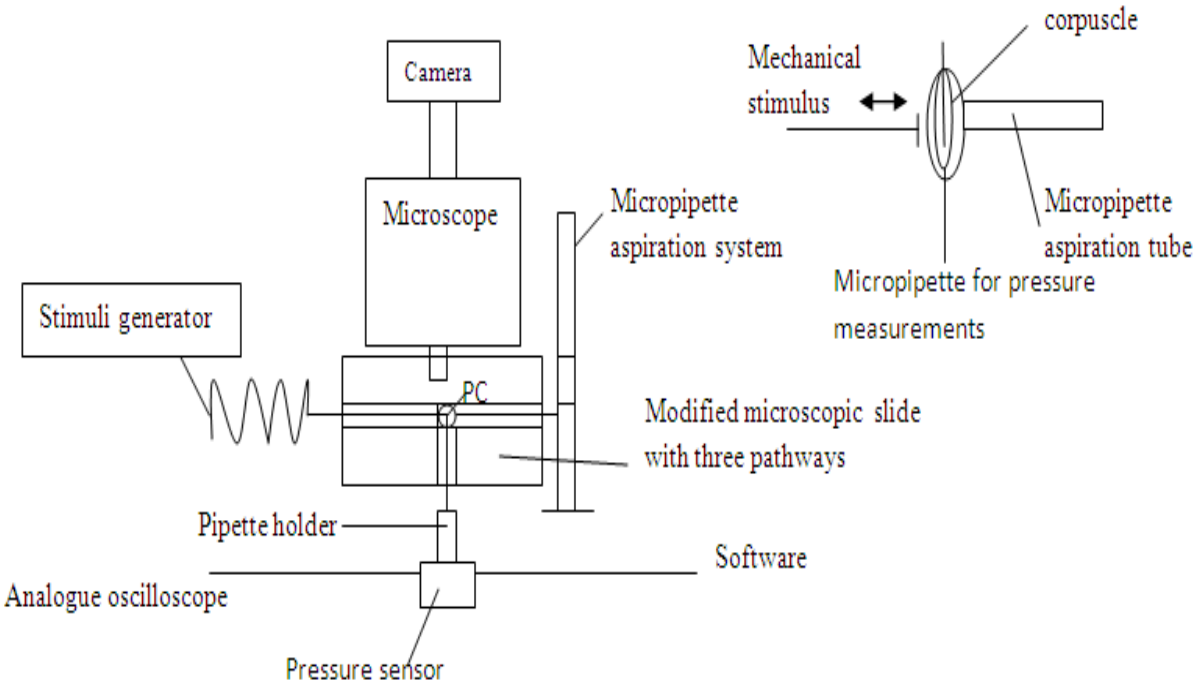

Figure 2.5. Schematic of the experimental set-up for measurement of intercellular pressure inside the PC. The PC is localised using one micropipette (right of figure), pressure is measured using a second micropipette (foot of figure) and there is provision for applying a mechanical stimulus (left of figure).

In pilot studies in advance of the present study (carried out in Exeter by Ian Summers and Natalie Garret) defrosted PCs from the *rat* foot were successfully penetrated without deflation and pressure measurements were obtained using the servo-null pressure transducer. However, despite numerous attempts it was impossible to replicate these measurements of intercapsular pressure in a fresh PC from the *horse* hoof. These *horse* PCs were much more difficult to penetrate and when this was achieved the lamellar structure was so badly disrupted that the

results were considered unreliable and the study was not pursued due to lack of time – no results are presented in this thesis. These observations are consistent with reports in the literature that the capsule is “deflated” once punctured [33], [42], but it remains to be established whether the previous success arose because the capsule was already deflated by the freeze-thaw procedure or because the *rat* PC has different mechanical properties.

2.5.2 Micropipette Aspiration

Micropipette aspiration is a well-established method of measuring the mechanical properties of cell membranes [79]. An aim of this project was to investigate the feasibility of scaling up this approach to investigate the local mechanical properties of the outer capsule of the PC and the mechanical coupling between lamellae.

The apparatus shown in figure 2.6 was constructed consisting of a hydrostatic pressure reservoir on a calibrated support connected via a 3-way tap to a glass micropipette. The pipette, prepared as described in section 2.5.I, but with a flat, smooth tip 20-150μm in diameter finished by soda glass annealing, was filled with 0.15M NaCl and mounted on a micromanipulator. A fresh PC from *horse* hoof was placed in an observation chamber on the microscope stage and the pipette was then positioned on its surface. The pressure reservoir was then lowered in order first to trap the PC and then to draw a tongue of the PC capsule into the tip of the

pipette, on which the microscope was focussed, using a 60X water immersion objective.

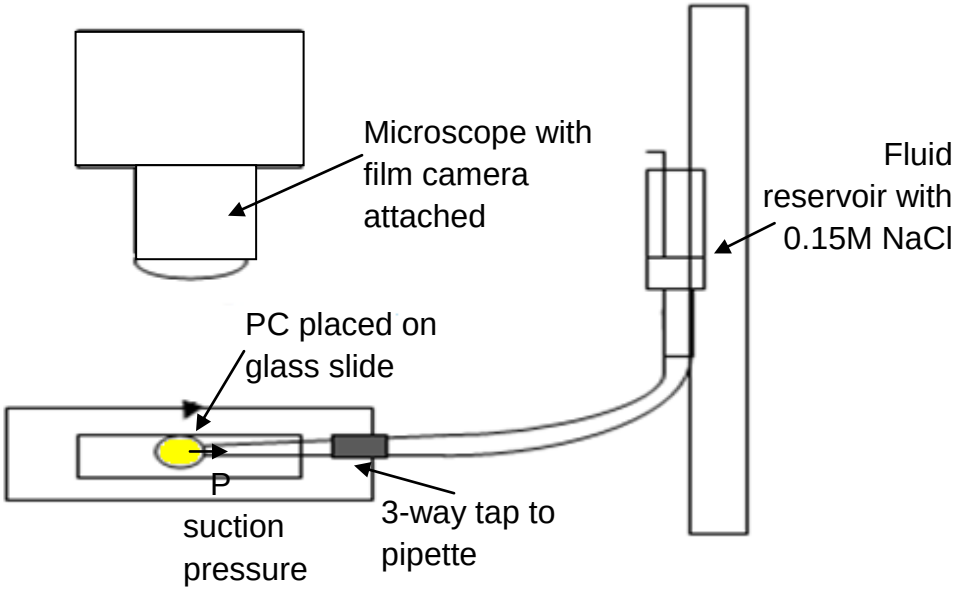

Figure 2.6. Micropipette aspiration system consisting of a hydrostatic pressure reservoir on a calibrated support connected via a 3-way tap to a glass micropipette.

2.5.3 Lamella displacement under static and dynamic compression of the corpuscle

The behaviour of lamellae under dynamic and static compression of the corpuscle was investigated by two approaches. Experimental measurements on corpuscles were complemented by the construction of an electrical analogue of the theoretical model of mechanotransduction proposed by Loewenstein and Skalak [36], outlined in chapter 1.

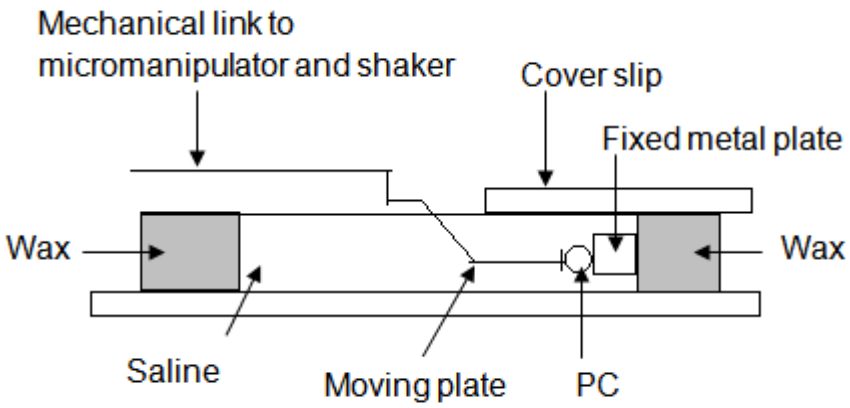

Figure 2.7. The experimental set-up for experiments involving static or dynamic compression. The corpuscle (PC) sits in saline solution between two metal plates.

The experimental set-up is based around a microscope slide observation chamber, as shown in figure 2.7. The corpuscle immersed in 0.15M NaCl in saline solution is positioned between two metal plates, one fixed and the other moving under the control of a micromanipulator and a mechanical stimulator. The direction of movement (left to right or right to left in fig. 2.7) is such that a compressive load can be applied to the corpuscle. The micromanipulator determines the baseline position of the moving plate, upon which a sinusoidal displacement from the shaker can be superimposed with a peak-to–peak amplitude of approximately 20 microns. Transmitted light microscopy is used to image a central plane of the corpuscle. For experiments involving static compression, the stimulator is not used and the compression is determined purely by the micromanipulator: images are acquired at

different positions of the moving plate, corresponding to different amount of compression. In order to determine local properties in some experiments the mechanical distortion of the corpuscle was achieved using a pointed probe 10-20 μm in diameter rather than the flat plate.

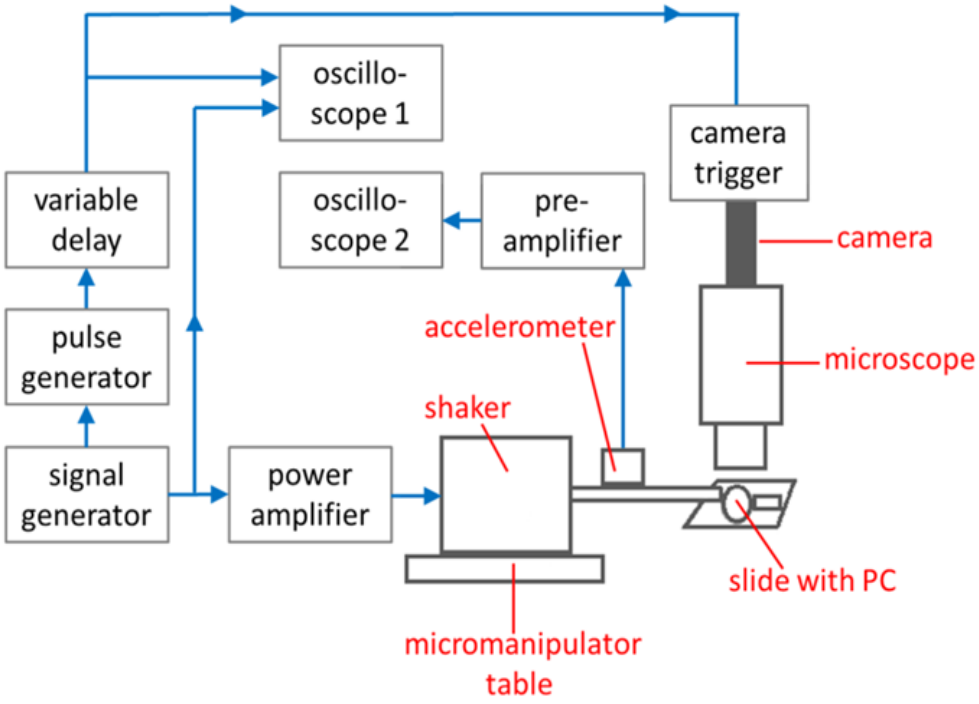

Figure 2.8.Schematic overview of the apparatus: signal paths are indicated by the blue arrows.

Figure 2.8 shows an overview of the complete apparatus. This set-up was developed over a period of many months, originally with the intention of simultaneously measuring pressure variations within the corpuscle in response to sinusoidal mechanical stimulation. In the event, the micropipette technique for

intra-capsular pressure measurement proved impossible to implement reliably. However, visualisation of the lamellae proved easier than expected and so the experimental focus was changed to a study of lamellar displacement in response to sinusoidal mechanical stimulation. The signal paths in figure 2.8 are indicated by blue arrows. The signal generator provides a sine wave which drives the stimulator (Bruel and Kjaer type 4810) via a power amplifier. The vibratory motion of the shaker, corresponding to the mechanical stimulation applied to the corpuscle, is measured by an accelerometer (Knowles type BU1771) whose output signal, after passing through a preamplifier, is displayed on Oscilloscope 2. Observation of this signal on the oscilloscope allows the amplitude of the vibration to be set as required, and provides a check that the displacement waveform in the steady state is indeed sinusoidal. (Harmonic distortion is observed if the drive voltage to the shaker is too high or if the movement of the mechanical system is not completely free.) The signal generator also triggers a pulse generator, producing a short rectangular pulse once per cycle of the mechanical stimulation. A variable time delay is given to this pulse before it is applied to the trigger circuitry of the microscope camera. The camera thus takes one image per cycle of the mechanical stimulation, at a phase in the sine wave cycle that is determined by the time delay which has been applied to the trigger pulse. This is effectively a stroboscopic imaging technique. Oscilloscope 1 is used to simultaneously display the sine wave from the signal generator and the trigger pulse sent to the camera; this allows adjustment of the time delay to correspond to a specified phase within the sinusoidal mechanical stimulation.

When investigating response to sinusoidal mechanical stimulation, the camera (QImaging type Retiga 2000R) was set to an acquisition time of 0.12ms. This was short enough to “freeze” sinusoidal motion at frequencies up to approximately 500 Hz. Images were acquired at phase steps of 36°, i.e., ten per cycle, at frequencies of 50, 100, 200 and 400 Hz. (See fig. 2.9 for examples; each complete data set consists of 21 images covering two compete cycles). By observing the accelerometer signal on Oscilloscope 2 (see fig. 2.8), the displacement amplitude of the moving plate was set to a nominal value of 20μm peak to peak (subsequently determined more accurately from measurements on the acquired images); at 400 Hz the available displacement amplitude was limited to around 8μm peak to peak because of the need to avoid overheating the shaker with high drive currents.

The layered structure of the corpuscle provides visible landmarks (see fig. 2.10) whose position along a suitable chosen line can be tracked over a set of images at different phases in the cycle of mechanical stimulation (see fig. 2.11). The sinusoidally varying position of these visible landmarks provides amplitude and phase information for the tissue displacement, as a function of position (depth) within the corpuscle.

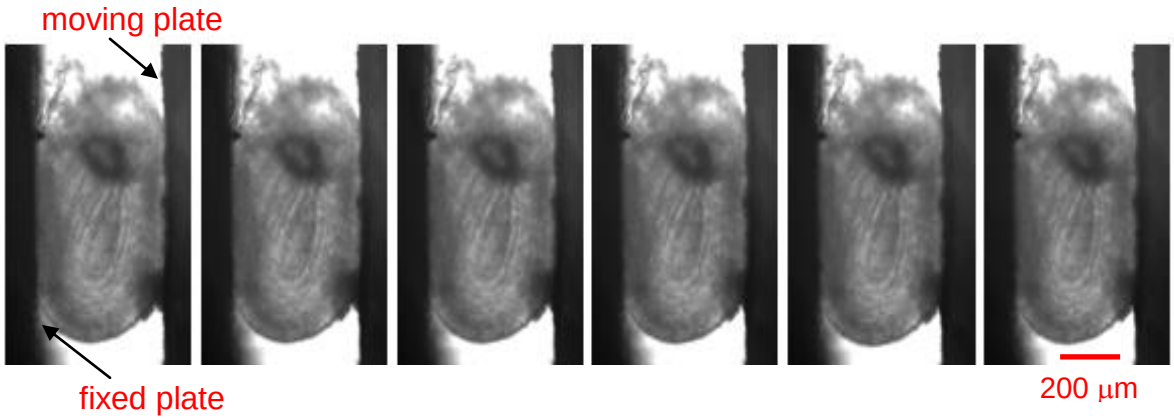

Figure 2.9. A sequence of images (FOV 600 μm × 900 μm) covering one half cycle of 100 Hz stimulation in phase steps of 36° (time difference 1 ms, exposure time 120 μs). The moving plate (black band on the right of each image) is seen to move inwards. PC from heel area of hind hoof of 8-year-old *mixed-breed horse*.

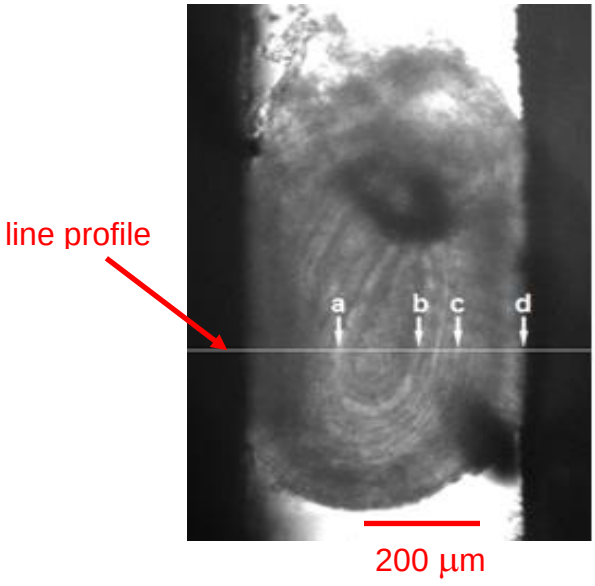

Figure 2.10. A corpuscle positioned between (left) the fixed metal plate, and (right) the moving metal plate (FOV 600 μm × 900 μm). The features a and b mark the boundary between inner and outer regions of the corpuscle; c is a lamellar feature in the outer region and d is the surface of the corpuscle. The position of such features can be determined from a profile along a line such as the one shown.

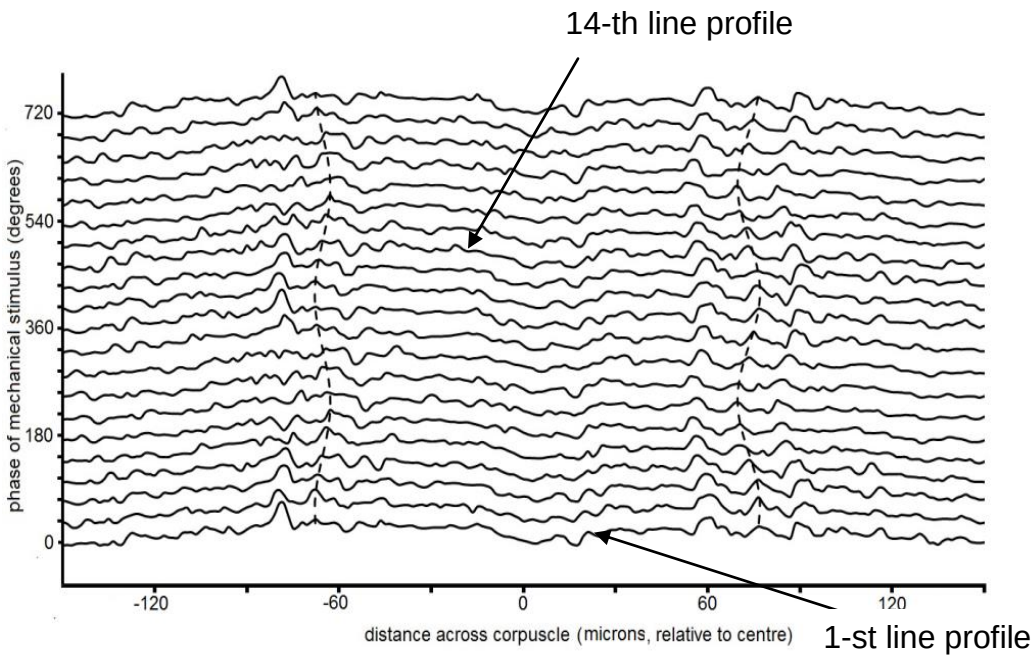

Figure 2.11. Line profiles (see fig. 2.9) across the corpuscle, for 21 phase steps over two cycles of stimulation at 100 Hz. Dotted lines are fits to 2 selected features. (Note position is measured relative to the corpuscle centre, so left and right move in antiphase.)

2.6 Electrical Analogue of Pacinian Corpuscle

The theoretical model of Loewenstein and Skalak [36] has been outlined in Chapter 1. As described in section 1.3, Loewenstein and Skalak also proposed an electrical analogue of their mechanical model, as a network of capacitors and resistors (figs. 1.24 and 2.12) whose values correspond to the compliances and resistances of the mechanical model (fig. 1.23).

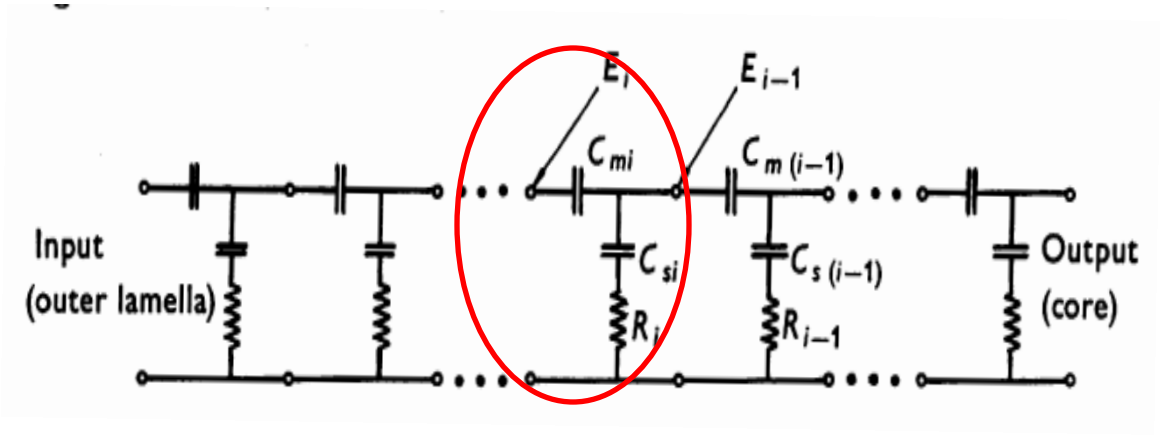

Figure 2.12. The model of the PC represented by an electrical analogue in which all components of the mechanical model are converted into electrical equivalents. The red circle indicates a single network, corresponding to a lamella with the associated interlamellar fluid. Adapted from [36].

Each lamella in the 30-lamella structure of the mechanical model is represented by a network of the type circled in figure 2.12 with 30 similar networks connected in series to form an analogue of the entire corpuscle. Pressure in the mechanical model is represented by voltage in the electrical analogue. As shown in figure 2.12, the pressure applied to the i-th lamella is represented by the voltage E_i and the pressure applied to the (i −1)th lamella is represented by the voltage E_{i-1}. These voltages are determined by equations (13) and (14).

$$E_{i-1} = \frac{Q_{si}}{C_{si}} + R_i \dot{Q}_{si} \qquad (13)$$

$$E_i - E_{i-1} = \frac{Q_{mi}}{C_{mi}} \qquad (14)$$

where Q_{mi} and Q_{si} are the charges on capacitors C_{mi} and C_{si}, respectively. Charges are also related by

$$Q_{mi} - Q_{m(i-1)} = Q_{si} \tag{15}$$

Substituting (15) into (13) gives

$$E_{i-1} = \frac{Q_{mi}}{C_{si}} - \frac{Q_{m(i-1)}}{C_{si}} + R_i\dot{Q}_{mi} - R_i\dot{Q}_{m(i-1)} \tag{16}$$

Now substituting (16) into (14) leads to

$$\frac{Q_{mi}}{C_{mi}} = \frac{1}{C_{s(i+1)}}(Q_{m(i+1)} - Q_{mi}) - \frac{1}{C_{si}}(Q_{mi} - Q_{m(i-1)}) + R_{i+1}(\dot{Q}_{m(i+1)} - \dot{Q}_{mi}) - R_i(\dot{Q}_{mi} - \dot{Q}_{m(i-1)}) \tag{17}$$

which has a direct correspondence to equation (12), derived in section 1.3 for the mechanical model:

$$\frac{B_i}{K_i} = R_{i+1}(\dot{B}_{i+1} - \dot{B}_i) + \frac{B_{i+1} - B_i}{h_{i+1}}\alpha E - R_i(\dot{B}_i - \dot{B}_{i-1}) - \frac{B_i - B_{i-1}}{h_i}\alpha E \tag{12}$$

From comparison of equations (12) and (17), we see that displacement amplitude B_i is represented by charge Q_i, compliance K_i is represented by capacitance C_{mi}, compliance $h/\alpha E$ is represented by capacitance C_{si} and mechanical (viscous) resistance R_i is represented by electrical resistance R_i.

The electrical analogue models the transmission of pressure (voltage) and displacement (charge) through the set of 30 lamellae (networks) from surface to core, and forms the basis of the comparison with experimental data in Chapter 5.

Loewenstein and Skalak suggested appropriate values for the compliances and resistances in their electrical model (see fig. 2.13), from which component values for the electrical analogue may easily be derived. In the practical implementation of the electrical analogue, values for the capacitance C_m, which represents the lamella compliance, are in the range 4.4 to 0.047 μF; values for the capacitance C_s, which represents the compliance of radial elements, are in the range 330 to 12,000 pF; values for the resistance R, which represents viscous resistance, are in the range 2000 to 5.6 kΩ. (Note: these values give an electrical analogue which operates 100 times faster than the mechanical model, i.e., the behaviour of the electrical analogue at 5 kHz corresponds to the behaviour of the mechanical model at 50 Hz; experimental measurements on the electrical analogue are quoted at a frequency 100 times less than that actually used; resistor and capacitor values were rounded to the nearest preferred value.) Figure 2.14 shows the practical implementation of the electrical analogue. Measurements were made at a range of frequencies by applying a voltage sine wave to the input terminals and measuring (a) the variation in voltage through the series of 30 networks, representing the change in pressure from the surface of the corpuscle to the core, and (b) the variation of charge (capacitance×voltage) on the capacitor C_m, representing the variation of displacement through the set of lamellae.

Table I

Lamella no.	Radius (μ)	Lamella compliance* K_l(cm³/dyn)	Radial springs' compliance, $h_l/\alpha E$* (cm³/dyn)	Viscous resistance,* R_l(dyn sec/cm³)
Core	20·0	—	—	—
1	21·7	$1{\cdot}69\times10^{-3}$	$1{\cdot}32\times10^{-7}$	$4{\cdot}88\times10^{5}$
2	23·5	$1{\cdot}44\times10^{-3}$	$1{\cdot}59\times10^{-7}$	$3{\cdot}24\times10^{5}$
3	25·4	$1{\cdot}23\times10^{-3}$	$1{\cdot}89\times10^{-7}$	$2{\cdot}27\times10^{5}$
4	27·5	$1{\cdot}05\times10^{-3}$	$2{\cdot}22\times10^{-7}$	$1{\cdot}66\times10^{5}$
5	29·8	$8{\cdot}96\times10^{-4}$	$2{\cdot}57\times10^{-7}$	$1{\cdot}25\times10^{5}$
6	32·3	$7{\cdot}65\times10^{-4}$	$2{\cdot}95\times10^{-7}$	$9{\cdot}72\times10^{4}$
7	34·9	$6{\cdot}54\times10^{-4}$	$3{\cdot}36\times10^{-7}$	$7{\cdot}70\times10^{4}$
8	37·8	$5{\cdot}58\times10^{-4}$	$3{\cdot}80\times10^{-7}$	$6{\cdot}21\times10^{4}$
9	41·0	$4{\cdot}77\times10^{-4}$	$4{\cdot}28\times10^{-7}$	$5{\cdot}09\times10^{4}$
10	44·4	$4{\cdot}08\times10^{-4}$	$4{\cdot}80\times10^{-7}$	$4{\cdot}22\times10^{4}$
11	48·1	$3{\cdot}49\times10^{-4}$	$5{\cdot}37\times10^{-7}$	$3{\cdot}54\times10^{4}$
12	52·1	$2{\cdot}99\times10^{-4}$	$5{\cdot}98\times10^{-7}$	$3{\cdot}00\times10^{4}$
13	56·4	$2{\cdot}56\times10^{-4}$	$6{\cdot}64\times10^{-7}$	$2{\cdot}56\times10^{4}$
14	61·1	$2{\cdot}19\times10^{-4}$	$7{\cdot}36\times10^{-7}$	$2{\cdot}20\times10^{4}$
15	66·1	$1{\cdot}88\times10^{-4}$	$8{\cdot}14\times10^{-7}$	$1{\cdot}91\times10^{4}$
16	71·6	$1{\cdot}62\times10^{-4}$	$8{\cdot}98\times10^{-7}$	$1{\cdot}66\times10^{4}$
17	77·6	$1{\cdot}39\times10^{-4}$	$9{\cdot}89\times10^{-7}$	$1{\cdot}45\times10^{4}$
18	84·0	$1{\cdot}20\times10^{-4}$	$1{\cdot}09\times10^{-6}$	$1{\cdot}27\times10^{4}$
19	91·0	$1{\cdot}03\times10^{-4}$	$1{\cdot}19\times10^{-6}$	$1{\cdot}12\times10^{4}$
20	98·5	$8{\cdot}94\times10^{-5}$	$1{\cdot}31\times10^{-6}$	$9{\cdot}87\times10^{3}$
21	108·4	$7{\cdot}53\times10^{-5}$	$1{\cdot}77\times10^{-6}$	$4{\cdot}79\times10^{3}$
22	119·2	$6{\cdot}37\times10^{-5}$	$1{\cdot}97\times10^{-6}$	$4{\cdot}18\times10^{3}$
23	131·2	$5{\cdot}41\times10^{-5}$	$2{\cdot}18\times10^{-6}$	$3{\cdot}64\times10^{3}$
24	144·3	$4{\cdot}62\times10^{-5}$	$2{\cdot}42\times10^{-6}$	$3{\cdot}18\times10^{3}$
25	158·7	$3{\cdot}98\times10^{-5}$	$2{\cdot}68\times10^{-6}$	$2{\cdot}77\times10^{3}$
26	174·6	$3{\cdot}44\times10^{-5}$	$2{\cdot}97\times10^{-6}$	$2{\cdot}41\times10^{3}$
27	192·0	$3{\cdot}01\times10^{-5}$	$3{\cdot}29\times10^{-6}$	$2{\cdot}09\times10^{3}$
28	211·2	$2{\cdot}65\times10^{-5}$	$3{\cdot}64\times10^{-6}$	$1{\cdot}81\times10^{3}$
29	232·3	$2{\cdot}36\times10^{-5}$	$4{\cdot}02\times10^{-6}$	$1{\cdot}56\times10^{3}$
30	255·6	$2{\cdot}13\times10^{-5}$	$4{\cdot}45\times10^{-6}$	$1{\cdot}34\times10^{3}$

Table II

Mechanical quantity	Electrical quantity
Pressure, p, dyn/cm²	Voltage, E, volts
Displacement, w, cm	Charge, Q, coulombs
Velocity, $\dot{w}$, cm/sec	Current, I, amperes
Mass, M, g	Inductance, L, henries
Viscous resistance, R, dyn sec/cm³	Resistance, R, ohms
Compliance, K, cm³/dyn	Capacitance, C_m, farads
Compliance, $h/\alpha E$, cm³/dyn	Capacitance, C_s, farads

Figure 2.13. Table 1 summarises the mechanical components of the Loewenstein and Skalak model. The viscosity of the fluid is assumed to be that of water and the solid mechanical properties are assumed to be similar to those of the arterial wall. Table II summarizes the relationships between mechanical and electrical parameters. (Because the mechanical model neglects inertial effects the electric analogue in fact contains no inductances.) Adapted from [36].

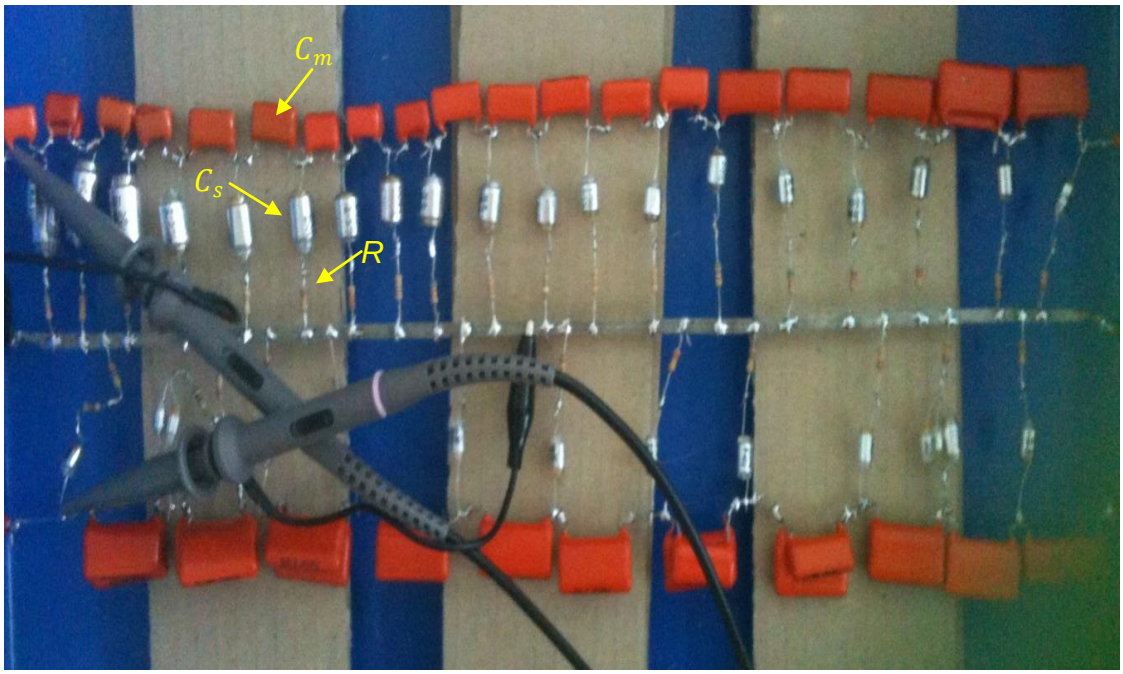

Figure 2.14. Practical implementation of the electrical analogue, with oscilloscope probes connected. The input terminals are at the top left of the picture; the signal travels left to right through the first 19 networks C_s (top half of picture) and then right to left through the next 11 networks (bottom half of picture). Each network consists of two capacitors (C_m with a range of 4.4 to 0.047 μF, with arrange of 330 to 12,000 pF), and a resistor (R with a range 2000 to 5.6 kΩ).

Voltage measurements were made using a two-channel digital oscilloscope with high-impedance probes; on-screen cursors were used to measure signal amplitudes; differential measurements of voltage were required to establish the C_m charge.

Chapter 3

Investigations of the distribution and structure of PCs

This chapter describes investigations of PCs of the horse hoof. Section 3.1 first describes the anatomy of the *horse* hoof, the distribution of PCs and aspects of the structure of the surrounding tissue that may be important in mechanotransduction. Section 3.2 reports on the structure of the corpuscle and variations in the structure of PCs obtained from *horses* of different breeds and ages, and compare these observations with those reported in the literature. Section 3.3 describes in more detail the structure of the corpuscle as revealed by histological staining and confocal microscopy. Section 3.4 describes the first application of nonlinear microscopy to reveal the structure of the fresh, unstained corpuscles.

3.1 Gross Anatomy

3.1.1 The Structure and Mechanics of the *Horse* Hoof

The distribution of PCs in the *horse* hoof is highly localised and needs to be considered in relation to the biomechanics of the hoof whose expansion and recovery under transient loading is central to the processes of locomotion and shock absorption.

The hoof consists of a relatively rubbery sole with an extremely hard wall made out of keratinized structures surrounding the toe (fig. 3.1 and 3.2). There are no muscles in the hoof, only bones, ligaments and tendons together with the requisite vascular network and the nervous system involved principally with mechanotransduction. The skeletal structure consists of three bones. The short pastern bone is located between the long pastern bone in the leg and the coffin bone, which is the largest bone and determines the shape of the hoof and affords protection to the vascular and nervous systems. There is a thin bone called the navicular bone located behind the coffin bone. The digital flexor tendon is attached to the coffin bone and goes across the navicular bone, which acts as a fulcrum for the tendon [24].

Figure 3.1. (a) relation between navicular bone (shown in green) and digital flexor (shown in purple); (b) a digital cushion located above the frog area and the lateral cartilages, the cushion acts as a shock absorber; (c) relative position of the digital cushion (red area) and the lateral cartilages (green areas) which are incorporated in the shock absorption mechanism. Adapted from [24].

The bones (coffin and navicular) are surrounded by a sensitive lamina, which provide pathways for nerves and blood vessels penetrating through the whole hoof. There is an elastic, fatty digital cushion located right under the lamina (fig. 3.1 b). The main function of the cushion is to absorb shock, which a horse receives from contact with the ground (fig. 3.1 c).

The digital cushion, with the extensive microcirculation it contains, also acts as a pump to drive venous blood back up the leg (fig .3.2).

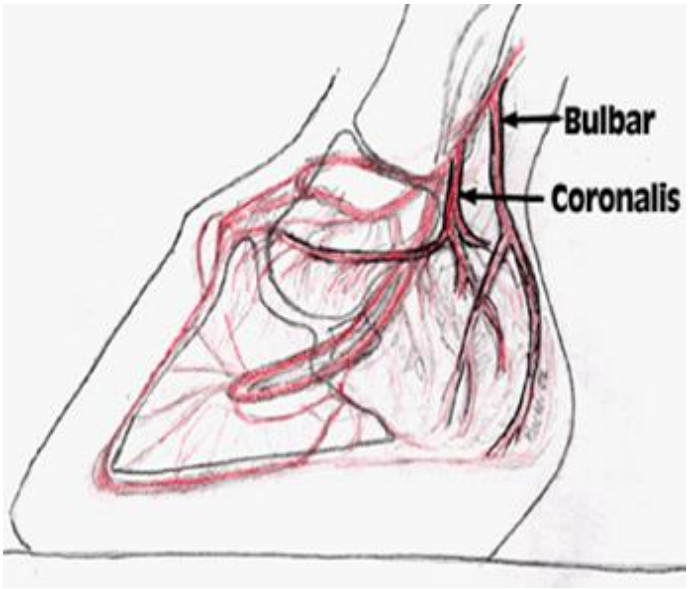

Figure 3.2. Diagram of the blood circulation in the hoof. Taken from [24].

3.1.2 Distribution of Pacinian Corpuscles in the *Horse* Hoof

Up to 60% of the *horse* body weight, including head and neck, is carried by the front limbs and more forces are applied to the front feet during movement than to the hind feet. The front feet mainly act as a shock absorber and give direction of movement while the hind feet push the *horse* forward. The differentiation between the biomechanics and function of the front and hind feet is reflected by the shape of the hoof capsule [80] and by localization and quantity of mechanoreceptors as observed in the present study (fig. 3.3).

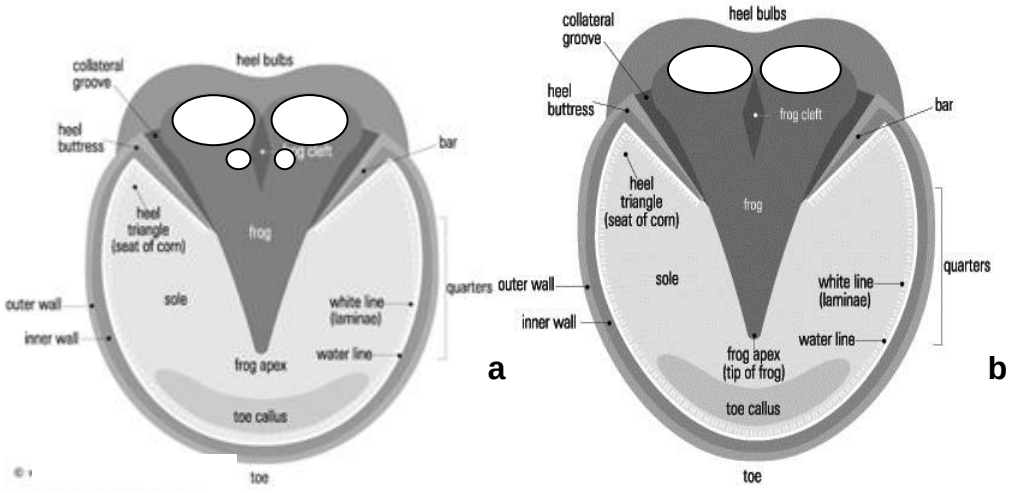

Figure 3.3. The front hoof (a) is wider and the hind foot hoof (b) is more pointed. He white area (4 in the front hoof and 2 in the hind) shows where PCs were identified in the present study. Adapted from [80].

The observation of histological sections revealed PCs generally close to blood vessels and hair follicles. They generally occur in clusters, and the axons which serve a group of PCs run in the same direction as blood vessels within the loose connective tissue and adipose fat (fig. 3.4).

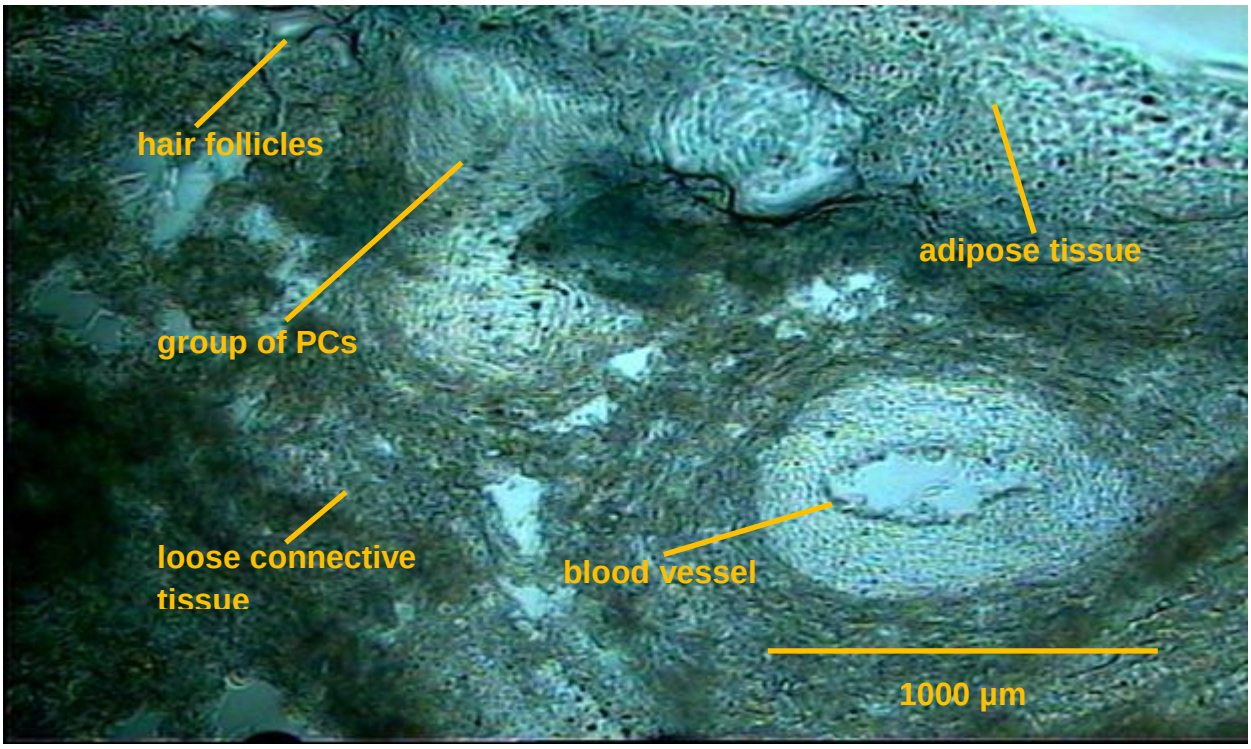

Figure 3.4. Histological section of tissue (stained with Evans Blue) from the digital cushion showing the typical location of a group of PCs between hair follicles and blood vessels, surrounded by adipose and loose connective tissue.

The corpuscles were generally quite uniform in size and shape in the smaller clusters (around clefts), but the larger groups (around blood vessels in heel bulbs) usually contained corpuscles differing in size and shape (fig. 3.5, fig. 3.6, fig. 3.7, and fig, 3.8). The size varied from 0.6 up to 2.5mm in length and 0.2 up to 1mm in

maximum diameter. The study was too small to investigate variation with size, age or breed of *horse*, but it is noticeable that the largest corpuscles, reaching up to 4 mm in length and 2 mm in diameter, were found in two *Shire horses*. The mean sizes of PCs observed in the heel area (*n* = 360) are 1.0 ± 0.6 mm (diameter) and 2.0 ± 0.8 mm (length). The mean sizes of PCs observed in the cleft area (*n* = 36) are 0.6 ± 0.4 mm (diameter) and 1.8 ± 0.4 mm (length).

The most commonly observed overall shape was ellipsoidal but some were round or conical (fig. 3.9). For example, in a large group of 13 PCs, ten corpuscles were ellipsoidal and two had conical shape. The large groups of PCs from the bulbar area were surrounded by a thin layer of fatty and connective tissue, which was difficult to remove. Individual PCs or small groups of PCs were also surrounded by a layer of loose connective and adipose tissue. Interestingly the layer that surrounds the corpuscle appeared as a sack of whitish colour but transparent enough to identify the onion-like structures of the corpuscle. Sometimes, there are conical-shaped PCs standing out from the group, each of them covered separately by a thin layer. This layer becomes visible during micro dissection only after surrounding tissue has been removed.

Results from dissection of hooves from 17 *horses* (age range 1 – 18 years, breeds ranging from *Dartmoor pony* to *Shire horse*) are summarised in fig. 3.10. Roughly twice as many PCs were observed in the front hoof than in the hind hoof.

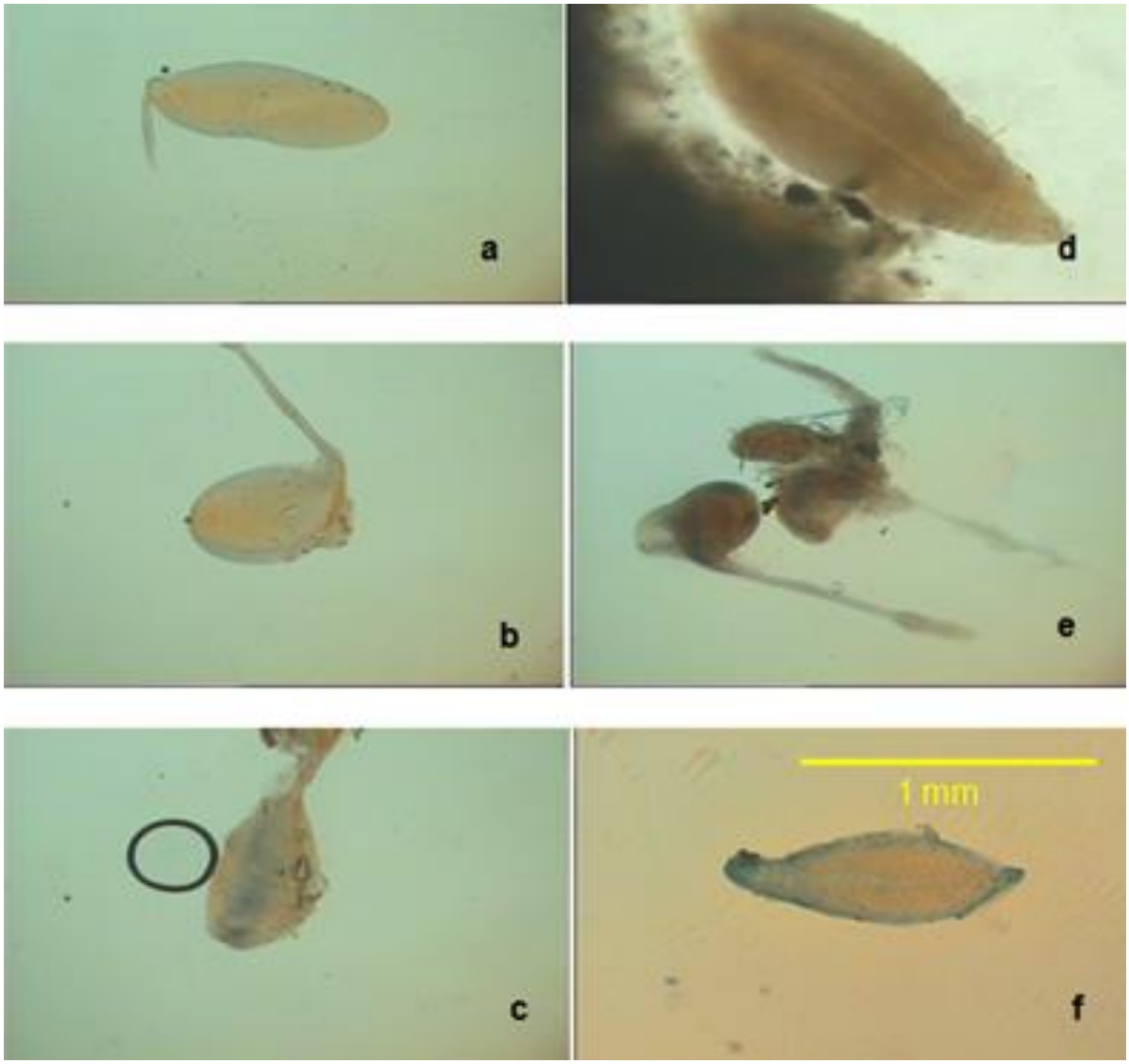

Figure 3.5. Different PCs from the same *horse*, with significant differences in size and shape: (a) & (c) ellipsoidal, (d) & (f) conical, (b) & (e) oval.

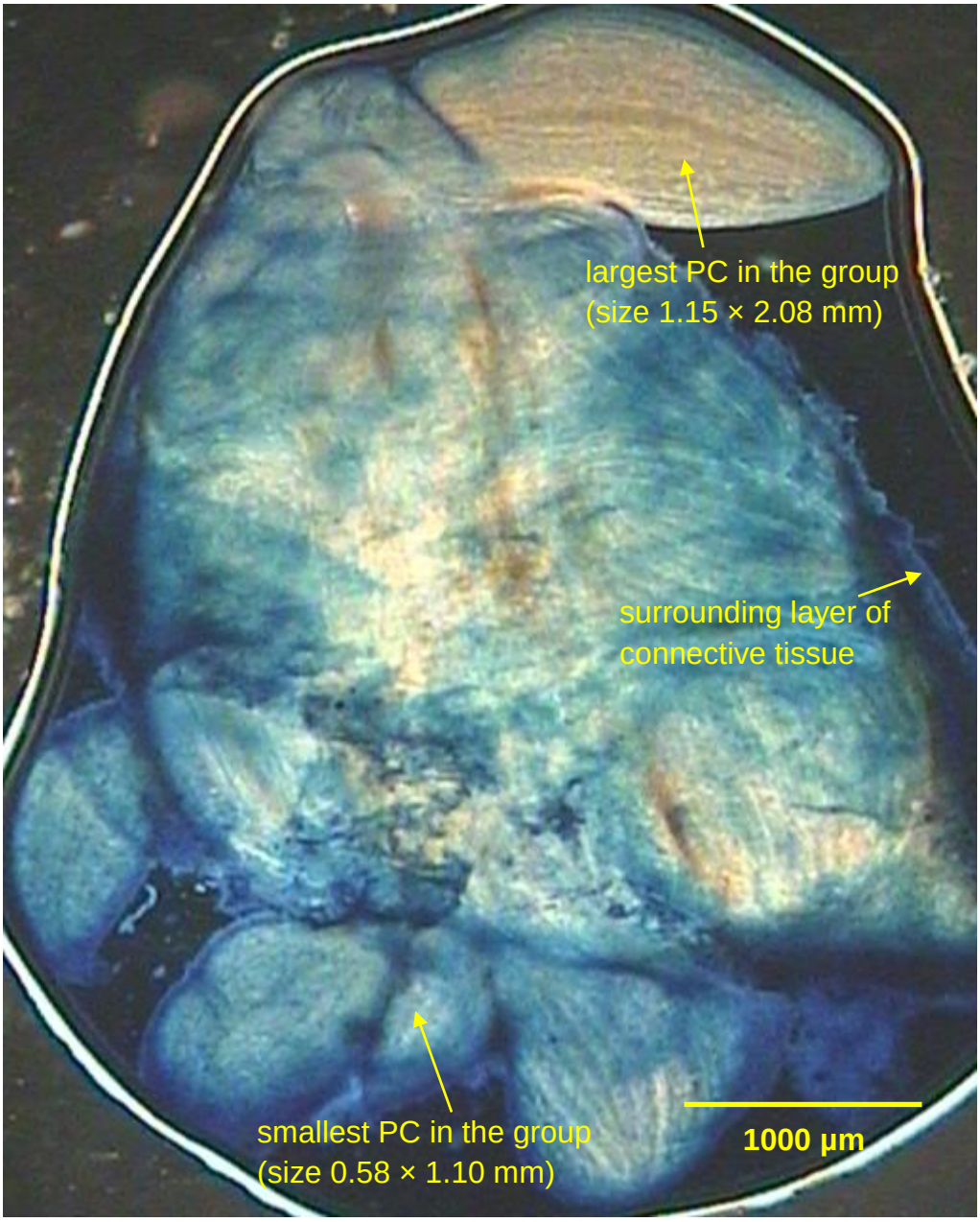

Figure 3.6. A large group of 13 PCs, found close to the bulbar artery in the bulb area of the digital cushion of the front hoof of a 15-year-old *mixed-breed horse* (sample was stained with Evans Blue). The mean sizes of PCs from three horses of this age/type are 0.87 ± 0.29 mm (diameter) and 1.59 ± 0.49 mm (length).

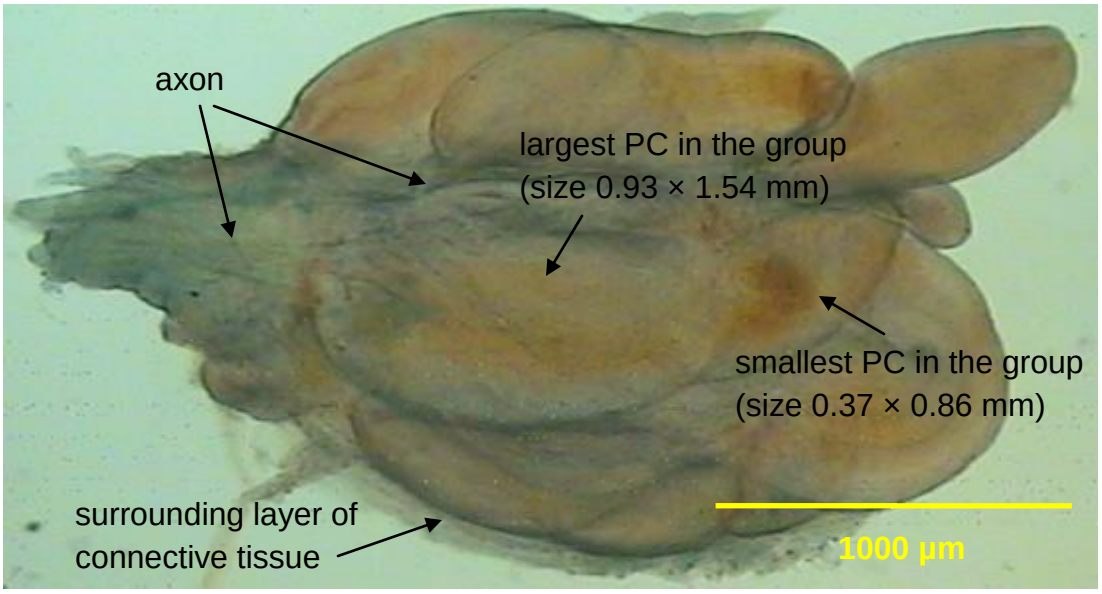

Figure 3.7. A large group of 12 PCs dissected from the front hoof (heel area) of a 3-year-old *racehorse*. The mean sizes of PCs from two *horses* of this age/type are 0.65 ± 0.28 mm (diameter) and 1.20 ± 0.34 mm (length).

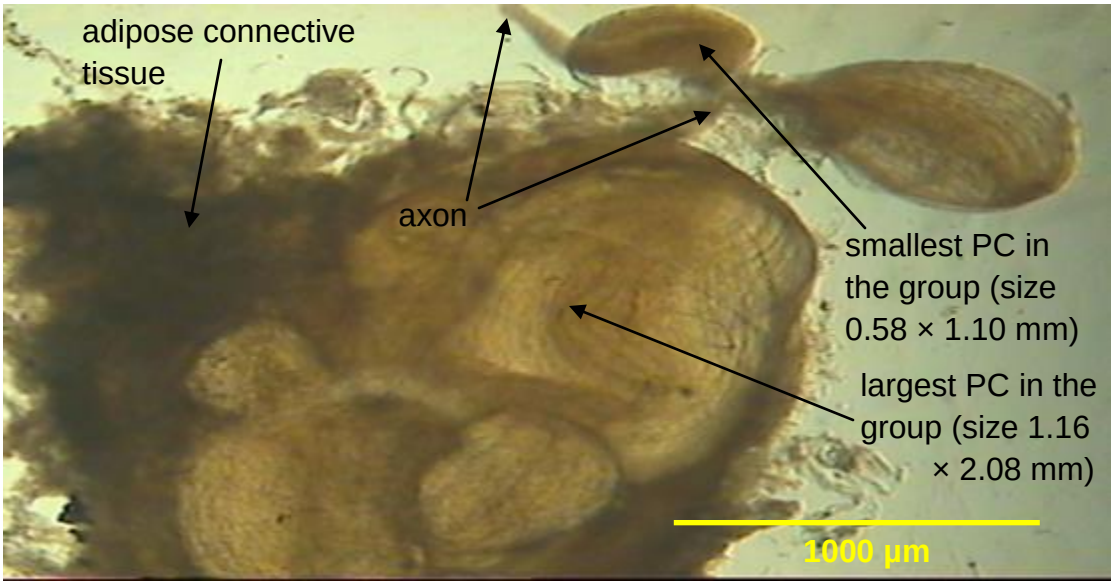

Figure 3.8. A large group of 7 PCs from a 15-year-old *mixed-breed horse*. This group of corpuscles was found next to the bulbar artery in the bulb of the heel area of the front foot. The mean sizes of PCs from three *horses* of this age/type are 0.87 ± 0.29 mm (diameter) and 1.59 ± 0.49 mm (length).

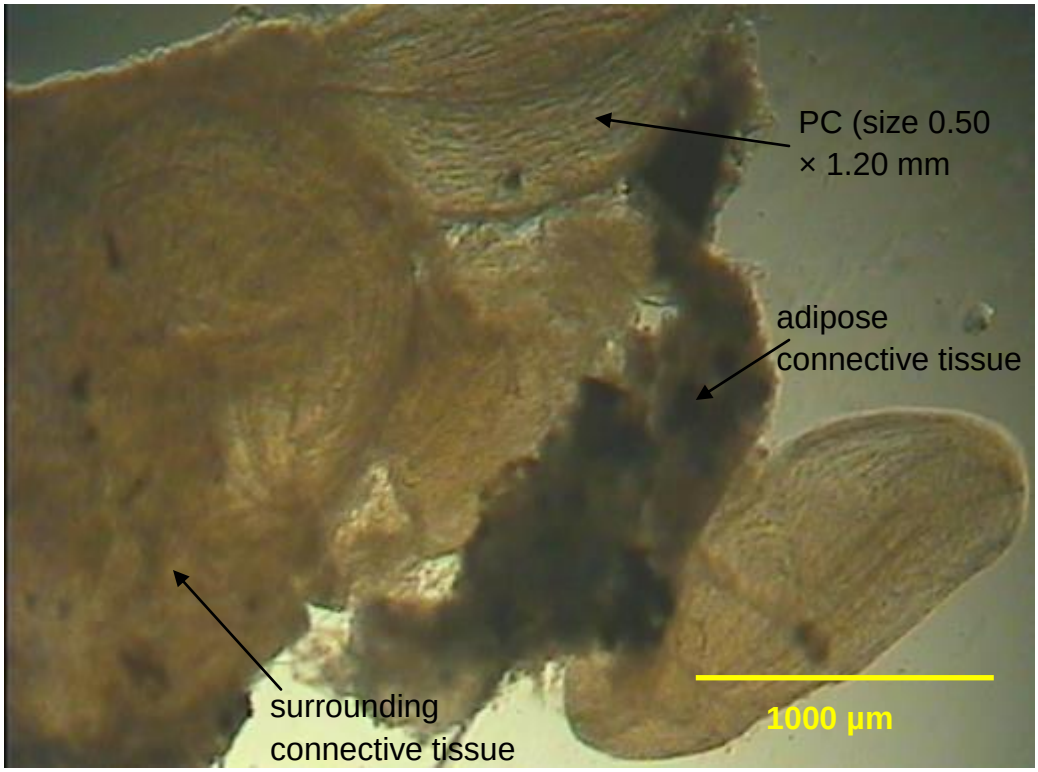

Figure 3.9. A group of 6 PCs found in a 1.5-year-old *racehorse*, next to the bulbar artery in the bulb of the heel area of the hind foot. The mean sizes of PCs from two *horses* of this age/type are 0.50 ± 0.26 mm (diameter) and 1.20 ± 0.50 mm (length).

Region	Typical number of PC clusters found per horse	Mean number of PCs in a cluster
front foot (heel)	1 or 2	9.6 (range 4−13)
front foot (cleft)	0 or 1	3.0 (range 2−4)
hind foot (heel)	1 or 2	5.6 (range 3−8)
hind foot (cleft)	always 0	−−

Figure 3.10. Table of observed PC distribution in *horses*' front and hind feet.

The frog is probably the principal site for the reception of the tactile stimuli for locomotion and this is the primary function of the PCs in this area, however, their

intimate association with the vasculature adds support to suggestions in the literature that some at least may have an additional role in monitoring haemodynamic conditions: in the *horse* hoof these two functions may be intimately connected.

Although the study group was too small for detailed analysis, differences were observed between PCs from the various horses, which may correlate with differences in the structure and biomechanics of the hoof in different breeds. It is clearly important that impact loads when the hoof hits the ground are distributed rapidly in order to prevent damage to bones and connective tissue. The efficiency of this mechanism in specific animals depends upon the conformation of the cartilages and the structural composition of the digital cushion. A study of the characteristics of the hoof in different breeds [71] found that structural organization was influenced by a genetic predisposition and an adaptation to various external stimuli (age, weight of horse, environment, etc.). Some breeds show a distinct cartilage and fatty cushion (a structure which can transfer impact forces to the level of the navicular bone) whilst others have a more uniform fibrocartilaginous fatty cushion. In mixed-breed or Arabian *horses*, fibrocartilaginous digital cushions are common, and fibrocartilaginous digital cushions predominate in the forelimbs of most types of horses. The venous complex incorporated into the fibrocartilaginous digital cushion encourages movement of venous blood as the hoof periodically contacts the ground [81].

As summarised in fig. 3.10, the experimental data from the present study indicate that PCs in front feet are distributed within the heel around the arteries with a small group of PCs located beside the cleft. As noted above, the front foot contains a fibrocartilaginous digital cushion [81], and PCs in the heel and cleft (both within this cushion) may be involved in monitoring or regulating both the shock absorption and blood pumping mechanisms. PCs in the heel area of the hind foot may be involved in monitoring impact forces on the navicular bone as an aid to locomotion.

3.2 Microscopic Structures

Light microscopic analyses were undertaken in 50 corpuscles taken from the frog regions of different breeds of horses, including *racing and mixed-breed horses, ponies and shire horses*, ranging in age from one up to twenty years old. All PCs have the same basic structure, which is represented in figure 3.11. The outer membrane has a smooth contour, suggesting that there may be a positive intracapsular pressure which keeps lamellae separated from each other; a prominent blood vessel can been seen passing through, which is seen in most corpuscles. There is a visible clear boundary between the outer and inner zones defined by a different density and structure of the lamellae; the inner zone and the outer zone are surrounded by a thin layer of connective and fatty tissue.

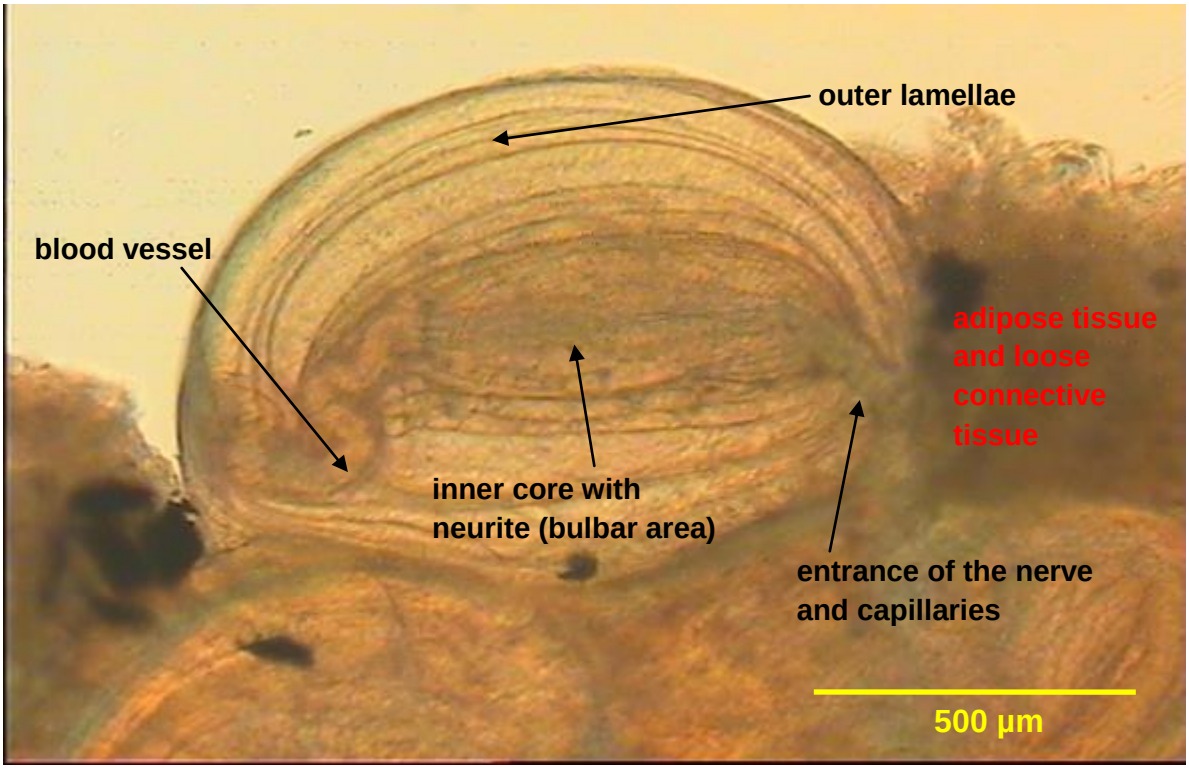

Figure 3.11. PC of oval shape, size 1.2 × 0.7 mm, dissected from a hind foot of a 4-year-old *mixed-breed horse*, 2 hours after euthanasia; (transmission light microscopy).

As mentioned above the size of PCs varied between groups, and the number of lamellae depended on the size of the corpuscle. The number of outer lamellae in large corpuscles (length up to 2.5mm) can reach up to 30 with a number of tightly packed inner lamellae. The interlamellar space generally ranged between 20−50 microns. In *horses* up to 15 years old, the typical radial thickness of the outer zone was roughly equal to that of the inner zone, but in older *horses* the outer zone occupied a greater proportion of the capsule. Associated with these changes was a reduction in the vascularity of the surrounding tissue.

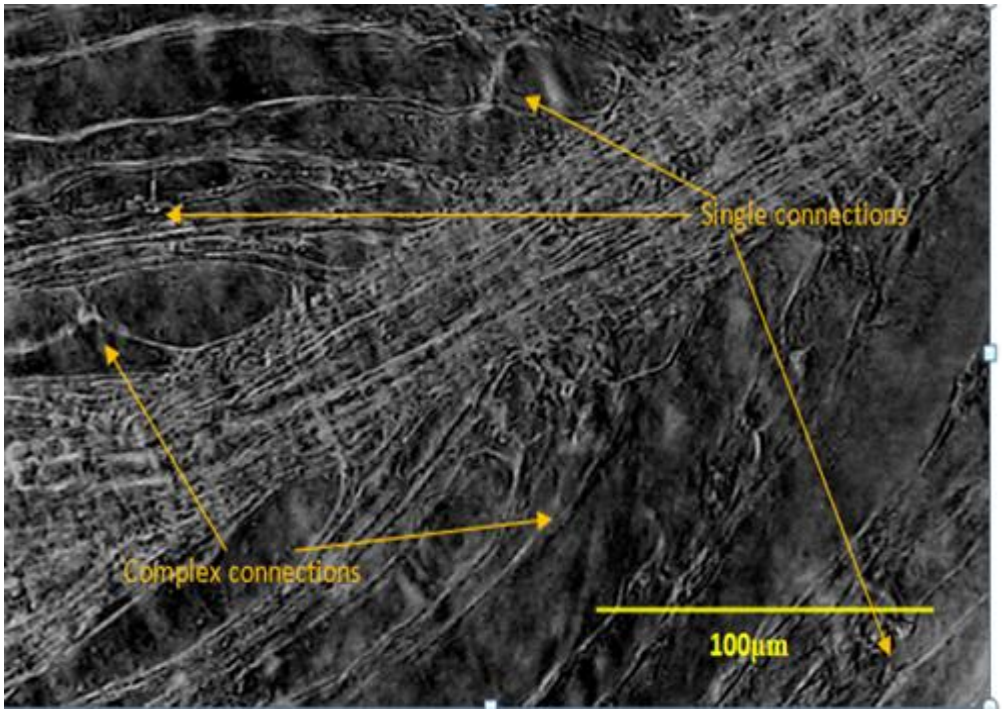

Figure 3.12. The area of the first Ranvier node in a PC from the heel (front foot) of a 4-year-old *mixed-breed horse*; (transmission light microscopy, inverted contrast). Single connections and complex connections (see text) are visible.

Two principal forms of connection within the lamellar structure were observed (figs. 3.12, 3.13, 3.14). The first type of connection is a single strand running between two neighbouring lamellae, roughly perpendicular to the lamellae, and the second is a more complex structure generally involving two (or more) strands crossing, with strands sometimes running roughly tangential to the lamellae. (The interlamellar spaces also contain fibrils, which are much thinner.) Single connections are relatively regularly distributed through the outer zone, while complex connections seems to be associated with extended radial strands which run through the lamellar structure towards the neurite. The spacing of complex connections in the outer zone is greater than in the inner zone. The connections

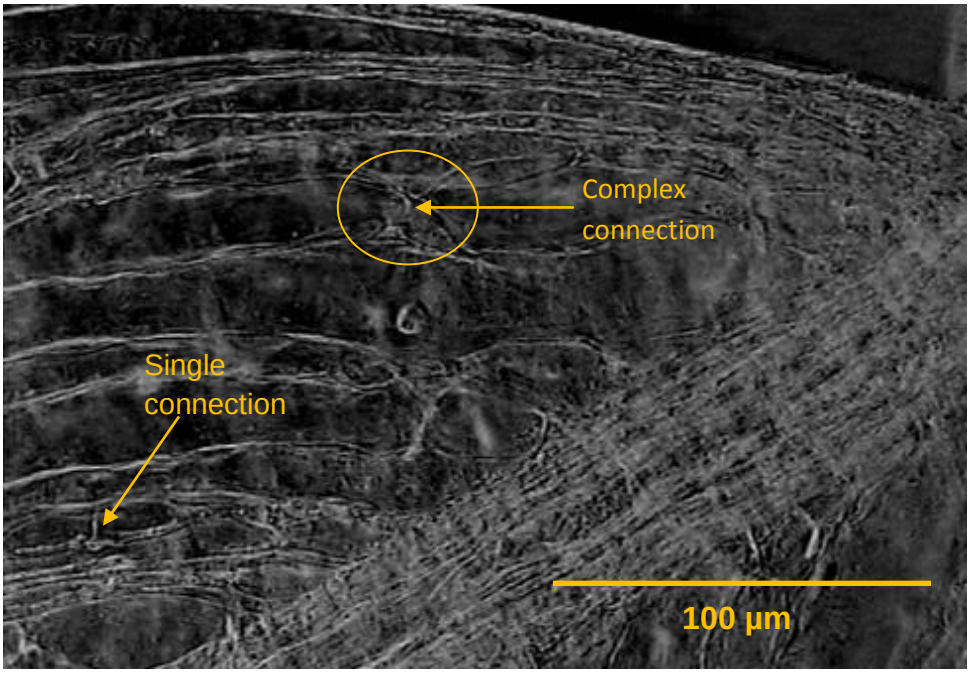

Figure 3.13. The outer zone and part of the zone of the first Ranvier node in the same PC as shown in fig. 3.12, showing single and complex connections; (transmission light microscopy, inverted contrast).

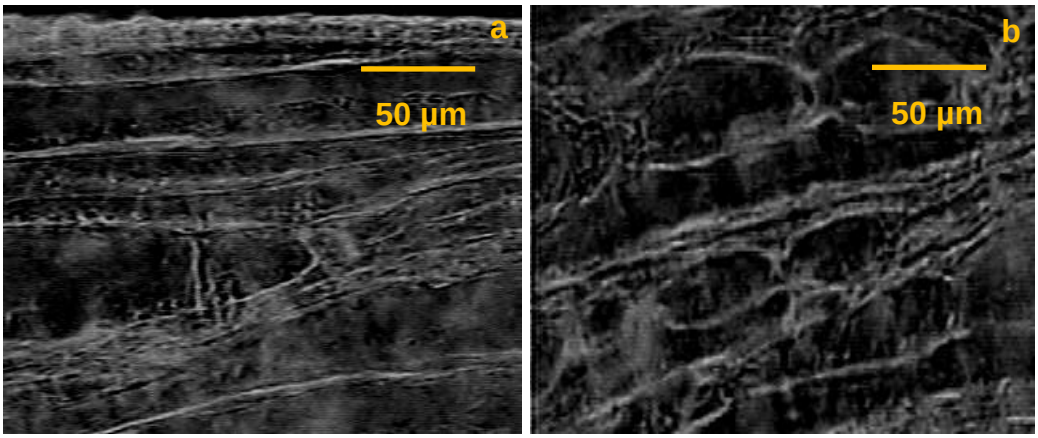

Figure 3.14. Images of the same PC as in figs. 3.12 and 3.13, showing (a) a single connection running orthogonally between two lamellae, (b) a complex connection running tangentially along the lamellae; (transmission light microscopy, inverted contrast).

appear to be cellular junctions that form “bridges” between neighbouring lamellae. Lowenstein and Skalak [36] remark that an “onion-like” structure of concentric lamellae separated by interlamellar fluid requires radial connections to achieve stability – if the interlamellar connections observed in the presents study are purely cellular, it is unlikely that they perform this mechanical function. (See section 3.3.1 for further information on the nature of these connections.)

3.2.1 Blood Vessels in Pacinian Corpuscles

A number of previous studies have raised questions about the role of blood vessels in the PC, as reviewed in Chapter 1. In the present study, most of the corpuscles examined had blood vessels entering the inner core and other vessels crossing the outer surface. Figures 3.15 and 3.16 demonstrate two blood capillaries with an approximate diameter of 10 microns, running close to the nerve fibre. In figure 3.15 the capillaries enter the capsule along the axon, and make a distinctive loop in the area of the first Ranvier node. The capillaries reappear at the end of the inner core area (fig.3.16), but it is unclear whether these capillaries join or run parallel to each other. The outer zone of the PC appears to have an independent blood supply: figure 3.17 shows two large capillaries (around 17 μm diameter) which follow the axon before running through the outer zone of the lamellar structure. (See Chapter 4 for a description of the role of blood vessels in solute transport.)

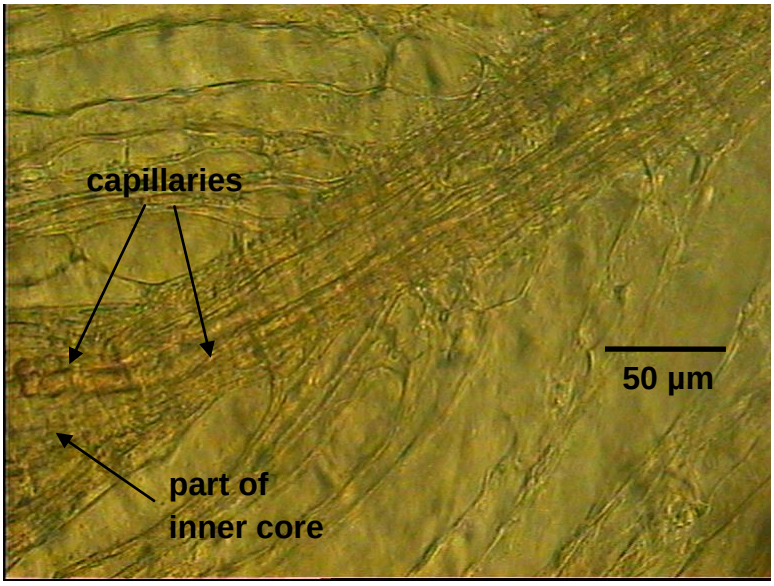

Figure 3.15. A region of the same PC shown in figure 3.12, where the nerve is losing its myelinated sheath and modified lamellae form around the nerve; blood capillaries share the entrance to the core with the axon and make a distinctive loop within the inner core; (transmission light microscopy).

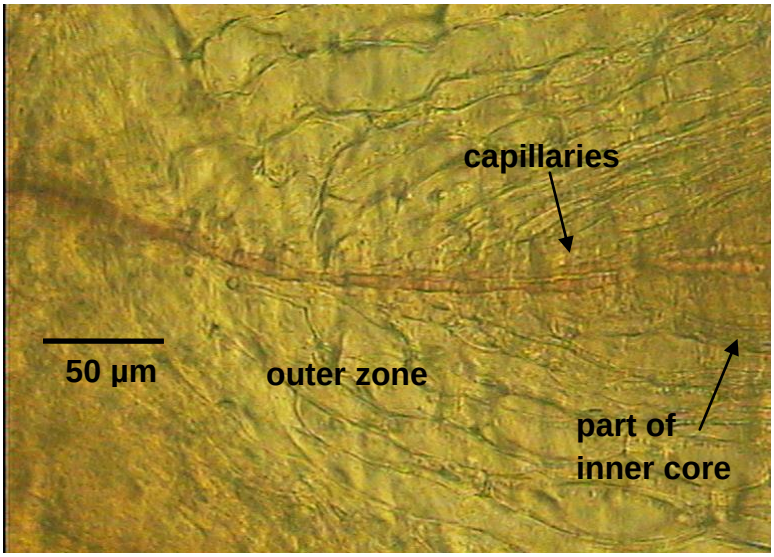

Figure 3.16. A region of the same PC shown in figures 3.12 and 3.15; the blood capillaries continue through the outer zone after a loop within the inner zone; (transmission light microscopy).

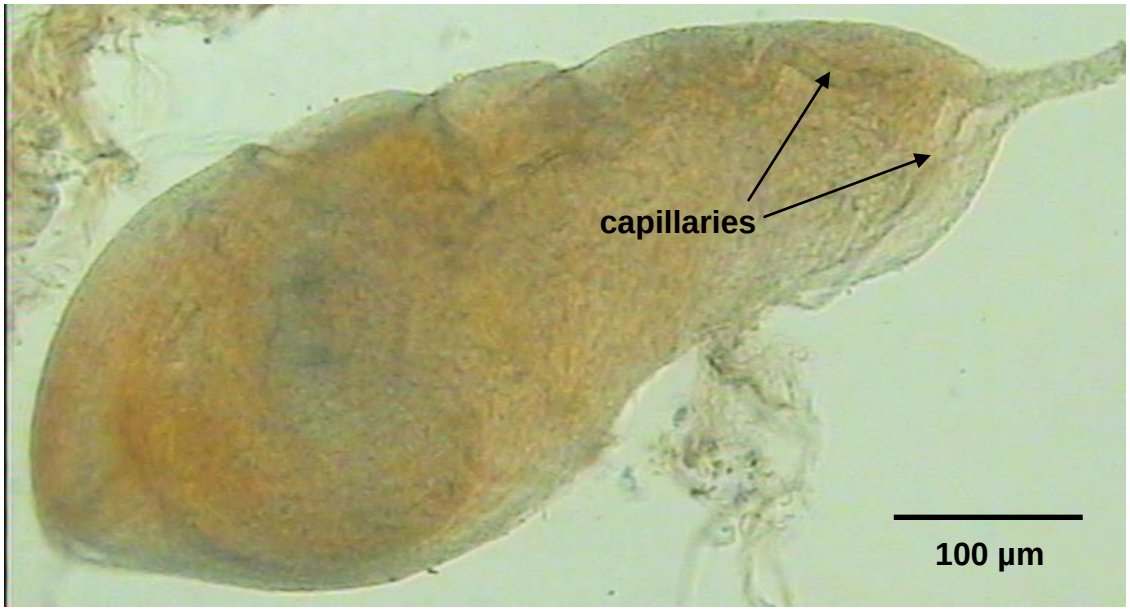

Figure 3.17. Two blood vessels following the axon and then appearing to run through the outer zone of a PC extracted from the hind hoof of a 10-year-old *Shire horse*; (transmission light microscopy).

3.3 Confocal Microscopy

Because frozen sectioning caused significant damage to the corpuscles, confocal microscopy was used to examine the structure of intact PCs from *horse* hoof. In order to observe 3-D structure staining and observation were performed on the intact corpuscles, although this produced some difficulties with stain penetration. Alcian Blue was used to stain for glycosaminoglycans, and Van Gieson's stain was used for collagen. Stains for elastin are rather unspecific (e.g. Weigert's) which was inadequate in the intact corpuscle. Elastin was searched for using its intrinsic fluorescence, but two photon excitation proved more sensitive, so these results are

presented in the following section. To complement efforts to detect cells by CARS, also described in that chapter, cell membranes and lipid deposits were stained with the lipid-soluble fluorophore di-8-ANEPPS.

3.3.1 Lipid Staining

Di-8-ANEPPS penetrated the intact corpuscle only slowly: 18 hours incubation revealed that the tissue is rich in lipids. An unexpected observation was the presence of vesicles or lipid droplets apparently freely floating in the interlamellar fluid. If these are indeed vesicles, they may be part of a signalling system – otherwise, it possible to assume they are involved in cellular metabolism. The interlamellar connections stained for lipid, confirming the hypothesis above that these are cellular junctions. The capsule stains intensely, though it is unclear whether this is because of a higher lipid content or because of limited dye penetration to the core.

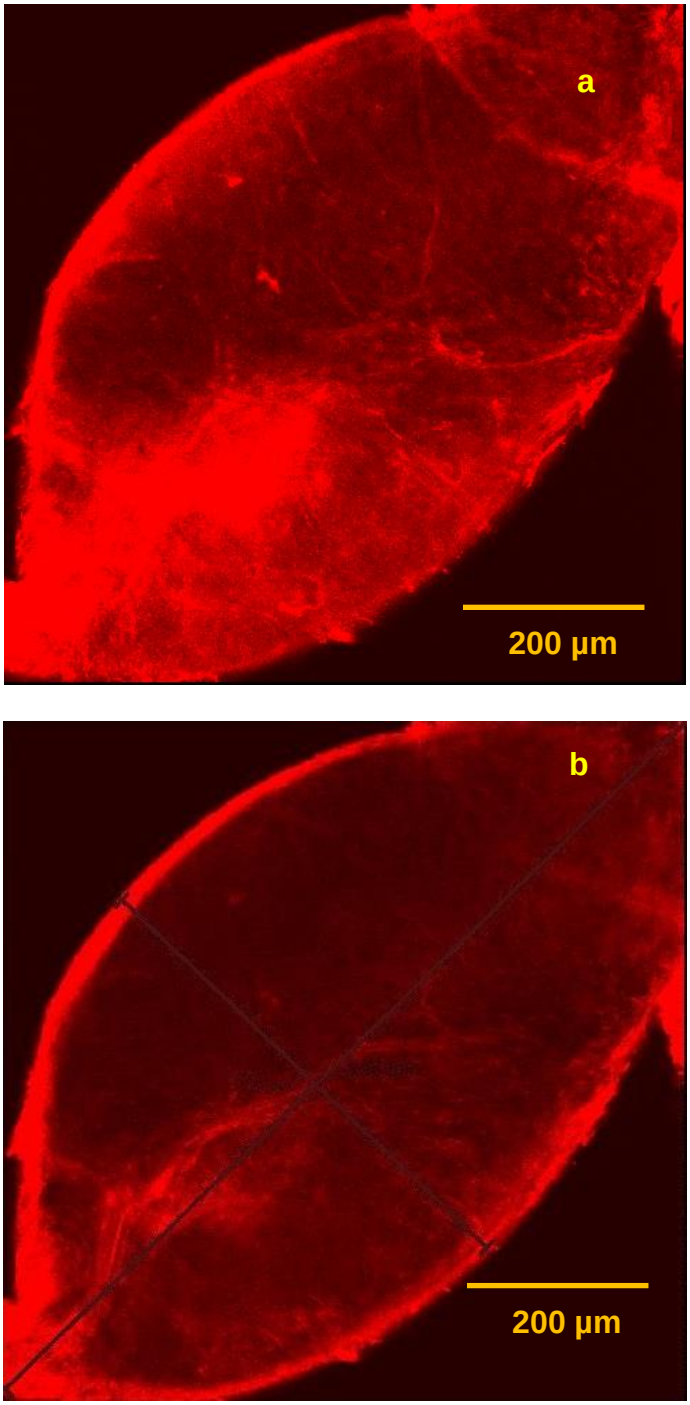

Figure 3.18. Confocal microscopy images (sections from a confocal stack with slice thickness 1µm) of a PC extracted from the cleft area of the front foot of a 4-year-old *mixed-breed horse*, after incubation in the fluorophore di-8-ANEPPS for 18 hours; excitation was at 488 nm and emission was at 530 nm: (a) staining of the surface of the corpuscle, (b) 25 µm deep in the tissue, showing weakly stained cell membranes and strongly stained axon.

3.3.2 Glycosaminoglycans

Alcian Blue staining revealed glycosaminoglycans particularly in capillaries penetrating the surface and outer zone and proved an unexpectedly effective way of observing their architecture and extending the observations made above. The capillaries branch from a main vessel which shares an entrance into the corpuscle with the axon (fig. 3.19 (a)) run in different directions throught the outer zone (fig. 3. 19 (b)).

Glycosaminoglycans were evident in all lamellae.The lamellae of the inner zone stain more intensely than the outer lamellae (fig. 3.20 (a)) particularly in the vicinity of the small capillaries. Staining is also more intense in what is generally referred to as the growth zone of the corpuscle, between the inner zone and the outer zone.

3.3.3 Collagen

The Van Gieson stain was applied to study the presence of collagen. As shown in figure 3.22, there was staining throughout the corpuscle. In the outer region the individual lamellae were well resolved, indicating that collagen is a major

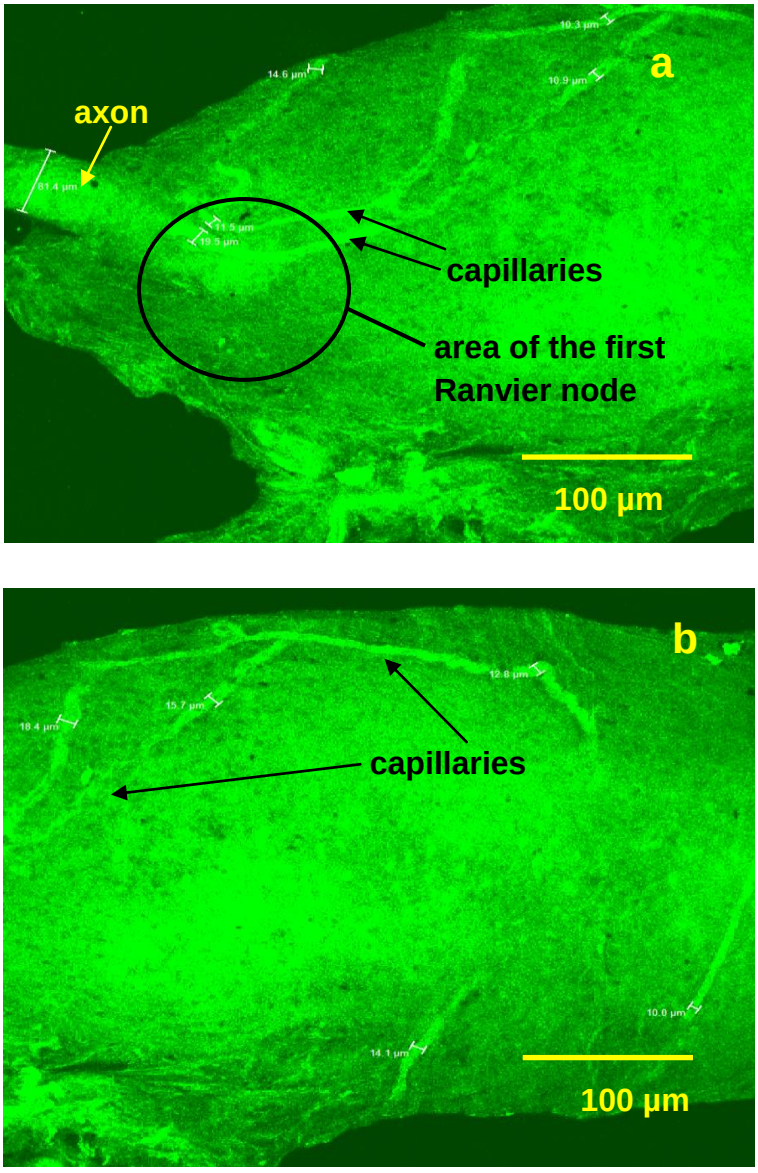

Figure 3.19. PC of size 1.20 × 0.63 mm, extracted from the heel area of the hind hoof of 4-year-old *racehorse* and incubated in Alcian Blue for 40 minutes; confocal microscopy, slice thickness 0.99 µm; (a) showing capillaries in the part of the PC close to the first Ranvier node; (b) showing capillaries running along the outer lamellae (capillary diameter in the outer zone is typically in the range 10 to 15 µm).

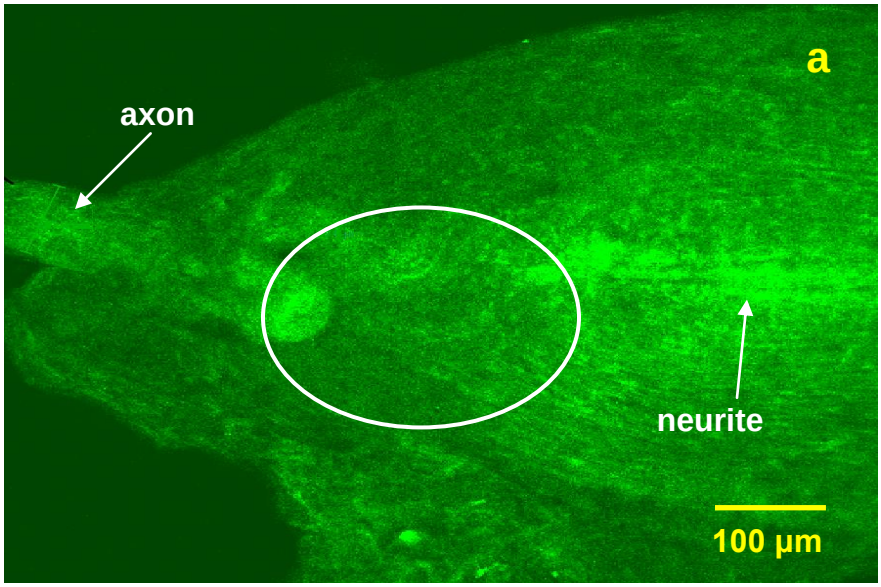

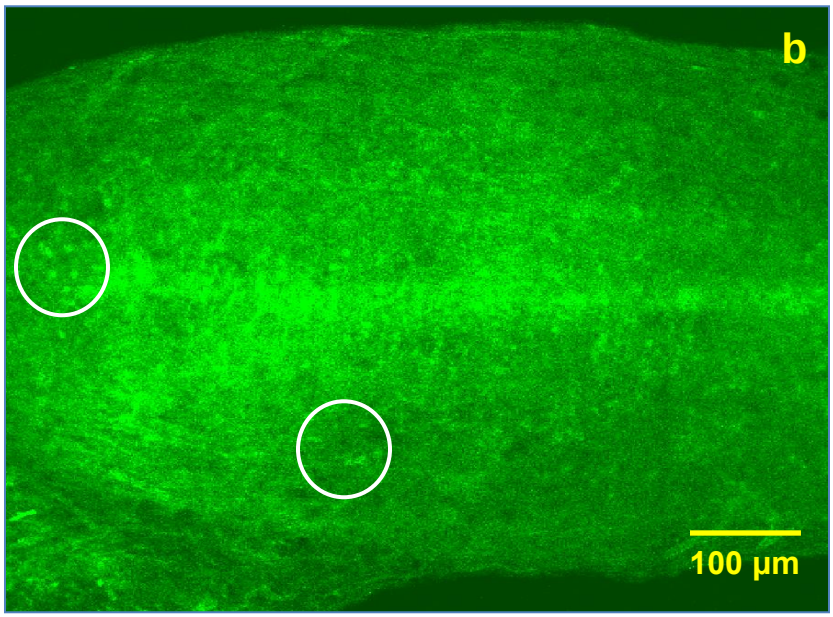

Figures 3.20 and 3.21. The same PC as in fig. 3.19, incubated in Alcian Blue for 40 minutes; confocal microscopy, slice thickness 0.99 µm; (a / fig.20) within the circled region, capillaries are seen entering the inner zone, which has highly packed lamellae; (b / fig. 21) the bright central band in this image corresponds to the plane of the growth zone; the circled regions indicate features in the proteoglycans distribution whose origin is unknown.

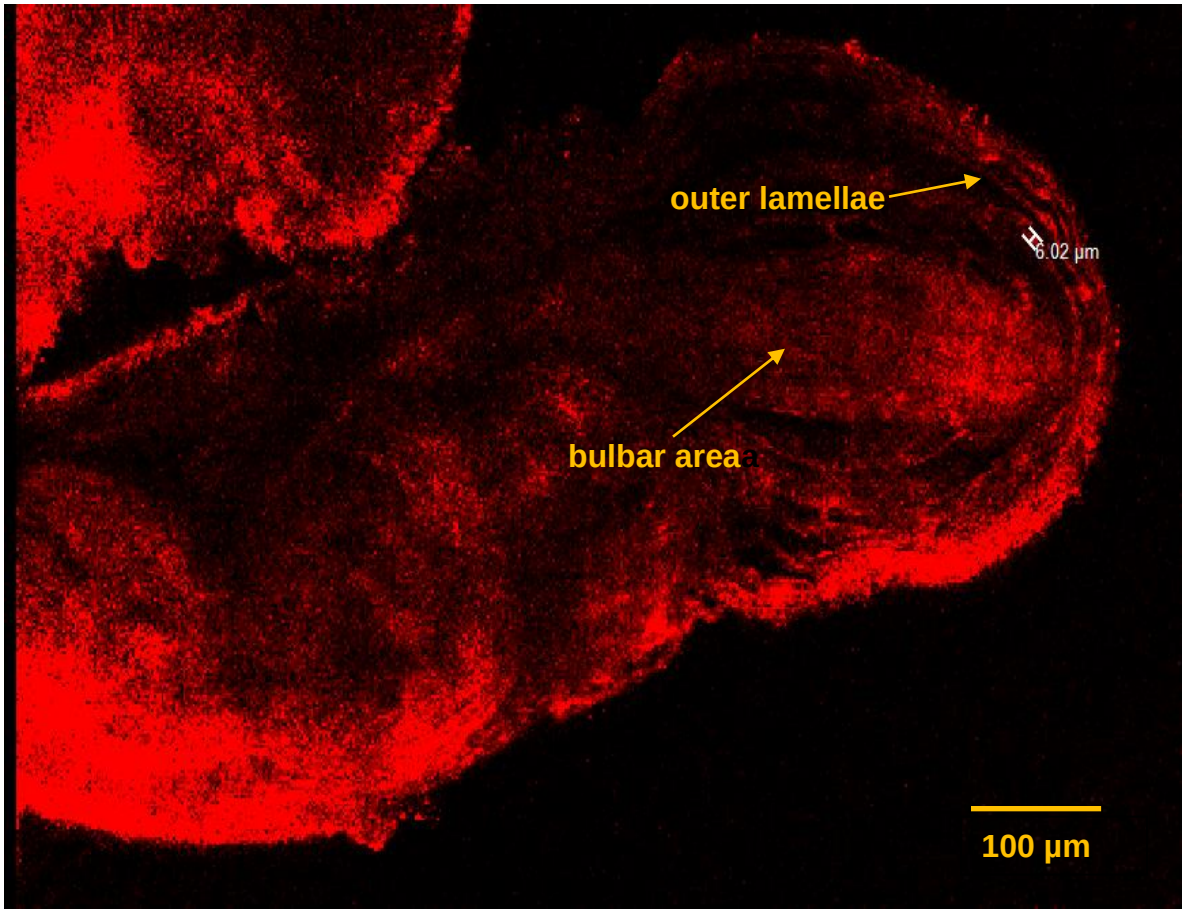

Figure 3.22. PC of size 1.10 × 0.45 mm, extracted from the heel area of the front foot of an 8-year-old *mixed-breed horse*, incubated in Van Gieson stain for 40 minutes; a single image from a confocal-microscopy stack shows a central section of the PC, through the core.

component of the structure, including the interlamellar struts. Collagen was also visible in the walls of the larger blood vessels. Staining was rather patchy and this was believed to be because of problems in dye penetration. Since SHG provided a much more powerful means of visualising collagenous structures in 3-D this approach was not pursued further and collagen organisation is discussed in more detail in section 3.4.

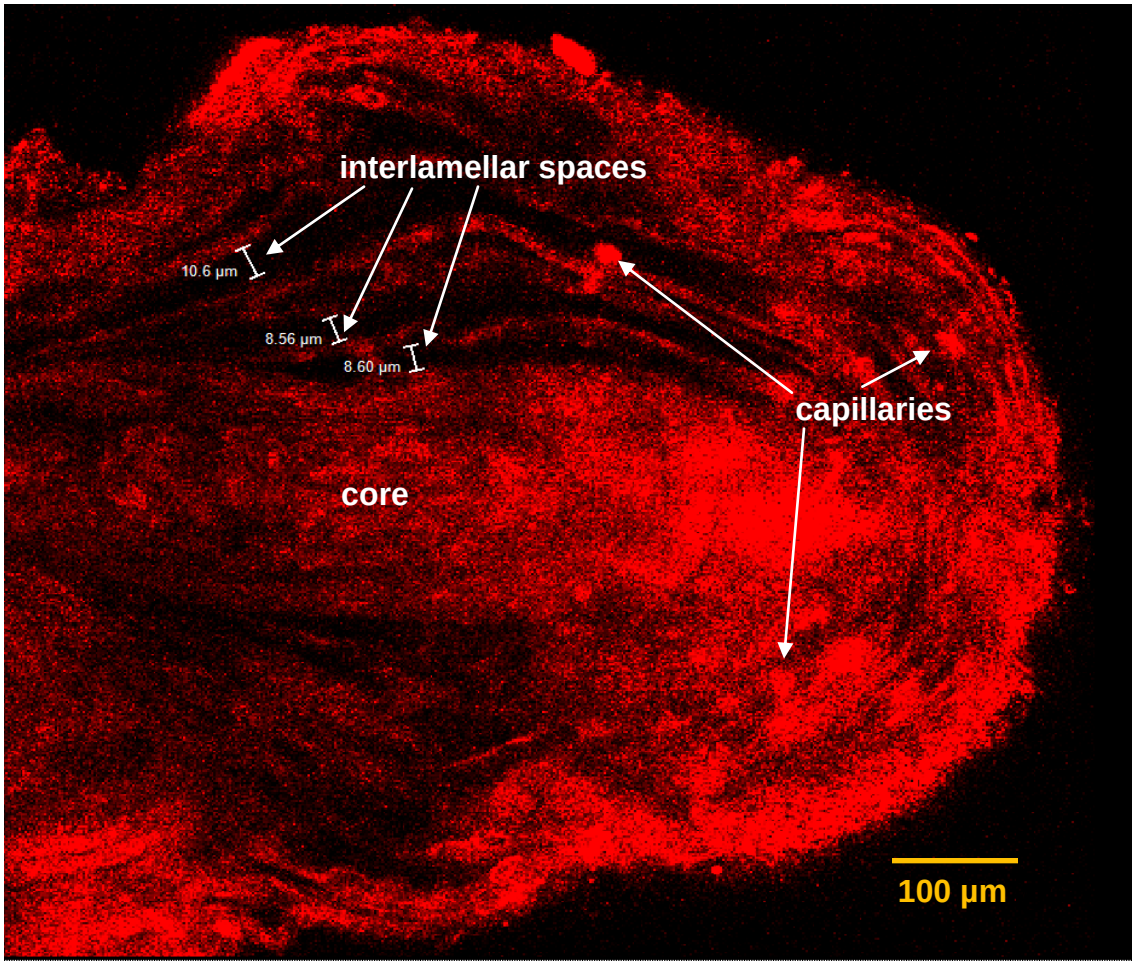

Figure 3.23. PC (as in fig. 3.22) of size 1.10 × 0.45 mm, incubated in Van Gieson; a single image from a confocal-microscopy stack, showing variation of interlamellar gaps. A number of capillaries pass through the outermost lamellae.

3.4 Nonlinear Microscopy

Nonlinear microscopy was used to investigate the structure of the fibre network within the extracellular matrix, which is likely to be the principal determinant of the elastic properties of the solid component of the PC.

Nonlinear microscopy was performed on fifteen fresh unstained PCs dissected from front and hind hooves of horses aged two, six and eight years old. As described above, fibrous collagens (types I, II and III) can be detected by second harmonic generation (SHG), elastin by its intrinsic two photon fluorescence (TPF) and cell membranes by tuning Coherent Anti-Stokes Raman spectroscopy (CARS) to the frequency of membrane phospholipids. In viewing the images below it should be noted that, in tissues with high collagen content, collagen gives a small fluorescence contribution in the TPF images and a protein-CH contribution to the CARS images. These contributions are easy to distinguish and have actually been used in checking the co-registration of the multimodal images displayed below (figs. 3.24- 3.32).

SHG imaging showed an extensive network of collagen fibres (fig. 3.24). Fibres within the lamellae were tentatively identified as type I collagen on the basis of their similarity in size, which was approximately 5 μm in diameter (fig. 3.25, red arrow head), to such fibres observed in tissues such as tendons and blood vessels. Collagen fibres are also observed linking to the lamellae (fig. 3.25, green arrow head). They are much thinner, approximately 1 μm in diameter, and appear to be related to the “simple” junctions observed with conventional microscopy, described above (section 3.2). It is possible that this is type II collagen, which has been reported in the interlamellar spaces [45], [43] or type III, which forms finer fibres

than type I. Collagen fibres were not observed in relation to the “complex” lamellar connections, suggesting that these are simply cellular junctions.

The orientation of collagen fibres within the lamellae will be a major determinant of their mechanical properties and is probably important in transducing mechanical stimuli through the PC. The majority of fibres were orientated longitudinally (with respect to the long axis of the PC) (fig. 3.27), some transverse (fig. 3.24) and also some in random networks (fig. 3.26). Longitudinal organization of collagen fibres, was most clearly observed in the first 10-14 outer lamellae. At the surface of the corpuscle the collagen network was denser (consistent with the staining results) and it organisation was more irregular, forming an isotropic network at the surface of the corpuscle (fig. 3.26, 3.27).

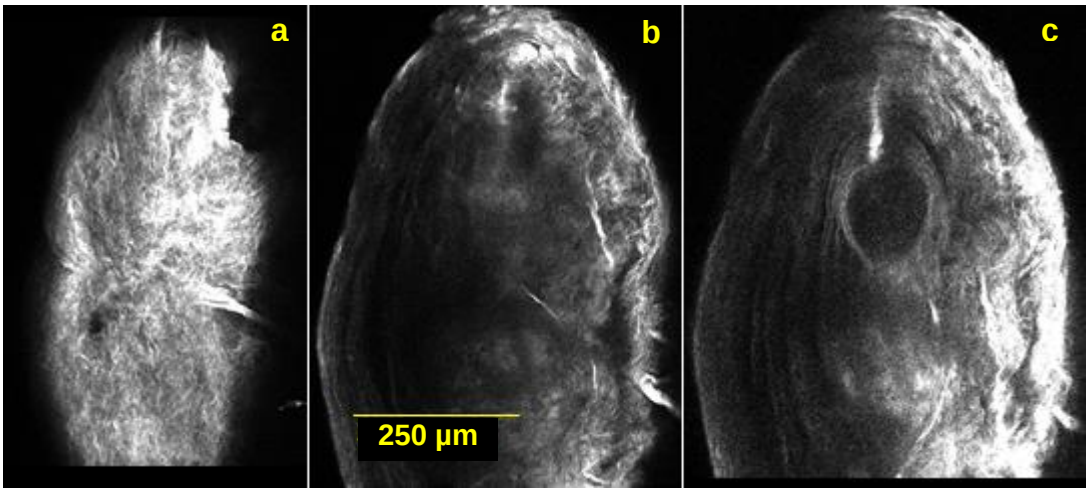

Figure 3.24. PC of size 1.0 × 0.5 mm, extracted from the heel area of the front foot of a 6-year-old *mixed-breed horse*; images from a SHG stack show (a) the surface of the PC, with complex collagen organisation, (b, c) planes at depth 100 µm and 150 µm, showing collagen network in lamellae and organisation of the outer core.

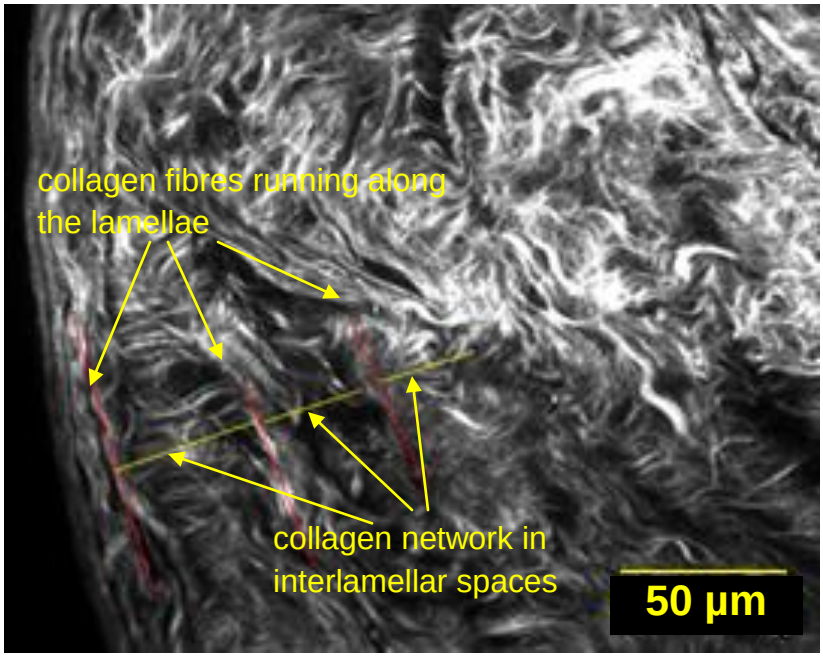

Figure 3.25. PC of size 1.3 × 0.6 mm, extracted from the hind foot (heel) of a 12-year-old *mixed-breed horse*; SHG image, showing collagen fibres running along the lamellae (following the red lines) and in the interlamellar spaces (following the yellow lines). Dehydration during imaging may have caused folding of some lamellae.

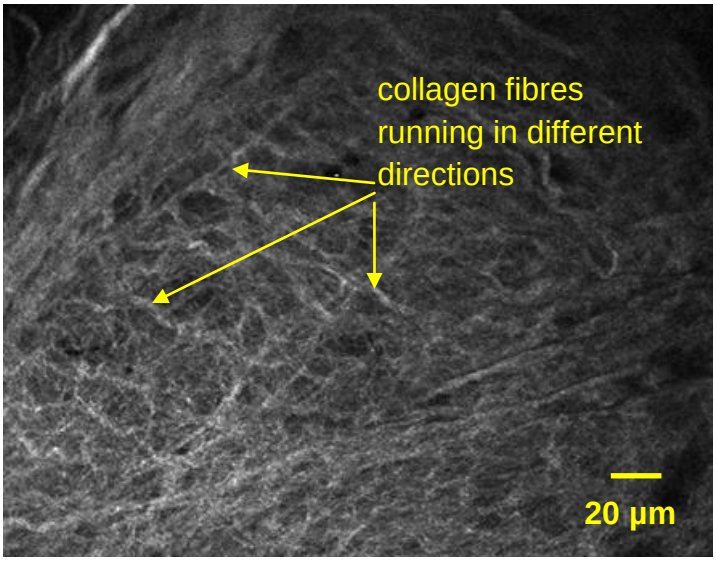

Figure 3.26. PC of size 1.20 × 0.52 mm, extracted from the heel area of the front foot of 4-year-old *racehorse*; the SHG image shows a detailed collagen organisation in the surface of the corpuscle.

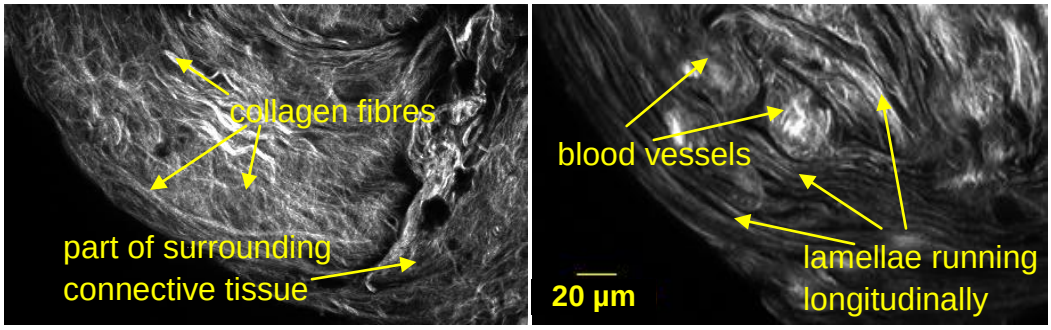

Figure 3.27. PC of size 1.0 × 0.4 mm, extracted from the cleft area of the front foot of a 4-year-old *mixed-breed horse*; SHG images demonstrate a complex organisation of collagen fibres at the PC surface (left) and longitudinal organisation in the outer zone (right); blood vessels can be seen in the outer zone.

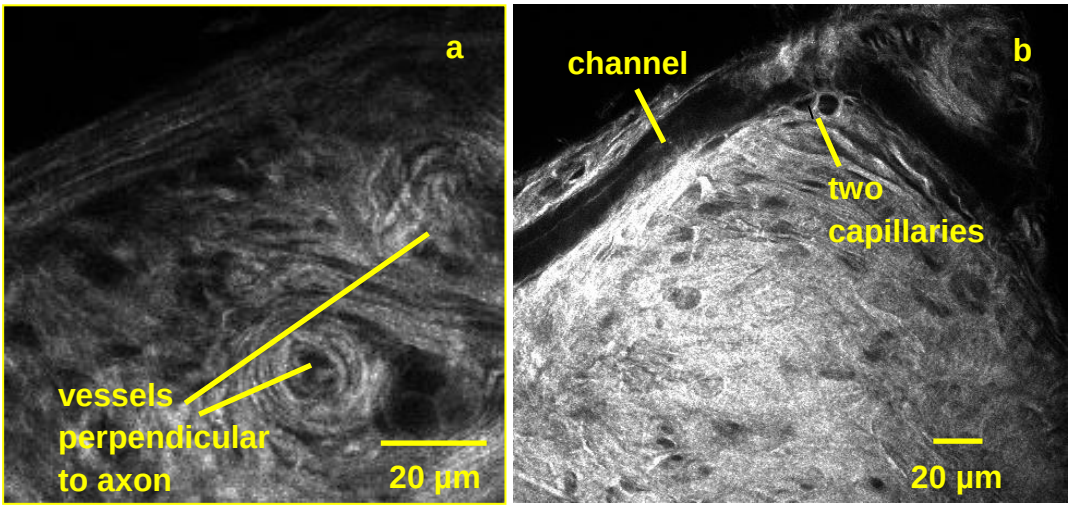

Figure 3.28. PC of size 1.20 × 0.52 mm, extracted from the heel area of the front foot of a 4-year-old *racehorse*; SHG images show (a) vessels (approximately 20 µm in diameter) perpendicular to the axon, (b) two longitudinally orientated channels (20 µm in diameter) along the outer lamellae, also two capillaries sharing the same entrance to the PC as the axon (they eventually reach the inner core).

Collagen was also evident in the walls of blood vessels, and in the neighbourhood of vessels the collagen organisation of the PC was disrupted. For example, figure 3.28b shows two 10 μm vessels, probably capillaries, which share the same entrance with the axon. Also visible are two 20 μm diameter channels, running through the outer zone, and two vessels of similar diameter running perpendicular to the axon (fig. 3.28a)

These observations on blood vessels are consistent with the light and confocal microscopy already described, and with tracer uptake experiments presented in Chapter 4.

It was difficult to entirely eliminate dehydration during the long time required for acquisition of the image stack and this may have caused slight folding of the lamellae and crimping of transverse fibres (fig. 3.25).

TPF imaging of the PC surface layer revealed elastin fibres weakly against the background of collagen fluorescence (fig. 3.29).

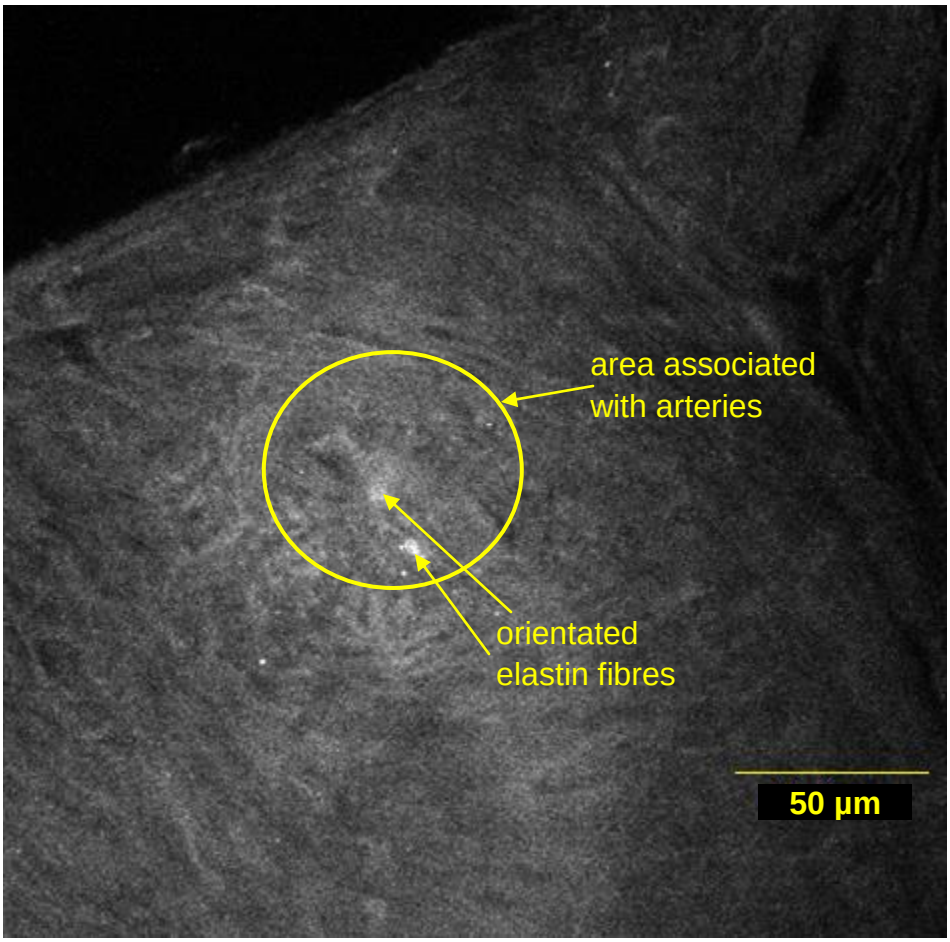

Figure 3.29. PC of size 1.20 × 0.52 mm, extracted from the heel area of the front foot of a 4-year-old *racehorse*; TPF image showing elastin fibres weakly against the collagen network; the circled area, associated with arteries, shows orientated elastin fibres (found in vessels perpendicular to the axon – see fig. 3.28 (a)) against randomly orientated collagen on the surface of the PC.

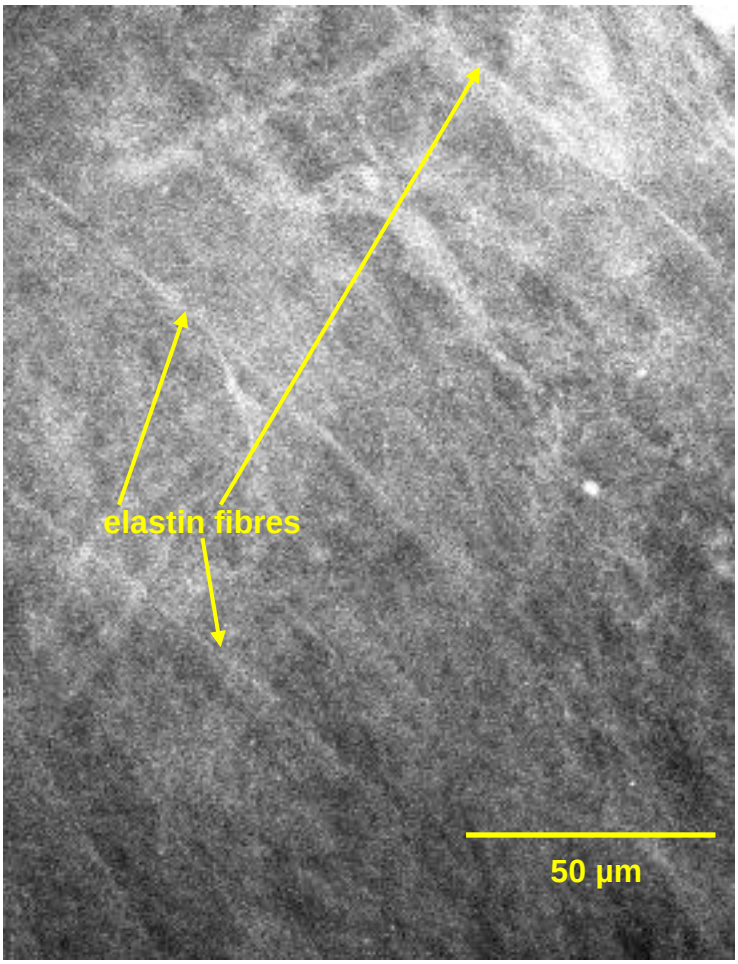

Figure 3.30. PC of size 1.20 × 0.52 mm, extracted from the heel area of the front foot of a 4-year-old *racehorse*; TPF image showing a network of elastin fibres running across the surface layer of the PC.

A sparse network of fibres approximately 1µm in diameter was present on the surface of the PC (fig.3.30). The appearance of these fibres is similar to that of elastin fibres recently found in tissues such articular cartilage [82]. Similar fibres were interwoven between the collagen fibres of the lamellae and some spanned lamellae (fig. 3.30).

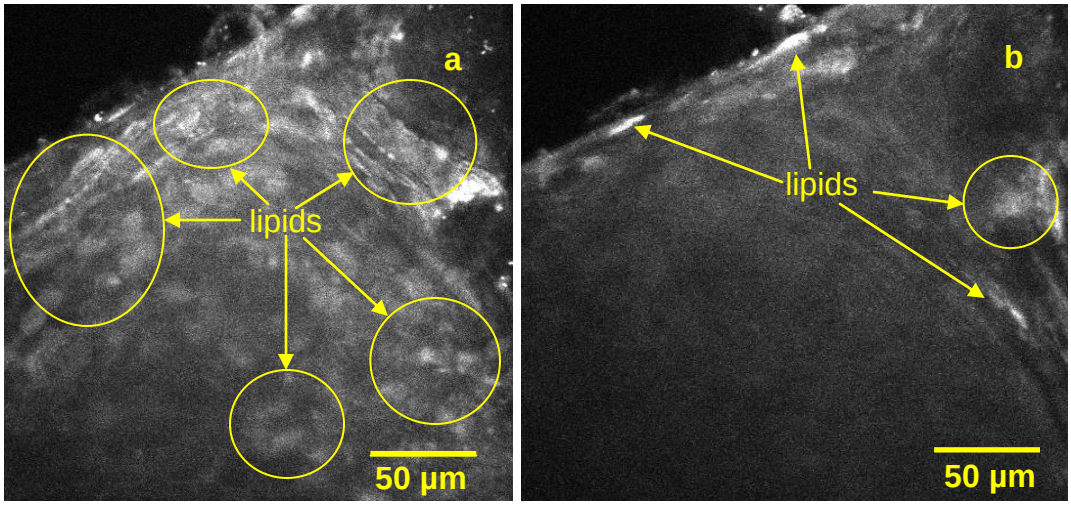

Figure 3.31. PC of size 1.20 × 0.52 mm, extracted from the heel area of the front foot of a 4-year-old *racehorse*; CARS imaging reveals a high density of fatty lipids within the surface layer (a), decreasing in the outer zone away from the surface (b).

CARS imaging, demonstrated the presence of a high density of lipids in the outer zone, perhaps related to surrounding adipose tissue, as noted by light microscopy. The density of lipids is highest in the surface and first few lamellae but decreases away from the surface (fig. 3.31). Because of the high fluorescence background, contrast was insufficient to delineate individual cell membranes.

Colour-coded SHG images (collagen), TPF images (elastin) and CARS images (lipids) can be combined to form a composite colour image, as shown in figure 3.32. The composite image shows, as expected, a high concentration of lipids (red) at the surface of the PC, and high concentration of collagen within the outer core.

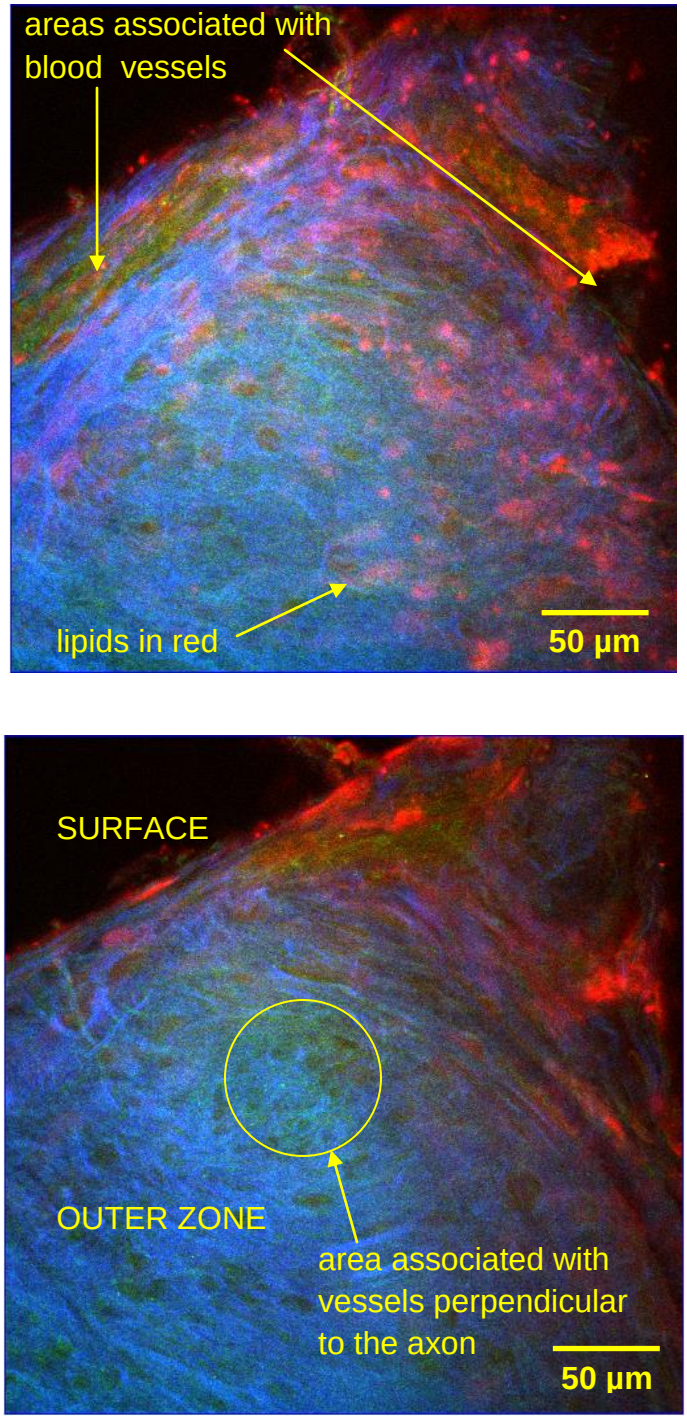

Figure 3.32. PC of size 1.20 × 0.52 mm, extracted from the heel area of the front foot of a 4-year-old *racehorse*; composite overlaid colour-coded images [SHG (collagen) − blue, TPF (elastin) – green, and CARS (lipids) – red] of (top) a plane at the PC surface and (bottom) a plane through the outer zone.

3.5 Discussion

PCs were found next to the primary blood supply in the hoof which is associated with the blood pumping during the movement. They are surrounded by a semi-transparent layer of adipose and loose connective tissue which needed to be removed before microscopic investigation. Confocal microscopy and CARS also revealed a high density of lipids on the surface of the PC, associated with relatively coarse collagen fibres and this may represent collapsed remnants of this encapsulating structure. Whether this structure has any role in transduction, perhaps by equilibrating the pressure distribution on the surface of the PC, would be an interesting topic of further research.

More than a hundred dissections of horse hooves revealed a similar PC distribution, with PCs varying in shape and size within the same cluster. Another question, which can only be resolved when a deeper understanding of the relationship between the structure of the PC and its transduction capabilities is better understood is whether these clusters function cooperatively, perhaps to cover a broad band of stimuli, or whether each is an independent sensor.

The microscopy revealed a number of significant aspects of corpuscular structure. The main component of the extracellular matrix was collagen, forming the skeleton

of each lamella, and showing slight variations with depth and particularly on the outer surface. The elastin fibre network was very sparse (probably accounting for the difficulty in detecting it with histochemical stains) and it is difficult to imagine that it directly supports mechanical loads. However, relatively recently it has been recognised that many collagen-rich tissues contain relatively sparse networks of elastin fibres and their presumed mechanical function is a topic of current research interest [82].

Proteoglycans were also present within the lamellae. These probably serve, as in the glomerular basement membrane, to regulate the movement of water and solutes across the lamellae. However, they may also have a direct role in determining the viscoelasticity of the matrix through their effect on the distribution and mobility of water.

Several forms of interlamellar connection were observed, some were fibrous – mainly collagen with small quantities of elastin, and these probably represent the mechanical connections envisioned in the Loewenstein-Skalak model. However, others appeared to be cellular processes and these are unlikely to have a mechanical role but to provide pathways of intercellular communication – a process in which lipid vesicles may also be involved.

Blood vessels were visualised in the PC by a number of techniques. It appears that there are independent supplies to the core and surface of the corpuscle, both of which may be necessary to meet its nutritional requirements, but the anatomical association between corpuscles and blood vessels adds support to the hypothesis that they may also be involved in some aspects of haemodynamic regulation. To investigate this possibility it would be important to explore the coupling of the corpuscle into the rest of the circulation – techniques such as corrosion casting of the microcirculation of the hoof would be a useful tool in this task.

Chapter 4

Water and solute transport

The pathways of water and solute transport into the PC are of interest in understanding how this unusual structure maintains its nutrition and integrity. However, the main aim of the work described in this chapter was in relation to understanding the process of mechanotransduction. The flow of fluid in the interlamellar space is important in most [83], [52], [64], [84], theories of mechanotransduction. However, the connectivity of the interlamellar spaces and the resistance to water flow across and along the lamellae are quite poorly investigated. This chapter describes two groups of experiments. The first group of experiments investigates osmotic swelling of the PC, described in section 4.1. Fluorescent tracer measurements of permeability are reported in section 4.2. Discussion on how obtained results may lead to better understanding of mechanotransduction in the PC is in section 4.3.

4.1 Osmotic Challenge

The permeability of the lamellar membranes to water and a range of solutes was investigated by measuring the response of the corpuscle to osmotic pressure gradients generated by these solutes (see section 2.4 for practical details). If the corpuscle is permeable to water but not the solute, the osmotic pressure gradient

generates a flow of water into or out of the corpuscle until it is resisted by tension in the structure of the corpuscle. If the membrane is partially permeable to the solute this pressure is then dissipated by the (slower) movement of solute into the corpuscle. This approach therefore gives insights into both the permeability of the corpuscle to a particular solute and to the mechanics of the corpuscle.

4.1.1. Osmotic Swelling

Eight corpuscles, dissected from different horses, were equilibrated in a bath of 0.15 M NaCl and the bathing solution was then exchanged for deionised water. Within 15 seconds the volume of the PC increased from the original, and then remained approximately constant for the next 30 minutes. The changes in length and width generally preserved the overall shape of the capsules (figs. 4.1, 4.2). In corpuscles incompletely dissected and retaining some surrounding tissue the changes were slower, presumably due to the buffering action of osmolytes diffusing in the tissue.

The overall change arose largely from an increase in interlamellar spacing, of (30 ± 2)% in the outer zone (fig. 4.4). There was no measurable change in spacing in the inner zone. The optical contrast between the lamellae and interlamellar space became less, presumably due to swelling of either the cells or extracellular matrix of the lamellae.

4.1.2. Hyperosmotic Solutions

The permeability of the corpuscle to molecules of different size and charge was investigated by monitoring changes produced by replacing the 0.15M NaCl bathing solution with various hyperosmotic solutions. Sucrose (4M) was used as a small, neutral solute, PEG (polyethylene glycol, 20,000 kD molecular weight, concentration 30% wt /vol) was used as an intermediate size solute, and albumin (0.1mM) was used as a representative protein. Sodium chloride (2M) was used to investigate ion transport. When exposed to hyperosmotic solutions, the spacings of the outer lamellae of the outer core were reduced, whilst the spacings of the inner lamellae again remained unchanged. The changes in overall PC dimensions generally preserved the overall shape of the capsule. This shrinkage occurred on a similar time-scale of a few seconds for all the osmolytes and to a similar extent for all the osmolytes (lamellar spacing decreasing by around 20%, see fig. 4.4) despite the differences in their size and osmotic pressure; (response to PEG was an exception, with no noticeable effects within 20 minutes). We therefore hypothesise that this shrinkage phase represents the rapid movement of water out of the capsule. The osmotic pressure of the low molecular weight solutions is many times higher than that of albumin. The similarity of their effects on interlamellar spacing could indicate that the lamellae are partially permeable to the smaller solutes, so that the full osmotic gradient is not generated across the lamellae, which is consistent with the recovery at longer times, discussed below. Alternatively, there may be a maximal state of collapse of the corpuscle where its mechanical strength is sufficient to prevent further collapse.

The subsequent behaviour of the corpuscle varied with the osmolyte, reflecting the different permeability of the corpuscle to the different solutes. For albumin there was no further change for up to 30 minutes. For the other solutes (excepting PEG) the volume of the corpuscle slowly increased as the solute diffused into the corpuscle. The response was similar for 2M NaCl and 4M sucrose, indicating that there is little charge interaction with the extracellular matrix. This is surprising, given the high concentration of proteoglycans in the matrix and perhaps suggests that the cell junctions constitute the major barrier. However it is clear that active cellular ion transport is not a factor in the response.

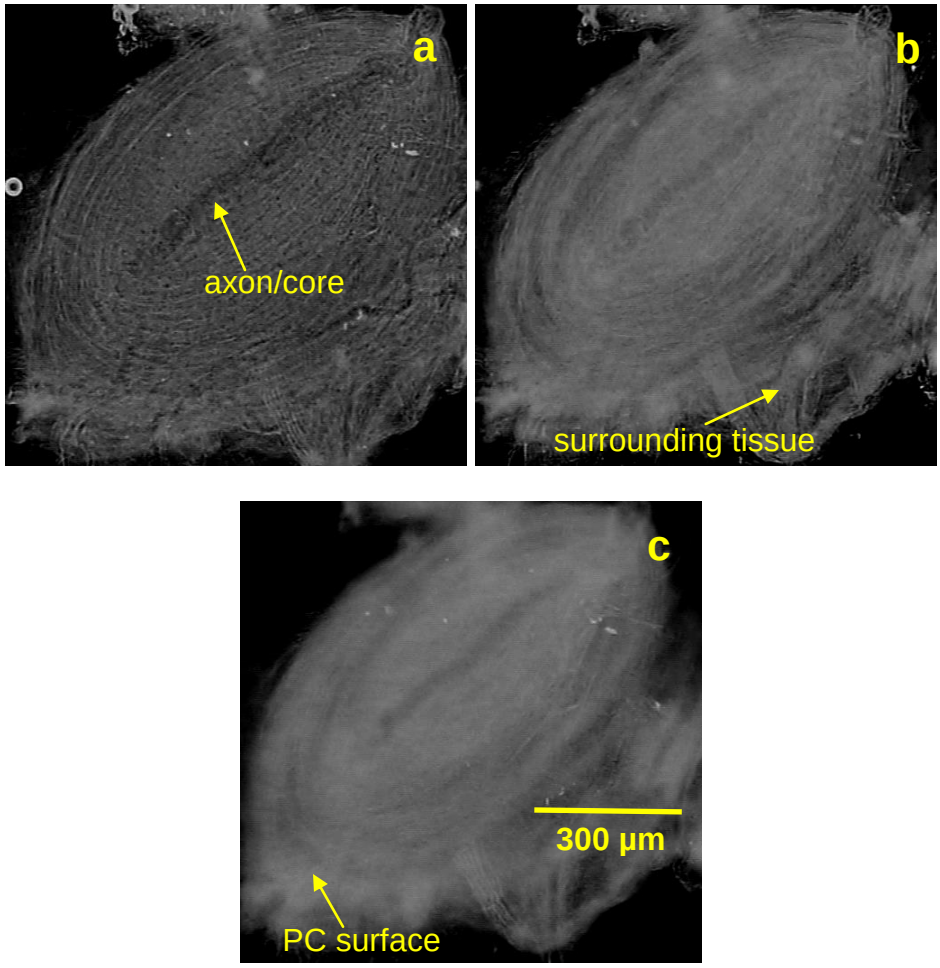

Figure 4.1.Osmotic swelling of a PC, extracted from the heel area of the front foot of an 8-year-old *mixed-breed horse*; (a) the initial state in 0.15M NaCl, (b) 15 seconds after exchange to deionised water, (c) the final state, when equilibrium was reached.

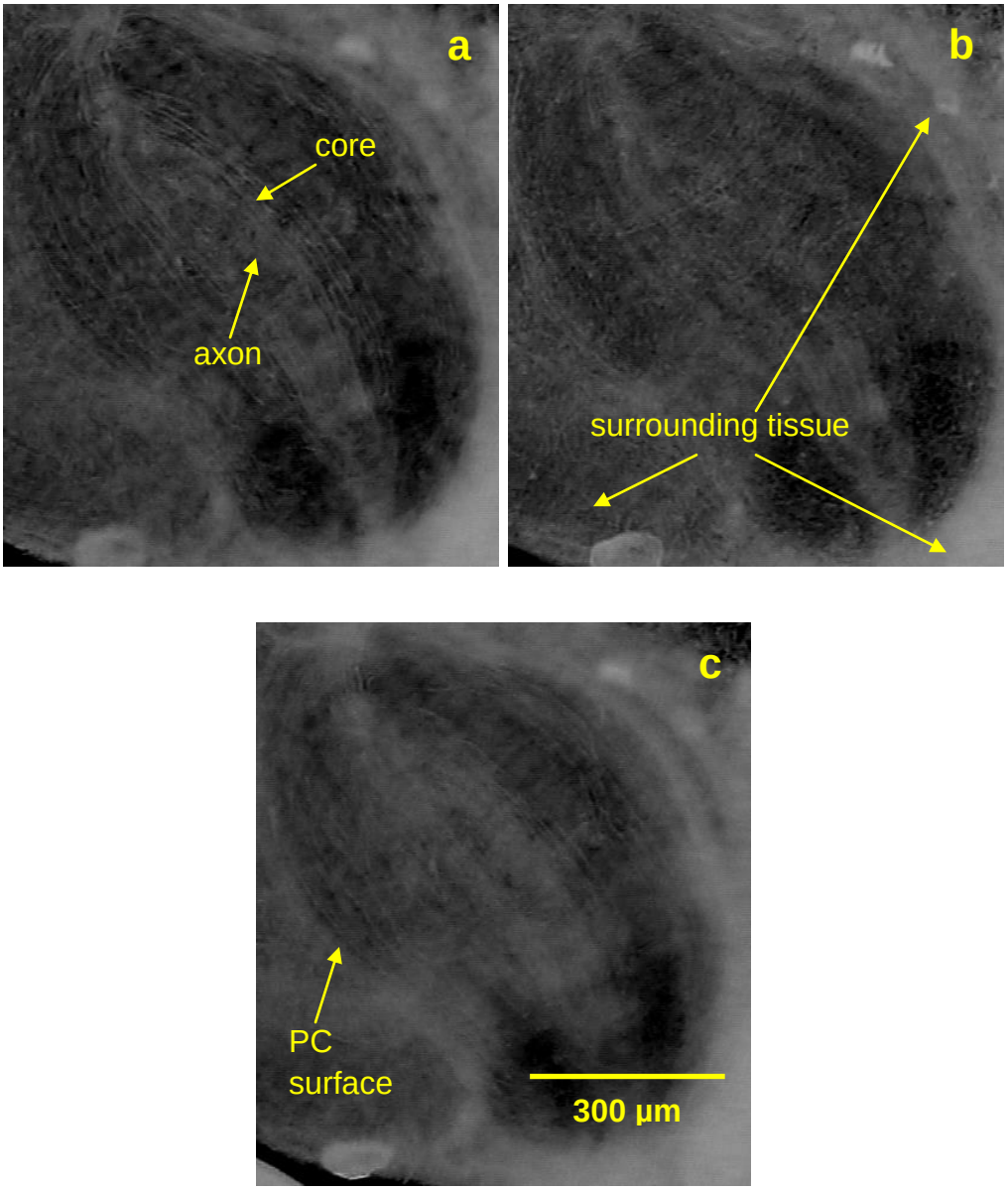

Figure 4.2. Osmotic swelling of a PC, extracted from the heel area of the hind foot of an 8-year-old *mixed-breed horse*; in this case the surrounding tissue was not removed and the osmotic response was attenuated; (a) in 0.15 M NaCl, (b) 30 seconds after exchange for deionised water, (c) equilibrium after 1h.

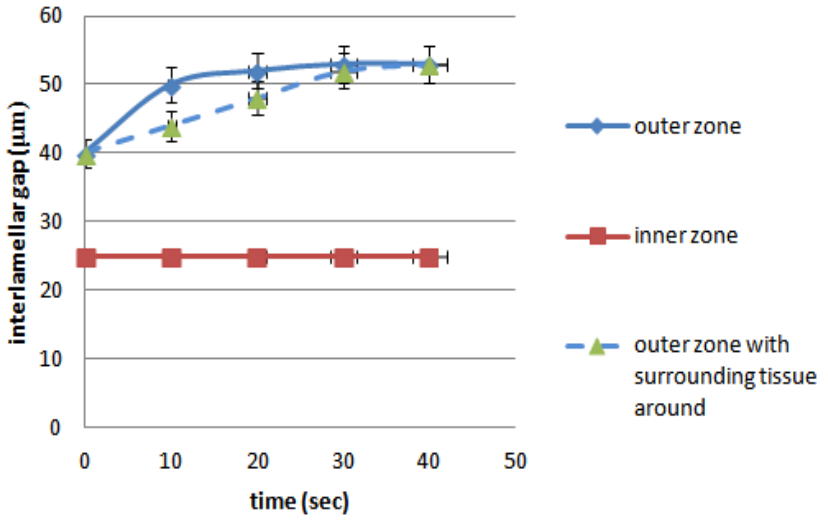

Figure 4.3. Time course of changes in interlamellar spacing in outer and inner zones (full blue and red lines, respectively) for the case of a PC completely separated from its surrounding tissue, following exchange of 0.15M NaCl for deionised water; the dashed blue line shows equivalent measurements for the case of a corpuscle incompletely separated from its surrounding tissue, showing an overall change of similar magnitude but on a longer timescale.

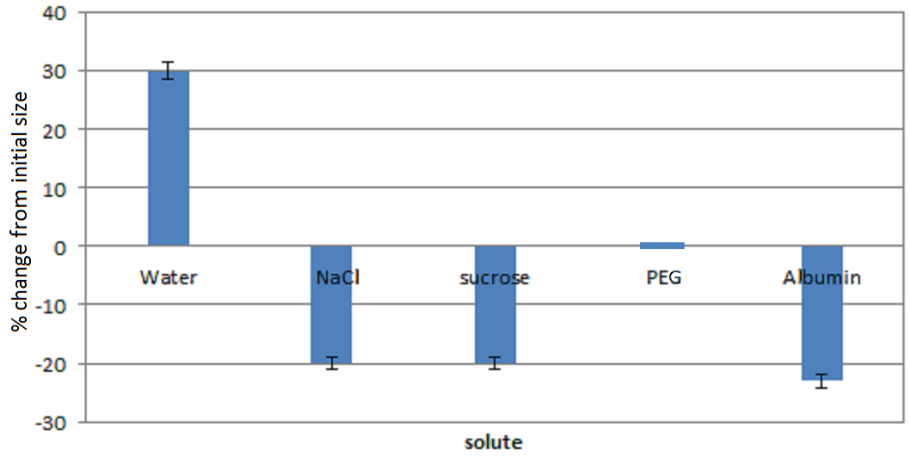

Figure 4.4. Changes in interlamellar spacing after 15 seconds incubation with deionised water or osmolytes (concentrations as in text). The error bars indicate the standard error in the mean (n = 8).

4.2 Tracer-Uptake Experiment

Solute diffusion was studied using two small, fluorescent molecules, rhodamine B (M.W 479 Da) and fluorescein (M.W 332 Da) representing the range of nutrients and metabolites whose exchange is important for the metabolism of the PC. A total of 20 corpuscles were used with incubation periods of 5min to 18h, generally using the two tracers simultaneously to facilitate detailed comparison of distributions. After the required incubation period the corpuscles were washed and transferred to a saline-filled chamber on the stage of the confocal microscope and image stacks were acquired at 1µm separation through the depth of the corpuscle. The distribution of fluorescence across selected line profiles was quantified using Image J, as described under Methods.

Figure 4.5 shows the time-course of uptake of fluorescein and rhodamine B. (Some higher resolution images are shown in fig. 4.6 for rhodamine B and fig. 4.7 for fluorescein.) Rhodamine B appeared in the tissue before fluorescein. Both tracers first appeared in the core of the corpuscle. The images suggest that the site of initial entry was close to the axon. As described in section 3.2, blood vessels share the same entrance as the axon, and at short times tracer was clearly visible in these vessels, before diffusing into the surrounding tissue. Rhodamine B was present in the core at high concentration (close to that in the perfusing solution) after only 5 minutes incubation (see image a' in fig. 4.5: this observation was repeated in ten PCs).

Images b and b' in fig. 4.5 (after 8 minutes incubation) indicate both tracers in high concentration along the axon and distribution through the inner zone towards the outer zone; however, there is a sharp change in concentration between the outer and inner zones, which may correspond to a barrier at the transition. In the outer capsule a high concentration of rhodamine B delineates the collagen network, but the distribution of fluorescein is more uniform. Despite rhodamine B being the larger molecule it appeared to diffuse faster into the core than fluorescein. This may be because rhodamine B is positively charged (its uneven distribution in the outer region probably arises from electrostatic interactions with the negative charges on the extracellular matrix) whereas fluorescein is negatively charged, demonstrating the existence here of a charged structure as the primary transport resistance – probably associated with basement membrane.

Figure 4.8 presents intensity profiles across the width of the PC, showing the distribution of fluorescein (top panel) and rhodamine (lower panel) at different times. After 18 h a uniform distribution has been attained throughout the corpuscle; at earlier times the intensity gradients indicate that there is transport across the outer surface with rapid initial transport into the core (at 8 minutes the distribution of both tracers is higher towards the centre of the PC). Superposition of fluorescence images and transmitted-light images at high resolution (fig. 4.7) shows that the fluctuations in fluorescence intensity which can be seen in fig. 4.8 are correlated with the lamellar structure, with regions of high intensity corresponding to the interlamellar spaces.

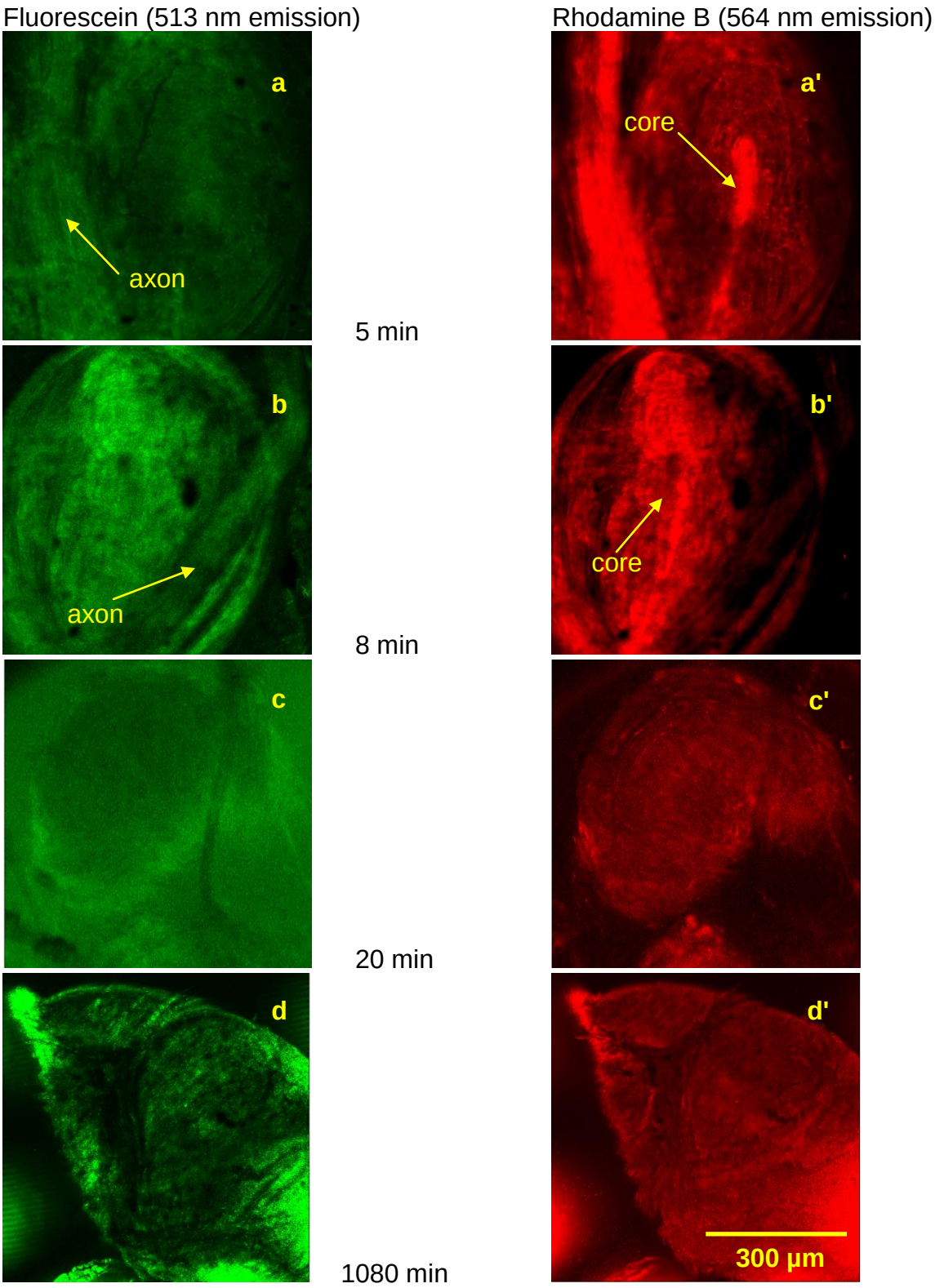

Figure 4.5. Fluorescence images of the time course of uptake of fluorescein and rhodamine B: (a & a') 5 min incubation, PC from the heel area of the hind foot of a 4-year-old *mixed-breed horse*; (legend continues on next page)

(b & b') 8 min incubation, PC from the front heel of a 4-y-old *mixed-breed horse*; (c & c') 20 min incubation, PC from the front heel of a 15-y-old *mixed-breed horse*; (d & d') 18 h incubation; PC from the front heel of a 6-y-old *racehorse*; the representative 1 µm slices from a confocal stack are not normalised; at 5 min and 8 min the dye distributions are non-uniform – higher in axon and core, at 20 min and 18 h the distributions are more uniform; quantitative analyses of tracer distribution are given in fig. 4.8.

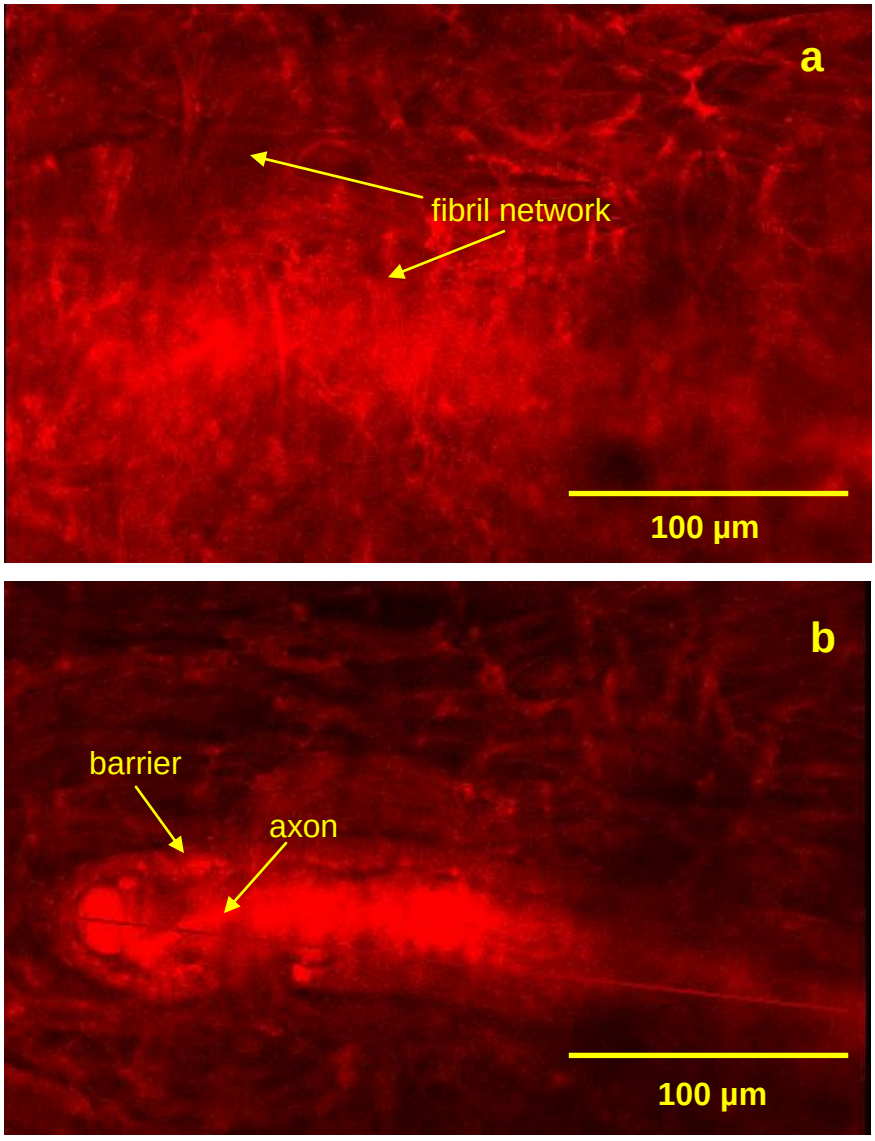

Figure 4.6. High resolution images of tracer distribution in a PC incubated in rhodamine B for 5 min: (a) 30 µm deep in the PC, showing the fibril network around the inner zone, (b) section showing dye distribution affected by an apparent barrier around the core; images are representative 1 µm slices from a confocal stack.

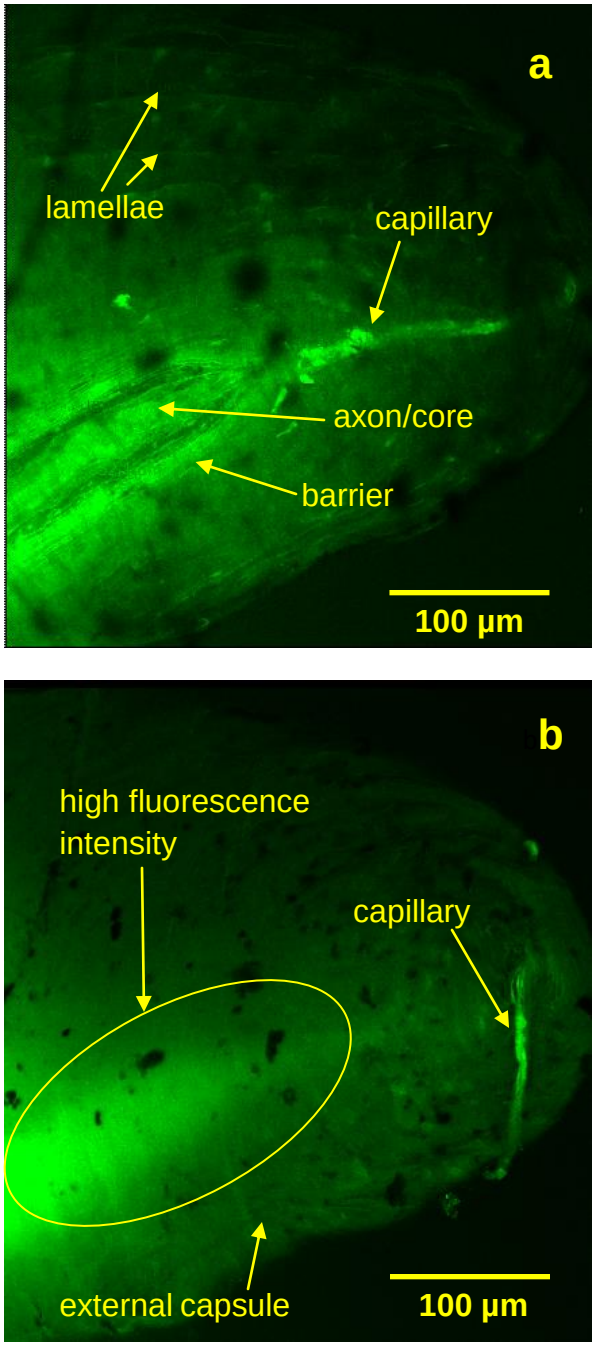

Figure 4.7. Superposition of fluorescence and transmitted light images at high resolution; PC incubated in fluorescein for 8 minutes; images are representative 1 µm slices from a confocal stack: (a) through the centre of the PC − regions of high fluorescence intensity correspond to the interlamellar spaces, (b) through the external capsule – the high fluorescence intensity in the circled region is probably a geometric effect (intersection of the image plane with the curved capsule surface).

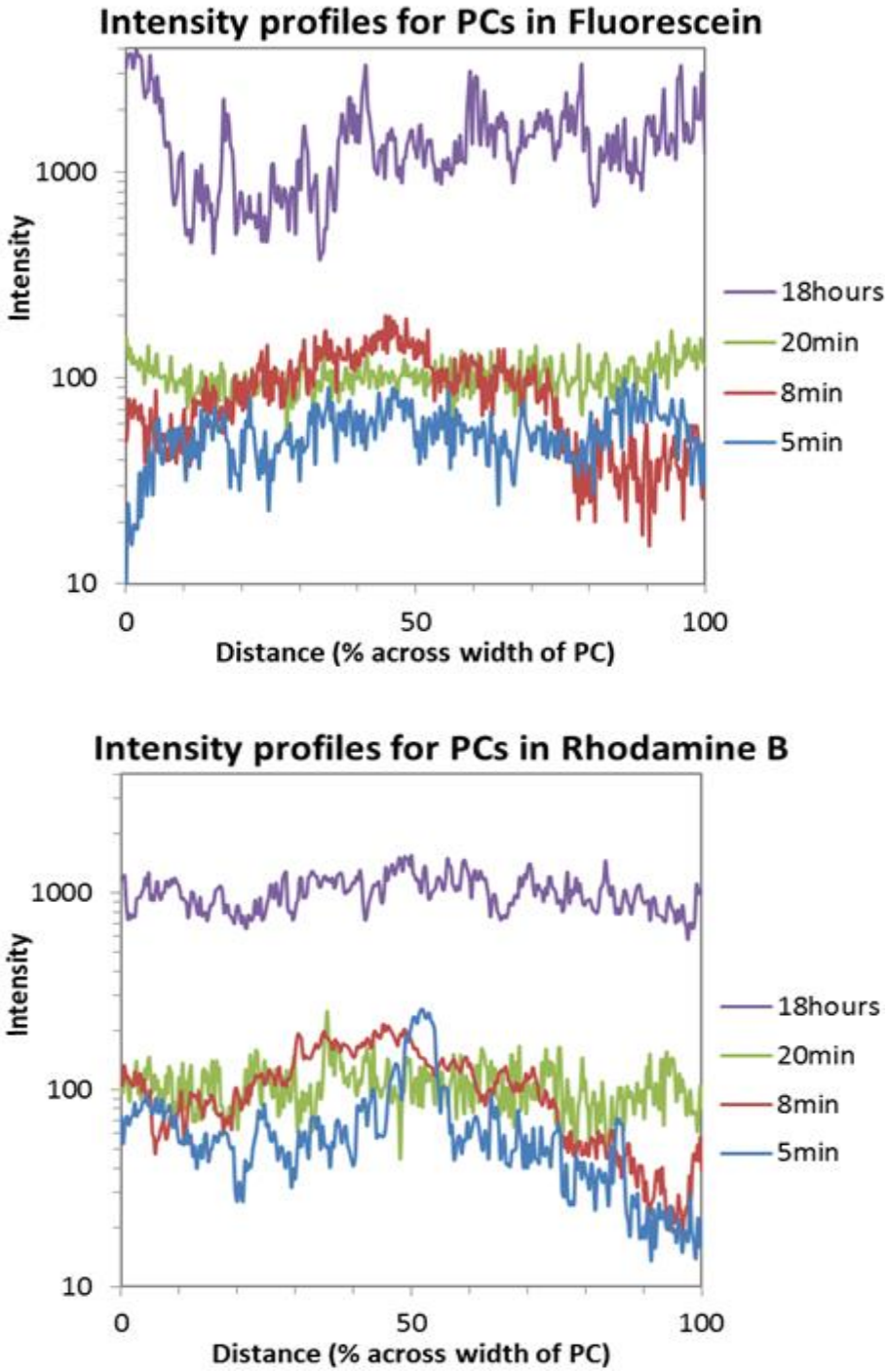

Fig.4.8. Intensity profiles showing the distribution of fluorescein (top panel) and rhodamine B (lower panel) at different times; profiles are taken (from fig. 4.5 images) through the midpoint (maximum diameter) of the corpuscle; Intensity (arbitrary units) is normalised to a stock solution of fluorophore; distance is scaled by maximum diameter to allow comparison between corpuscles of different size.

4.3 Discussion

The osmotic stress experiments revealed different properties in the outer and inner lamellae. The behaviour of the outer lamellae was consistent with them providing a partially permeable osmotic barrier. The limited extent of the swelling under hypo-osmotic conditions suggested that the capsule is either rather rigid or quite permeable. Comparison with other tissue such as the renal basement membrane suggests that the latter is unlikely to be the case for a large protein such as albumin; evidence for the former is provided by the rigidity found in the mechanical tests described in Chapter 5. That the capsule also shrank by relatively little in the face of high osmotic pressure gradients also suggests rigidity under compressive loads. This is also consistent with the mechanical testing and may be essential for the corpuscle to transmit mechanical loads from the periphery to the core. The lack of response in the core may suggest that it is mechanically even stiffer than the outer region or there are pathways that permit rapid and total equilibration with the osmolytes. One such pathway might be the blood vessels entering the core. However, most capillary beds, except the specialised fenestrated capillaries of organs such as the kidney, do not allow the unimpeded exchange of proteins. We cannot exclude the possibility that the corpuscle capillary beds became leaky during preparation, but the mechanical hypothesis seems plausible.

The sharp boundary between inner and outer regions was unexpected, but this was also seen in the tracer uptake experiments.

The tracer-uptake experiments demonstrated relatively rapid transport along blood vessels surrounding the axon, and suggest a barrier between the PC core and the inner zone. In Chapter 3 we discussed the two possibilities that blood vessels entering the core may be involved in haemodynamic sensing by the corpuscle or to deliver nutrition to the core. The tracer studies suggest a need for the latter, though they do not exclude the former.

The shape of the tracer concentration profiles in the outer capsule and their change with time suggest that transport occurs by diffusion [86]. More detailed structural analysis would be required to analyse transport in terms of a series of lamellar barriers separated by fluid spaces but it is useful to obtain an order of magnitude estimate of the overall process using dimensional arguments [87]. The diffusion coefficient has dimensions of length^2/time. We can estimate its magnitude by taking as the characteristic length the radius of the capsule (~300 μm) and the characteristic time as that required for tracer equilibration (~20 min). These give a value of diffusion coefficient ~ 8×10^{-7} cm^2 s^{-1}. This is almost two orders of magnitude lower than the free diffusion coefficients of these small molecules [88], but is comparable to coefficients found in tissues such as cartilage. We can therefore deduce that the lamellae do indeed constitute a significant barrier to the movement of solutes, such as those involved in nutrition – this provides further confirmation of the need for a blood supply to the core region.

Chapter 5

Corpuscle mechanics

Section 5.1 will discuss the mechanical behaviour of the PC under static compression and sinusoidal stimulation at 50, 100, 200 and 400 Hz; an aspiration test will be described in section 5.2. The results for sinusoidal stimulation will be compared to predictions obtained from the electronic analogue of a theoretical model of mechanotransduction in the PC (section 5.3). Results obtained from all the experiments on mechanical properties of the corpuscle will be summarized in section 5.4. A computer file of video recordings of mechanical stimulation of the PC is attached to this thesis.

5.1 Lamella displacement under mechanical load

The experimental method is described in section 2.6.3. A fresh PC was inserted into the paraffin-wax frame and covered with 0.15M NaCl solution. The corpuscle was positioned against a metal plate attached to the frame wall (see fig. 2.7) in order to fix its position during mechanical stimulation.

5.1.1 Dynamic displacement

In this case sinusoidal stimulation at 50, 100, 200 and 400 Hz was applied to the surface of the PC. Peak-to-peak amplitude was nominally 20 μm (8 μm at 400 Hz, see section 2.6.3); measured values of peak-to-peak amplitude (from microscope images, see below) were 15.1, 24.7, 28.4 and 8.1μm (± 1 μm) at 50, 100, 200 and 400 Hz, respectively. For more detailed explanation of how displacement measurements were made see section 2.5.3. Figure 5.1 (duplicate of fig. 2.10) shows a corpuscle positioned between fixed and moving metal plates, with features marked by arrows. The positions of these features were tracked from grey-scale profiles along the same line in a series of images (covering two stimulation cycles in phase steps of 36 degrees) and are shown as the data points in figure 5.2. (A few points are missing because not all of the four features were visible in every profile.) Figure 5.2 also shows sine-wave fits to these data points – to produce these fits, a sine wave of the appropriate frequency is specified by the variables of baseline, amplitude and phase, and these variables are adjusted to minimise the squared error between the sine wave and the chosen set of experimental data points; repeating this procedure for each data set provides amplitude and phase information for the tissue displacement at the four different frequencies, as a function of position (depth) within the corpuscle.

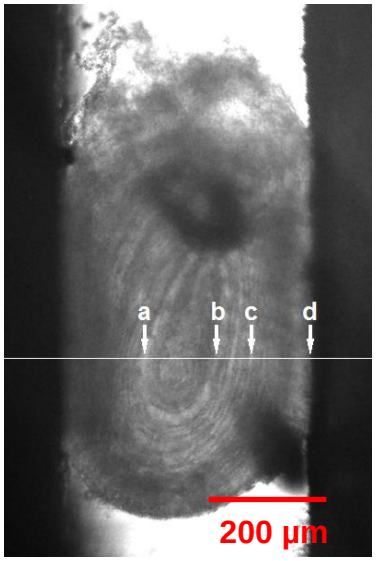

Figure 5.1. PC from the heel of the hind hoof of an 8-year-old *mixed breed horse*, positioned between (left) the fixed metal plate, and (right) the moving metal plate. The arrows indicate features selected for tracking during the motion.

The mid-point of the corpuscle may be defined as the average of positions *a* and *b* which define the inner zone (see fig. 5.1), and the sinusoidal displacement of this mid-point may be calculated as the mean of the sine-wave fits for *a* and *b* (see fig. 5.2). Hence the sinusoidal displacements of *a, b, c, d* can be calculated relative to the displacement of the mid-point, as in figures 5.3 and 5.4 which show amplitude and phase of the motions of *a*, *b*, *c* and *d*.

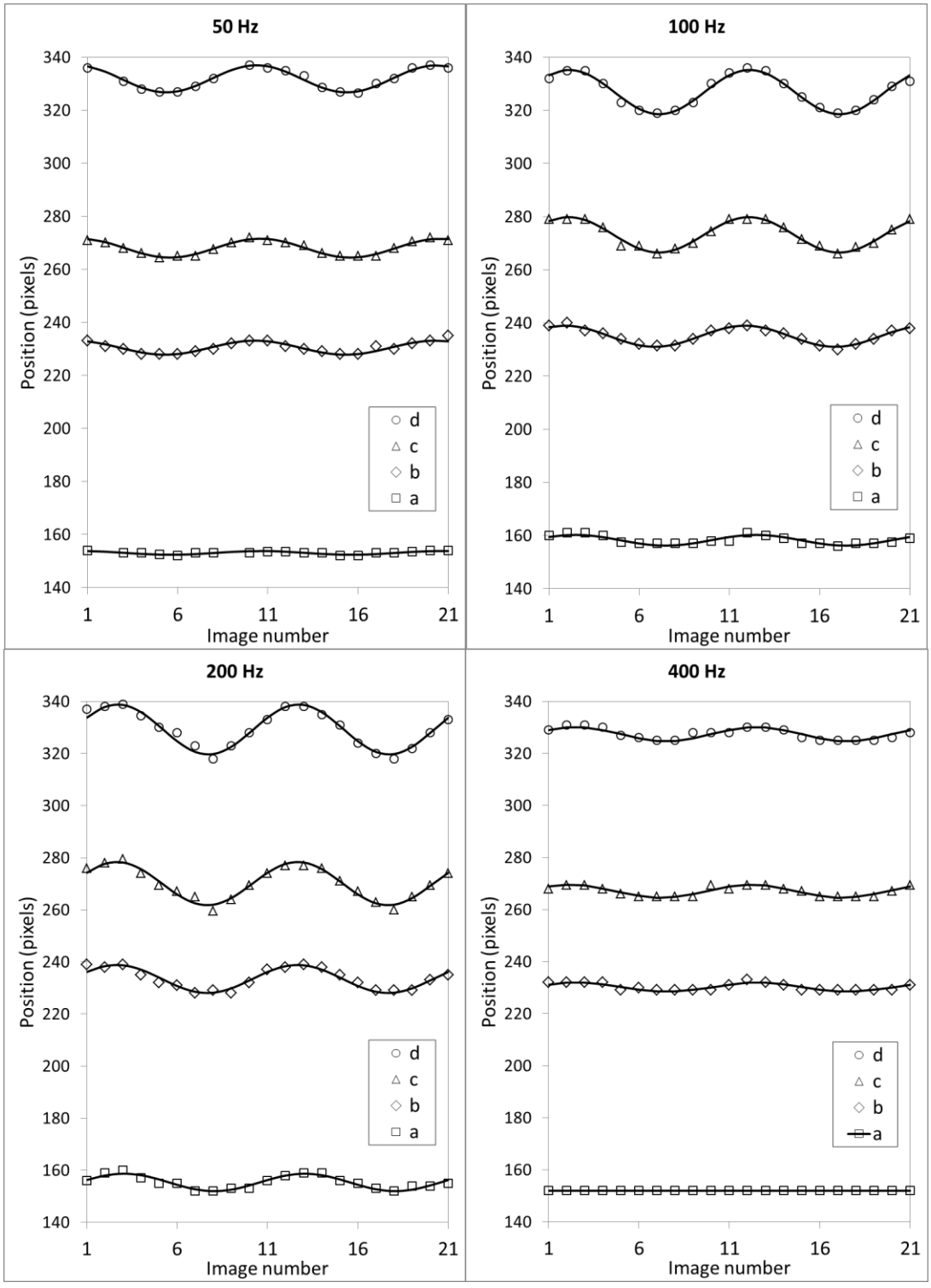

Figure 5.2. Positions of tracked features in series of 21 images of a PC (sample from fig. 5.1). The images cover two stimulation cycles in phase steps of 36 degrees. The features *a* and *b* mark the boundary between inner and outer zones of the corpuscle (see fig. 5.1); (legend continues on next page)

c is a lamellar feature in the outer zone and *d* is the surface of the corpuscle; the position of the centre of the corpuscle is assumed to be midway between the positions of the features *a* and *b*. The four panels show results for stimulation at 50, 100, 200 and 400 Hz. Estimated error in the individual data points is 1-2 pixels.

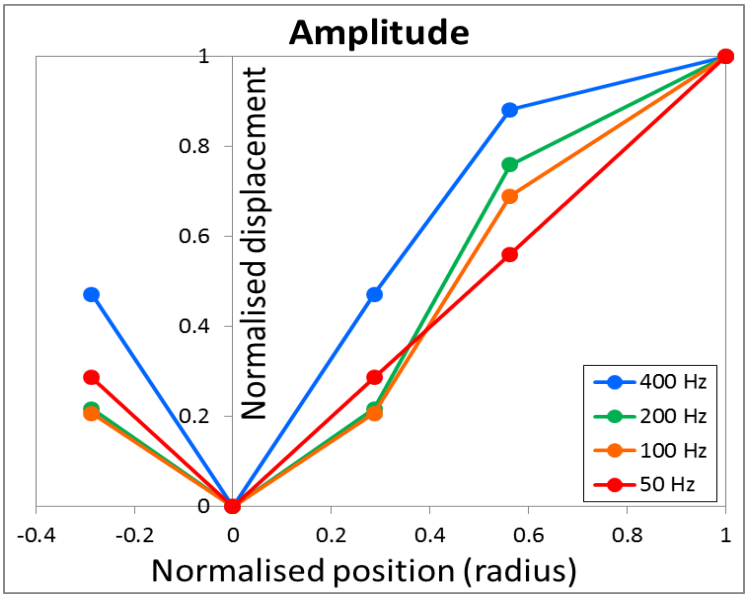

Figure 5.3. Displacement amplitude (relative to amplitude at the outer surface) as a function of position; all motions are measured with respect to the mid-point of the corpuscle (average position of features *a* and *b*); from right to left on the horizontal axis, the five sets of data points correspond to the following features: *d*, *c*, *b*, mid-point and *a* (as shown in fig. 5.1); estimated errors in normalised amplitude are in the range 5% to 10%. The graphs suggest that the outer zone of the PC acts as a high-pass filter for displacement, with 400 Hz signals undergoing less reduction in amplitude than 50 Hz signals as they travel through the outer zone (from *d* to *c* to *b*).

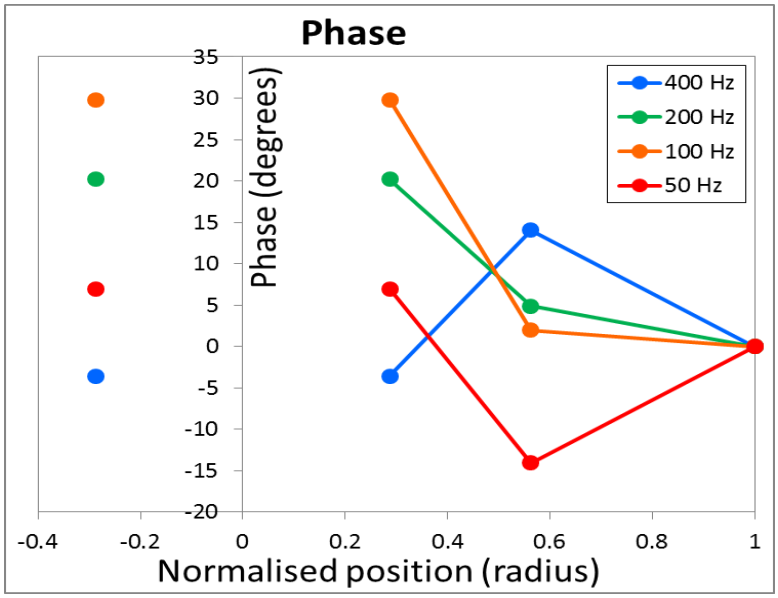

Figure 5.4. Displacement phase (relative to phase at the outer surface) as a function of position; all motions are measured with respect to the mid-point of the corpuscle; from right to left on the horizontal axis, the four sets of data points correspond to the features *d*, *c*, *b* and *a* (as shown in fig.5.1); estimated errors in relative phase are in the range 5 to 10 degrees.

5.1.2 Static displacement

To investigate the effect of static displacement of the outer surface, a fresh PC was subjected to a 30 μm compression (using the micromanipulator connected to the moving plate, see figs. 2.7 and 2.8). The compression was then released slowly (10 seconds per step) in steps of 5 μm. As in the case of sinusoidal displacement, the positions of image features were tracked via grey-scale line profiles across a sequence of images (fig. 5.5).

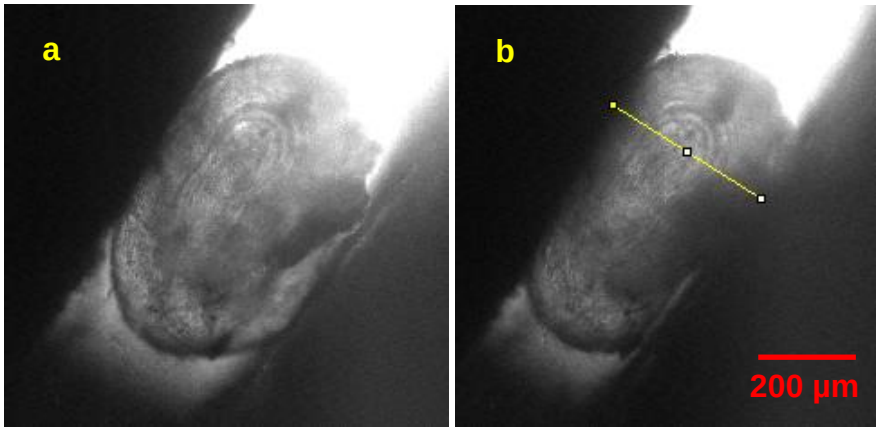

Figure 5.5. The PC (extracted from the heel area of the hind hoof of a 10-year-old *mixed-breed horse*) is placed between two plates, one of them (top left) stationary and the other (bottom right) moving; (a) uncompressed; (b) displacement of 30 µm applied at the surface of the capsule; line profiles across the corpuscle in fig .5.6 are based on the line shown in fig.5.5 (b).

In this case, in contrast to the response at frequencies of 50 Hz and above shown above, a change in shape of the corpuscle occurred only in the outermost layers, and the remainder of the corpuscle (including all features which could be easily tracked) did not demonstrate any geometrical distortion. This is most clearly seen in a video assembled from the sequence of still frames, but can also be seen in the line profiles in figure 5.6 – different parts of the corpuscle are displaced by the same amount, corresponding to an overall translation but no change of shape. It seems unlikely that this corresponds to the natural behaviour of the corpuscle – some transmission of the mechanical stimulus to the centre of the corpuscle is expected, at least according to accepted models.

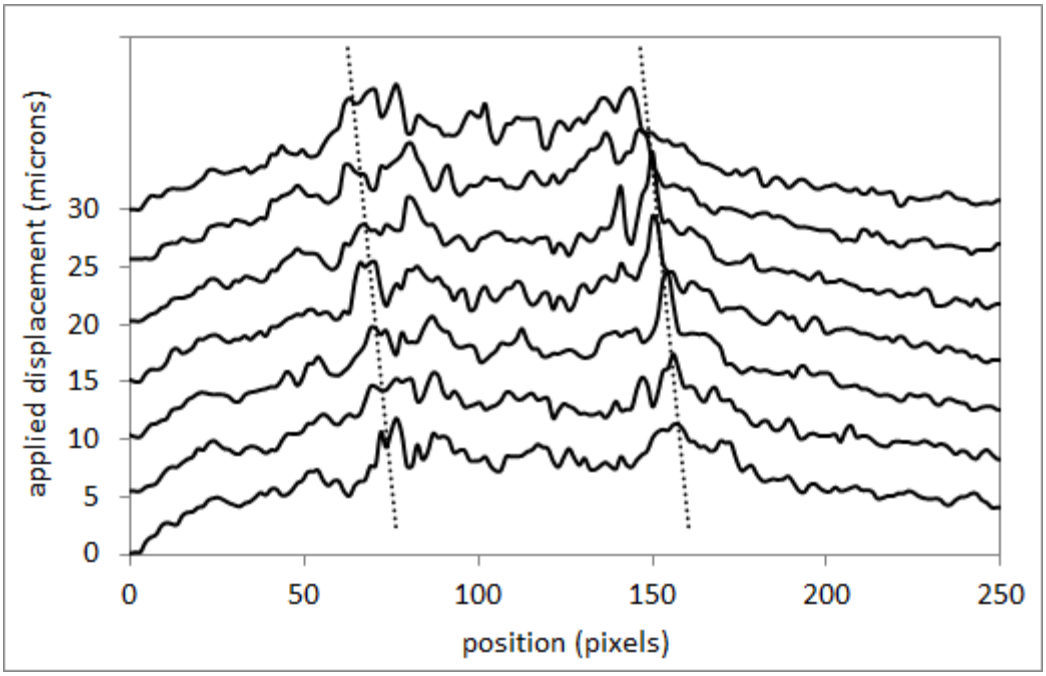

Figure 5.6. Line profiles across the corpuscle for static displacement of the surface in steps of 5 μm; dotted lines indicate translation of most of the corpuscle in this case (towards the fixed plate when pushed by the moving plate); 1 pixel = 1.48 μm.

Microscopic observation suggests that during lateral compression the PCs get longer, i.e., the compressive strain distributed perpendicularly to the lamellae is accompanied by a tensile strain along the lamellae (longitudinal direction). On removal of the compression, the PC tends to return to its original shape, presumably due to lamella stiffness and the resilience of the collagen fibril network. Similarly, a microindentation test described below confirms the ability of the PC to restore its shape after significant localized distortion (fig. 5.7).

The difference with the high frequency behaviour could indicate that the corpuscle does not transduce at low frequencies. This may perhaps because the lamellae are

permeable to water on these time scales, although it is difficult to reconcile this possibility with the permeability measurements above. However, it is possible that the corpuscle does not transduce low frequencies because of the difficulty in distinguishing signal from noise associated with movement etc.

Figure 5.7. PC extracted from the heel area of the hind foot of a 5-year-old *Shire horse*. Indentor diameter 604 µm. Mechanical deformation of the lamella structure produced by microindentation; the right panel shows restoration of shape when the probe is removed, presumably due to lamellae stiffness and the resilience of the collagen fibril network. Apart from the recoil the main point of interest is that the lamellae only ~ 1 indentor diameter away from the site are completely unaffected by a rather large indentation of almost 1/3 diameter of the corpuscle

5.2 Micropipette aspiration

The experimental method and purpose of the aspiration experiments are described in section 2.6.2. In summary, suction is applied to a circular region of the PC surface, with a view to producing a “bulge”. Attempts were made to perform this

technique on a fresh PC, but it was found that the maximum available (negative) pressure of around 5 kPa was insufficient to aspirate the external membrane, using a pipette of 0.3 mm internal diameter. [A similar observation had been made previously in the Exeter laboratory, as part of a pilot study for the present project (personal communication from N Garrett).] Consequently, it was decided to disconnect the hydrostatic system (fig. 2.6) so that increased suction could be applied directly, using a syringe. Measurable distortion could now be produced, as shown in fig. 5.8, although it was not possible accurately to measure the applied (negative) pressure.

Aspiration produced a roughly hemispherical protrusion of the outer surface, which was followed faithfully by around five of the underlying lamellae. As pressure was maintained constant the length of the protrusion increased, as shown in figure 5.9. After approximately 5 minutes the movement became much slower and interlamellar struts running straight between the deformed and undeformed lamellae became very clearly visible, suggesting that tension in these was limiting further movement. (Note that this timescale is much longer than the adaptation timescale of the PC's neural response.) As in the indentation experiments, deformation was limited to the region of force application.

An order of magnitude estimate of the forces involved can be obtained by assuming the cap is hemispherical and applying Laplace's law for the deformation of a thin shell: $P = T/R$

where P is the aspiration pressure, T is the lamellar tension and R is the radius of curvature of the protrusion. Estimating $P = 2.5 \times 10^4$ Pa and $R = 150$ µm, we obtain $T \sim 4$ N m^{-1}.

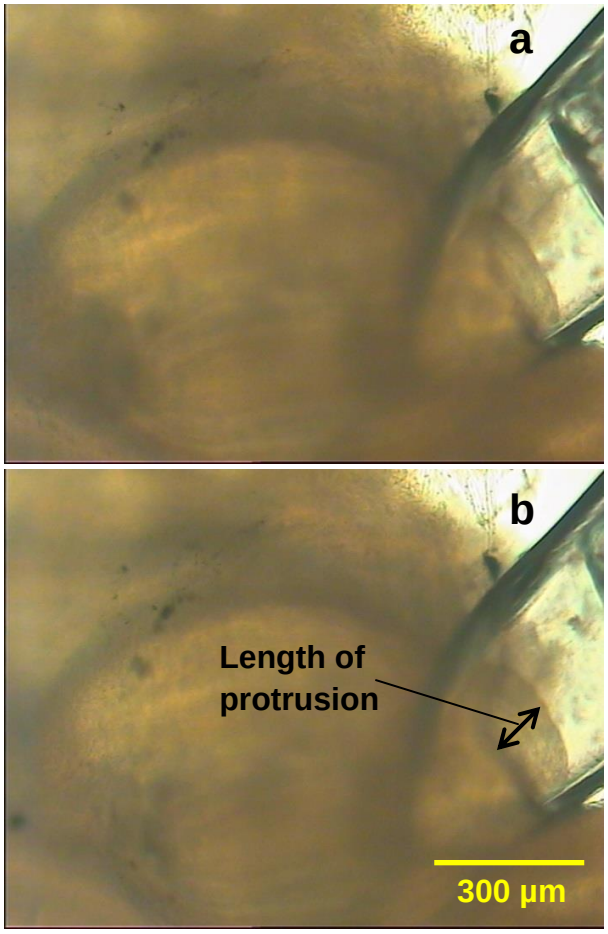

Figure 5.8. Aspiration of a PC, size 1.2 × 0.7 mm, extracted from the heel area of the front foot of a 12–year-old *mixed-breed horse*; pipette diameter 0.3 mm; (a) at the time that the suction is applied; (b) 210 seconds later; (the arrow indicates the length of protrusion).

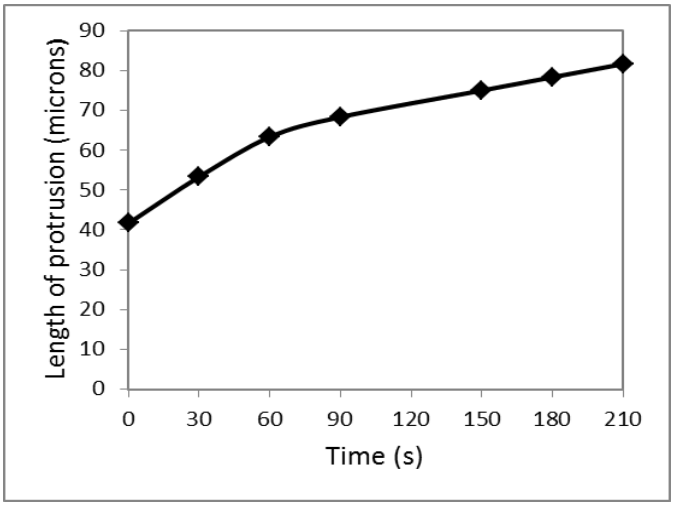

Figure 5.9. The graph represents variation of length of protrusion of part of the corpuscle sucked into the pipette with time after application of the suction. The measurements were stopped after 210 seconds.

5.3 Electrical analogue of the model of the Pacinian Corpuscle

A wide range of measurements was made on the electronic analogue of the theoretical model of Loewenstein and Skalak [36], described in chapter 2, section 2.5.1. The data obtained provide a broader overview of the model's performance than that presented in Loewenstein and Skalak's original paper, particularly in terms of the variation of pressure and displacement as a function of position within the corpuscle.

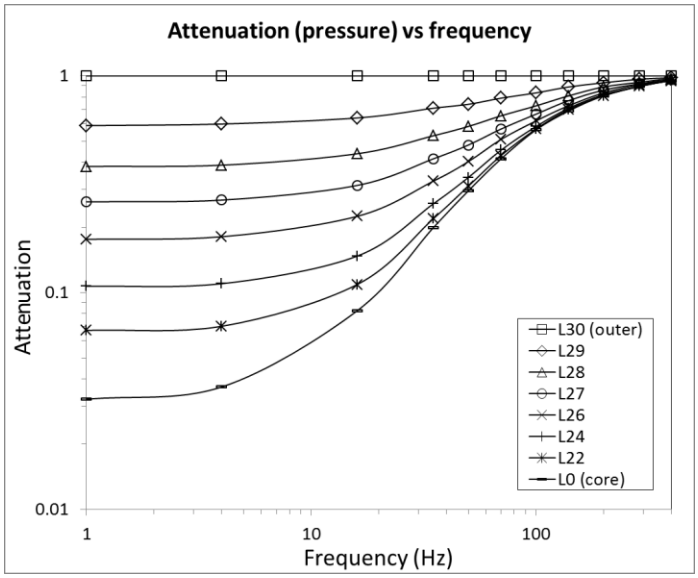

Figure 5.10. Sinewave response for pressure amplitude (attenuation factor as a function of frequency) measured at eight positions within the model corpuscle. Pressure is represented by voltage in the electrical analogue.

Figure 5.10 shows the attenuation of pressure (measured as voltage amplitude at the nodes of the 30-stage electrical analogue) for sinusoidal stimuli in the frequency range 1 to 400 Hz. It can be seen that attenuation factors at the various positions with the model corpuscle are close to unity at higher frequencies, but decrease as frequency falls, with the responses flattening below 5 Hz. This variation with frequency is due to the decrease in the impedance of the capacitative (compliance) elements as frequency rises; the capacitative (compliance) impedances become negligible compared to the resistive impedances at high frequencies, see figure 2.12, chapter 2.

The same data are plotted as a function of position (lamella number) in figure 5.11. It can be seen that the majority of the fall in pressure amplitude occurs over the outer lamellae, L20 to L30.

Figure 5.12 shows the phase of the pressure wave (measured as voltage phase at the nodes of the 30-stage electrical analogue, with respect to the phase of the input sine wave) as a function of position (lamella number) and frequency. Comparing to figure 5.10, it can be seen that the slope of the amplitude-response curves (fig. 5.10) is related to the magnitude of the phase shifts (fig. 5.12); slopes and phase shifts both fall as frequency rises from 50 Hz to 400 Hz.

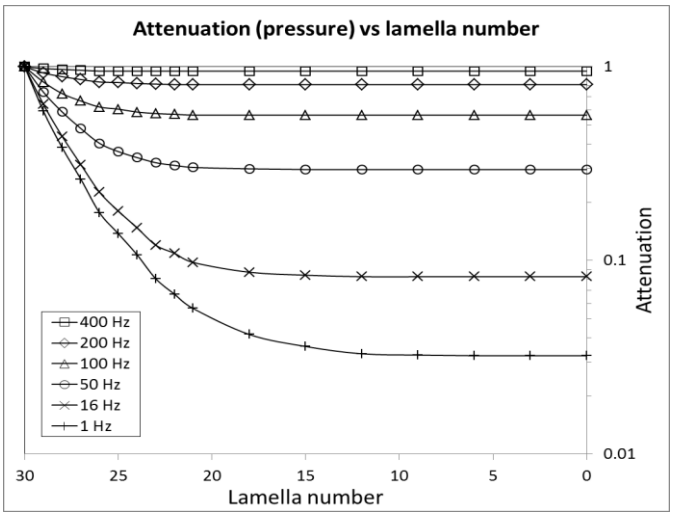

Figure 5.11. Sinewave response for pressure amplitude (attenuation factor as a function of position, i.e., lamella number) measured at various frequencies in the range 1 to 400 Hz; (data from fig. 5.10). Pressure is represented by voltage in the electrical analogue.

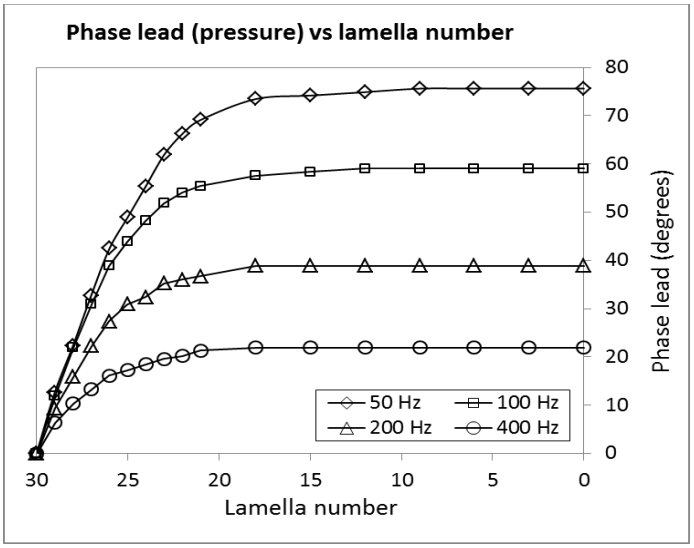

Figure 5.12. Sinewave response for pressure phase as a function of position (lamella number) measured at various frequencies in the range 50 to 400 Hz. Pressure is represented by voltage in the electrical analogue.

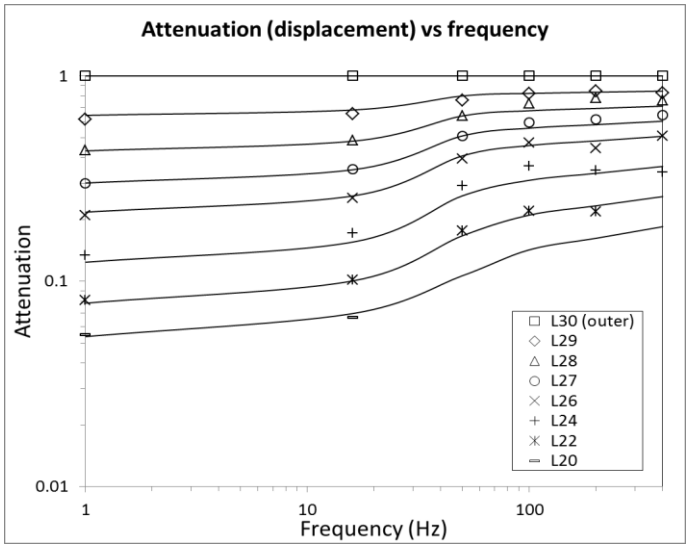

Figure 5.13. Sinewave response for displacement amplitude (attenuation factor as a function of frequency) measured at eight positions within the model corpuscle. Displacement is represented by electric charge in the electrical analogue.

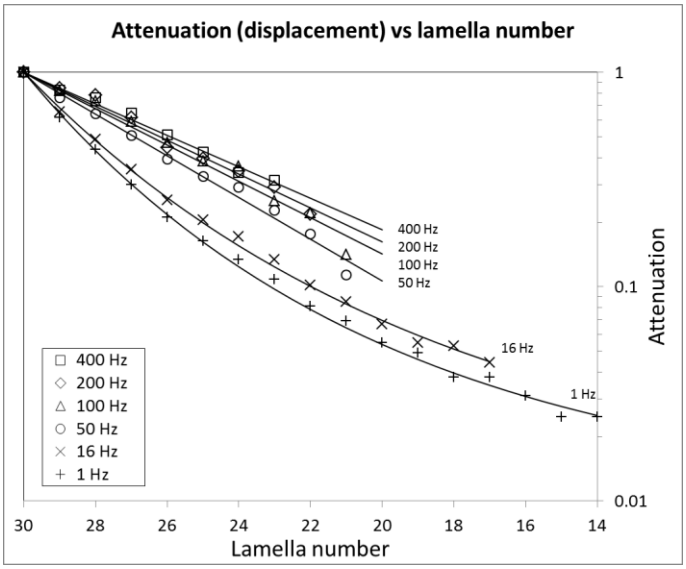

Figure 5.14. Sinewave response for displacement amplitude (attenuation factor as a function of position, i.e., lamella number) measured at various frequencies in the range 1 to 400 Hz; (data from fig. 5.13). Displacement is represented by electric charge in the electrical analogue.

Figure 5.13 shows the attenuation of displacement for sinusoidal stimuli in the frequency range 1 to 400 Hz. (Displacement is measured in terms of charge on the various capacitors C_{mi} in the electrical analogue – see section 2.6; in practice this involves a differential measurement of voltage across each capacitor.) It can be seen that the attenuation factor for displacement is less strongly dependent on frequency than that of pressure (fig. 5.10). The same data are plotted as a function of position (lamella number) in figure 5.14 (data for higher frequencies are limited because the differential signal corresponding to displacement (see section 2.6) becomes too small to measure accurately). Figure 5.15 shows displacement phase as a function of position (lamella number) and frequency, measured in terms of the phase of the measured differential voltages – as for the case of pressure, phase

shifts are higher at 50 Hz than at 100 Hz; this is related to the variation of slope with frequency for the curves in fig 5.13.

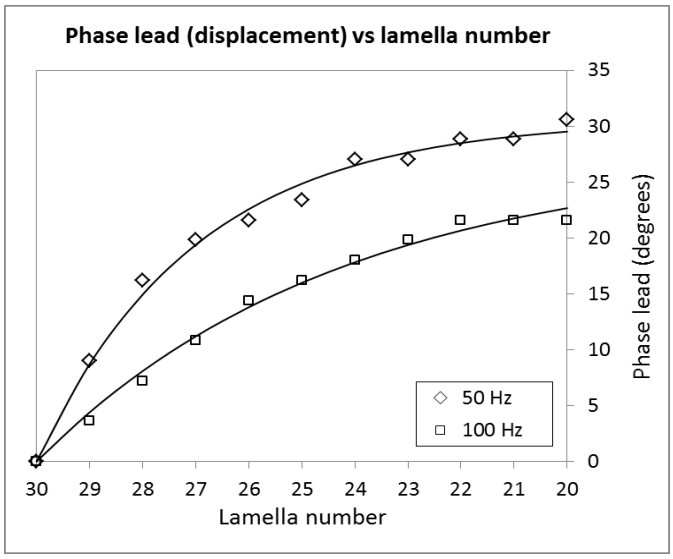

Figure 5.15. Sinewave response for displacement phase as a function of position (lamella number) measured at 50 and 100 Hz. Displacement is represented by electric charge in the electrical analogue.

5.4 Discussion

Sections 5.2.1 and 5.2.2 present microscope measurements on the effect of dynamic and static mechanical stimuli on the corpuscle. Although these experiments were repeated many times, there were few successful outcomes. In particular, the dynamic experiment in section 5.2.1 was successfully completed only once – in addition to difficulties in preparing and mounting the corpuscle

without damage, only a small proportion of corpuscles were sufficiently transparent to allow good visualisation of the lamellae.

The experimental results for sinusoidal stimulation in section 5.2.1 may be compared to predictions of the electrical analogue in section 5.4. Figure 5.16 shows the experimental results for amplitude and phase (duplicates of figs 5.3 and 5.4) and corresponding predictions of the electrical analogue (curve-fits from figs 5.14 and fig 5.15, replotted in terms of distance in microns as opposed to lamella number, using data on lamella spacing from [36]). Some discrepancies are apparent but, given the approximate nature of the model and the difficulties involved in obtaining the experimental data, the overall agreement is surprisingly good. In particular, both experiment and model show phase shifts of less than 30° in all cases – this is perhaps unexpected because a multi-element network has the potential for much larger phase shifts. This point is worth further consideration.

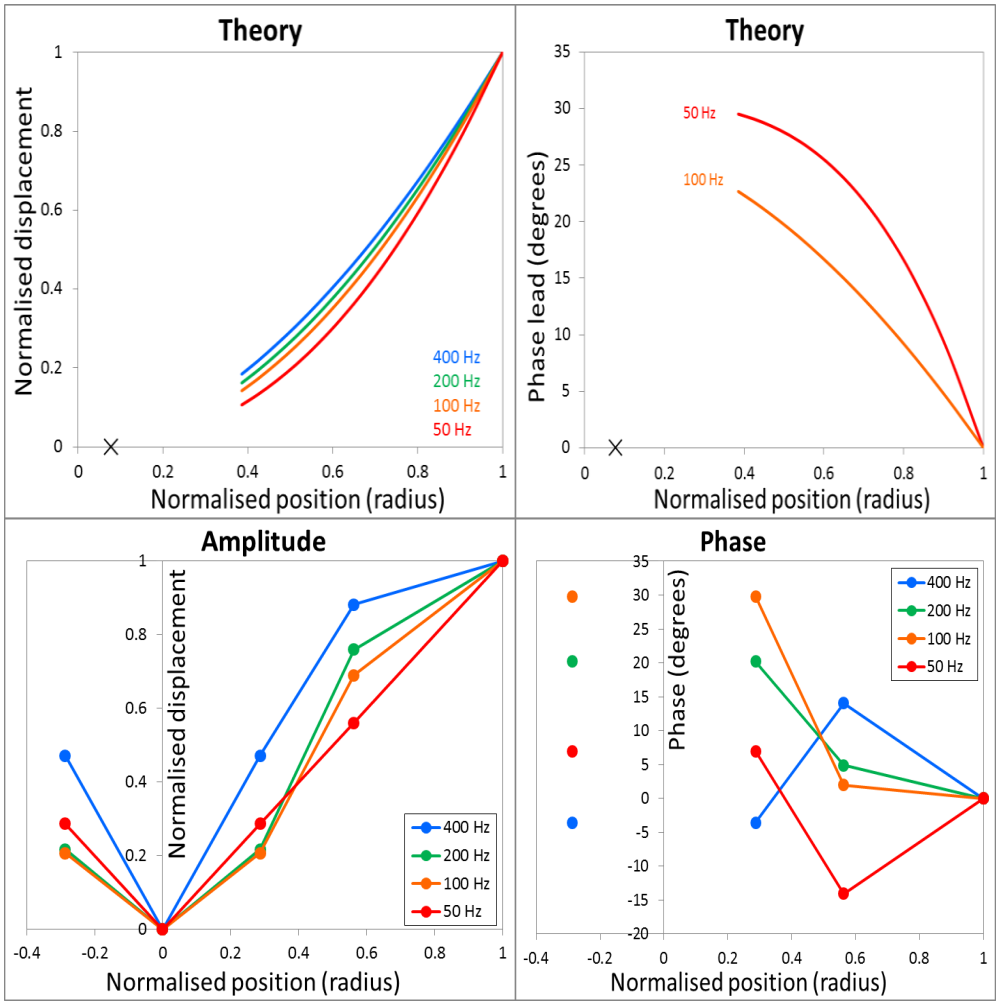

Figure 5.16. Experimental measurements of lamellar displacement observed in an equine PC in response to external, sinusoidal mechanical stimulation (lower panels, taken from figs. 5.3 and 5.4) and corresponding model data from the electrical analogue of Loewenstein and Skalak (upper panels, replotted from figs. 5.13 and 5.14); in the top left and bottom left panels, displacement amplitude is shown as a function of position (radius), normalised to a value of unity at the PC surface (input); in the top right and bottom right panels, displacement phase is shown as a function of position (radius), measured with respect to displacement phase at the PC surface (input).

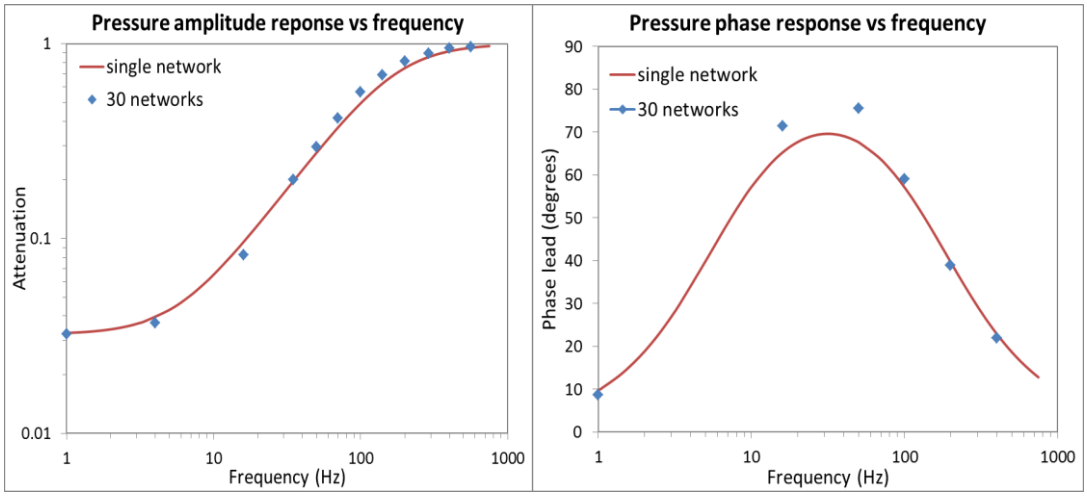

Figure 5.17. Pressure amplitude and phase response for 30 networks (Loewenstein & Skalak model) and a single network.

Figure 5.17 compares the amplitude and phase responses for pressure transmission through the chain of 30 networks in the Loewenstein-Skalak model, with those from a single network of the same type (fig. 5.18) whose components (two capacitors and one resistor) have been chosen to give the best match to the 30-network responses. It can be seen that, with a suitable choice of components, it is possible to achieve responses from a single network which are very similar to those from the 30-element network. This suggests that the function of the multi-lamella structure of the PC is not to produce a particular amplitude and phase response. A single lamella could produce the same response and a multi-lamella structure has the capability of producing much larger phase shifts and much greater variation of pressure attenuation factor with frequency than observed in the PC.

In the single-network equivalent (fig. 5.18) the capacitor C_m provides a global representation of the lamella compliances and the capacitor C_s provides a global representation of the radial-spring compliances. At low frequencies the attenuation factor of the network is given by $C_m/(C_m + C_s)$ and this is much less than unity because the global lamella compliance C_m is much less than the global radial-spring compliance C_s. (In other words, at low frequencies when the interlamellar fluid is easily displaced, the lamella stiffness resists the transmission of mechanical signals via the radial springs.)

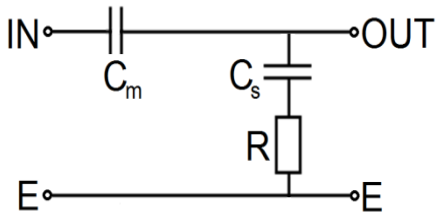

Figure 5.18. A single network with the same configuration as one of the networks in the Loewenstein-Skalak model.

The micropipette aspiration experiment described in section 5.3 demonstrates that the external membrane of the PC is particularly stiff for distortions in this geometry. This may be attributable to the network of collagen fibrils between lamellae, which act against pulling one lamella away from another. It is difficult to interpret the “creep” observed in this experiment, i.e., the slow increase in membrane distortion over a timescale of a few minutes, in response to continuously maintained suction (fig. 5.9). This is not in line with the “rapidly adapting” nature of the PC that is

generally assumed [32-50], according to which mechanical distortions develop on a timescale of less than a second.

Chapter 6

Conclusions and Future Work

Chapter 6 is an overview of experimental work undertaken for this thesis on PCs from the horse hoof. It reviews research that arises from the main points in the literature review in Chapter 1. Novel methods, and techniques which have not previously been applied to study PCs, have been used to develop a better understanding of the structure and function of the PC.

Three main areas were investigated in this work: the physiology of the PC; the mechanical properties of the structure and interconnectivity of fluid spaces; the mechanism of the PC response to external mechanical stimuli.

Histological and anatomical investigations informed the process of obtaining PCs by dissection of the hoof, allowing exact localization of the PCs in relation to the pattern of surrounding structures such as blood vessels and adipose tissue. It provides a starting point for a possible future study on the involvement of surrounding tissue in the transduction process.

Dissection of PCs is not easy – they are difficult to locate and difficult to remove without damage to their delicate structure. For microscopy studies it is necessary to remove the opaque external membrane – another difficult operation. A topic for further study is the structure, biomechanics and possible functions of this layer. In addition, fresh PCs degenerate after a few hours, despite our adoption of procedures which preserve other tissues in much better condition. The availability of suitable PCs was a limiting factor in many experiments.

The variety in size and shape of the corpuscles within a cluster, observed among horses of different ages may lead to two hypotheses: differences in shape and size are related to different ranges of sensitivity, or some corpuscles grow more than others through the life span of the animal. The experimental data were too limited to test the first hypothesis and application of the best current theoretical model posed fresh questions about the structure-function relation in the corpuscle whose resolution is a prerequisite for addressing this issue. Testing the second hypothesis would be an enormously time-consuming task.

Each microscopic technique provided specific structural information. Light microscopy is able to reveal basic information on anatomy of PCs which has already been described in the literature. However, we obtained new evidence of two different types of mechanical linkage between lamellae. Each of them may carry its own specific role, contributing to the overall receptor function. The staining techniques of whole PCs have not been documented before. Hence, to establish

the best incubation time for labelling collagen, proteoglycans, lipids in a whole capsule was a challenge. A high density of collagen was found in lamellae close to the surface and around the core. Confocal microscopy confirmed the presence of separate blood supplies to the inner and outer zones. Vessels that penetrate the outer zone may have a role in controlling the amount and composition of the interlamellar fluid and regulation of internal pressure. They may also be related to the putative function of PCs in regulation of the circulation.

The density of proteoglycan increases towards the inner zone, with less in the outer zone. A common role of proteoglycans in extracellular matrix is structural support and provision of resistance against compression. However, they also confer size- and charge-selectivity to transport of solutes through basement membranes and other extracellular matrices. In the PC it is possible that proteoglycans in the interlamellar spaces contribute to flow resistance and hence to the overall mechanical stresses of the lamellar structure. They are also probably responsible for the charge selectivity we observed in the transport of fluorescein and rhodamine B. A high density of lipids was observed on the surface of the corpuscle, decreasing towards the inner zone. Since lipids are associated with energy storage and protection from the environment, it is possible to assume that lipids found on the surface and through the outermost lamella may carry these functions within the process of mechanotransduction. Corpuscles were always surrounded by adipose tissue and it is possible that it has a role in the transduction

process in, for example making external forces more isotropic before they reach the corpuscle surface. Such hypotheses could be a major area for future work.

The collagen fibres occupy approximately 25% of the whole corpuscle, particularly in the outer zone. They are probably the major determinant of the degree of swelling and shrinkage of the outer zone induced by different osmotic forces. They may also produce the high stiffness of the outer lamellae demonstrated in the micropipette aspiration test.

There are occasional single elastin fibres uniformly distributed across the outer zone, becoming less distinguishable in the complex network of collagen and proteoglycans towards the inner zone. These elastic fibres may be associated with radial connections described by Lowenstein and Skalak [36] and may be involved in the recovery of the structure after the application of loads.

The complex network around the core is associated with increased density of proteoglycans which, in addition to the functions discussed above, will influence the distribution of cations such as can attract Na^{+}, K^{+}, Ca^{++}, and may thereby play a role in the electrochemistry of the nerve. Deformation of the lamellar structure may also be associated with ionic effects [42]. Electrochemical effects of PC function have not been investigated in the present study. Measurement of changes

in ionic composition and electrical potential, within the PC and across the nerve membrane, in response to mechanical deformation, remains an exciting topic for future work.

Experiments involving osmotic challenge show differences in behaviour between the inner and outer zones. However, it remains unclear whether these two zones have different roles in the process of mechanotransduction. Both the osmotic swelling and tracer uptake experiments indicated that the lamellae are partially permeable to water and solutes. This may be important in nutrition. It may also be important in the long-term accommodation of the corpuscle to continued loading.

Investigation of the theoretical model proposed by Lowenstein and Skalak [36] has provided a wide range of predicted responses to mechanical stimuli, considerably extending the scope of the original study. Corresponding measurements of the displacement response of the PC to sinusoidal mechanical stimuli show reasonable agreement with predictions, both in terms of amplitude and phase. These measurements were particularly challenging, involving many months of development work, and it is to be hoped that further measurements of this type will be carried out in future, to confirm and extend the present results. A weakness of the existing set-up is that experiments are performed at room temperature – experiments at body temperature (37°C) may produce different results [56]. If pressure measurement could also be implemented alongside measurement of

displacement, this would provide a very powerful technique for studying the mechanical behaviour of the corpuscle, allowing a rigorous test of theoretical models. Again, a great deal of effort was devoted to pressure measurements and whether the problems encountered with leakage could be circumvented by further attention to pipette tip design or the use of piezoelectric drivers still remain to be investigated.

At the end of the present study, there remains the question of why the Pacinian corpuscles have their complex lamellar structure. As discussed in Chapter 5, it seems unlikely that such a complex structure is required to produce the observed variation of response with frequency. Brisben et al [53] suggest that the function of the lamellar structure is “to protect the extremely sensitive receptor ending from the high static and low-frequency forces that occur in many motor acts, thereby leaving the ending sensitive to transmitted vibrations with amplitudes as small as 10nm”. The author is unaware of evidence in the literature that receptor endings of nerves associated with PCs are more susceptible to mechanical damage than nerve endings associated with other types of touch receptors, so this argument by Brisben et al is open to question. It may be that the most important function of the lamellar structure is to increase the size of the receptor, providing a large volume and large surface area, and hence a mechanism to efficiently transmit mechanical signals to the receptor ending from a large region of surrounding tissue (i.e., to achieve the spatial summation which is an important aspect of perception via PCs).

The work presented in this thesis provides a wide range of new information on the PC. Other researchers are encouraged to further investigate this fascinating subject for study.

References

[1] Magee, D., Zachawski, J., Quillen, W. (2007*) Scientific Foundations and Principles of Practice in Musculoskeletal Rehabilitation.* Sounder Elsevier.

[2] http://wiki.bethanycrane.com/somaticsenses

[3] Cauna, N., Leonard, R. (1960) *The fine structure of Meissner`s touch corpuscles of human fingers.* Journal of Cell Biology 8(2) 467–82.

[4] Hoffmann, J.N., Montag, A.G., Dominy, N.J. (2004) *Meissner corpuscles and somatosensory acuity: the prehensile appendages of primate and elephants.* Anat. Rec. A (Discov. Mol. Cell. Evol. Biol.) 281(1) 1138–47.

[5] Bongiorno, M.R., Doukaki,S., Aricò, M. (2010) *Neurofibromatosis of the nipple-areolar area: a case series.* Journal of Medical Case Reports 4(22), 22.

[6] Caceci, T. (2013) *Example: Lamellar Corpuscle,* from *Veterinary Histology* at http://www.vetmed.vt.edu/

[7] Maricich, S.M., Wellnitz, S.A., Nelson, A.M., Lesniak, D.R., Gerling, G.J., Lumpkin E.A., Zoghbi H.Y. (2009). *Merkel Cells are Essential for Light Touch Responses*. Science 324, 1580–82.

[8] Eric, R., Schwartz, J.H., Jessell, T.M. (2000). *Principles of Neural Science*. McGraw-Hill

[9] Barret, K.E. (2009) *Ganong's Review of Medical physiology*, 23rd Edition, McGraw Hill (Lange Basic Science). p. 150.

[10] Mountcastle, V.C. (2005) *The Sensory Hand: Neural Mechanisms of Somatic Sensation*. Harvard University Press. p. 34.

[11] Hamilton, N. (2008) *Kinesiology: Scientific Basis of Human Motion*. McGraw-Hill. pp. 76–7.

[12] Glickstein, M. (2014) *Neuroscience: a Historical Introduction*. Massachusetts Institute of Technology.

[13] Wolfgang, K., (2002) *Color Atlas of Cytology, Histology, and Anatomy*. Thieme. pp. 452-453.

[14] Heather Smith-Thomas, H. (2005) *The Horse Conformation Handbook*. Storey

[15] Lancaster, L.S., Bowker, R.M. (2012) *Acupuncture Points of the Horse's Distal Thoracic Limb: A Neuroanatomic Approach to the Transposition of raditional Points,* Animals 2(3), 455-471.

[16] http://understandingwilliamssyndrome.blogspot.co.uk/2011/10/curved-fingers-and-toes-clinodactyly.html

[17] Stark, B., Carlstedt, T., Hallin, R.G., Risling, M. (1998) *Distribution of Pacinian corpuscles in the hands: A cadaver study.* Journal of Hand Surgery (British & European) 23(7), 370-372.

[18] Cauna, N., Mannan, G. (1958) *The structure of human digital Pacinian Corpuscles and its functional significance.* Journal of Anatomy 92(1), 1-20.4

[19] Kumamoto, K., Takei, M., Kinoshita, M., Ebara, S., Matsuura, T. (1993) *Distribution of Pacinian corpuscles in the cat forefoot.* Journal of Anatomy 182(1), 23–28.

[20] Kumamoto, K., Takei, M., Kinoshita, M., Ebara, S., Matsuura, T. (1993) *Distribution of Pacinian corpuscles in the hand of the monkey, Macaca fuscata.* Journal of Anatomy 183(1), 149–154.

[21] Burg, E., Diepenbroek, C., Hoorneman, N., Lichtenberg, E. (2007) *AMC report: Explorative study of the natural balance method of hoof care in horses.* Master's dissertation, Wageningen University and Research Centre.

[22] Cauna, N., Mannan,G. (1959) *Development of postnatal changes of digital Pacinian corpuscles in the human hands.* Journal of Anatomy 93(3), 271-286.4.

[23] http://www.viovet.co.uk/knowledgebase/a177-A Guide To Horse Hoof Care

[24] *The Natural Hoof - Barefoot Horse Riding*, from www.thenaturalhoof.co.uk

[25] Chalisova, N.I., Kuznetsov, V.F., and Volkova, N.K. (1974) *Formation of new Pacinian corpuscles after additional somatic innervations of the mesentery*. Journal of Morphology and Pathomorphology (Translated from Byulleten`Eksperimental`noi Biologi i Meditsiny) 12, 84-87.

[26] Winkelmann, R. K. (1956) *The cutaneous innervation of human newborn prepuce.* Journal of Investigative Dermatology26(1), 53-67.

[27] Nishi, K. (1969) *Fine structure of Pacinian Corpuscle in the mesentery of the cat*. Journal of Cell Biology 43, 539-552.

[28] Michailow, S. (1908) *Die Struktur der typischen Vater-Pacinischen Korperchen und ihre physiologische Bedeutung*. Folia Neuro-Biol. Lpz. 2, 603-624.

[29] Gammon, G.D., Bronk, D.W. (1935) *The discharge of impulses from Pacinian Corpuscles in the mesentery and its relation to vascular changes.* Am J Physiol 114(1), 77-84

[30] *www.graysanatomyonline.com*.

[31] Tuttle, R.S., McCleary, M. (1975) *Mesenteric baroreceptors.* Journal of Physiology 229(6), 1514-1519.

[32] Glees, P.A., Mohiuddin, M. A, Smith, A.G. (1949) *Transplantation of Pacinian corpuscles in the brain and thigh of the cat.* Journal of Anatomy 7, 213-229.

[33] Pease., D.C., Quilliam, T.A. (1957) *Electron microscopy of the Pacinian Corpuscle*. J. Biophys. Biochem. Cytol. 3(3), 331–342

[34] Chouchkov, C.N. (1973) *The fine structure of small encapsulated receptors in human digital glabrous skin*. Journal of Anatomy 114(1), 25-33.

[35] Bell, J., Bolanowski, S., Holmes, M.H. (1964) *The structure and function of Pacinian Corpuscles,* a Review, Journal of Progress in Neurology 42, 79-128.

[36] Loewenstein, W.R., Skalak, R. (1966) *Mechanical transmission in a Pacinian corpuscle. An analysis and a theory*. Journal of Physiology 182, 346-378.

[37] Dubovy, P.(2000) *Restoration of lamellar structures in adult rat Pacinian corpuscles following their simultaneous freezing injury and denervation*, J. Anat. Embryos. 202, 235-245.

[38] Malinovski, L, Vega, J.A., Esteban, I., Naves, F.J., Valle, M.E. (1995) *Immunohistochemical localization of laminin and type IV collagen in human cutaneous sensory nerve formations*. Anat. Embryol. (Berl.) 191(1), 33-39.

[39] Loewenstein, W.R., Mendelson, M. (1965) *Components of receptor adaptation in a Pacinian corpuscle*, Journal of Physiology 177(3), 377-397.

[40] Pawson, L., Prestia, L.T., Mahoney, G.K. (2009) *GABAergic/Clutamateric-Glia/Neuronal Interaction Contributes to rapid adaptation in Pacinian Corpuscles*. Journal of Neuroscience 29 (9), 2695-2705.

[41] Spencer, P.S. (1973) *An ultrastructural study of the inner core of a Pacinian Corpuscle.* Journal of Neurocytology 2, 217-235.

[42] Ilyinsky, O.B., Krasnikova, T.L. (1972) *Changes in ionic composition of Pacinian corpuscular fluid with activity*, Fiziologicheskii Zhournal SSSR 58(3), 434-442.

[43] Sames, K., Halata, Z., Jojovic, M. (2001) *Lectin and Proteoglycan Histochemistry of Feline pacinian Corpuscles.* Journal of Histochemistry and Cytochemistry 49(1), 19-28.

[44] Van De Velde, E., (1909) *Die fibrillare Struktur der Nervenenden*. Int. Mschr. Anat. Physiol. 26, 225-298.

[45] Pawson, L., Slepecky, N.B., Bolanowski, S.J. (2000) *Immunocytochemical identification of protein within the Pacinian Corpuscle*. Journal of Somatosensory & Motor Research 17(2), 159-70.

[46] Gray, J.A.B., Malcolm, J. L. (1950) *The initiation of nerve impulses by mesentery Pacinian corpuscles*. Proc. Roy .Soc. B 137, 96-114.

[47] Adrian , E.D., Umrath, K. (1929) *The impulse discharge from the Pacinian corpuscle*. J. Physiol. 68, 139-154.

[48] Ramstrom, M. (1908) *Anatomishe und experimerntelle untersuchungen uber die lamelosn nervenedkorperchen im peritoneum parietale des menschen*. Anat. Hefte 36, 309-368.

[49] Loewenstein, W.R., Altamirano-Orrego, R. (1958) *The refractory state of the generator and propagated potential in a Pacinian corpuscle*. Journal of Physiology 41(4), 805-824.

[50] Bolanowski, S.J., Zwisloski, J.J. (1984) *Intensity and frequency characteristics of pacinian corpuscles. II. Receptor potentials.* Journal ofNeurophysiology 51(4), 812-30.

[51] Mendelson, M., Loewenstein, W.R. (1964*) Mechanisms of receptor adaptation*. Journal of Science 144, 554-555.

[52] Kajimoto, N., Kawakami, N., Tacji, S. (2009) *Psychophysical evaluation of receptor selectivity in electro-tactile display* http://files.tachilab.org/publications/intconf2000/kajimoto200312ISMCR.pdf

[53] Brisben, A.J., Hsiao, S.S., Johnson, K.O. (1991) *Detection of vibration transmitted through an object grasped in the hand.* Journal of Neurophysiology 81(4), 1548-1558.

[54] Koshima,I., Moriguchi, T., Soeda, S. (1992) *Electron microscopic observations of degeneration of human Pacinian corpuscles in amputated fingers.* J. Plast. Reconstr. Surg. 89, 243-248.

[55] Hubbard, S.J. (1957) A *study of rapid mechanical events in a mechanoreceptor*. Journal of Physiology142, 198-218.

[56] Sato, M. (1961) *Response of Pacinian corpuscles to sinusoidal vibration.* Journal of Physiology 159, 391-409.

[57] Gray, J.A.B., Sato, M. (1953) *Properties of the Pacinian corpuscles in the cat`s toe*. J. Physiol. 113, 475-482.

[58] Ilyinsky, O.B., Akoev, G.N., Krasnikova, T.L., Elman S.I. (1976) *K and Na Ion Content in Pacinian Corpuscle Fluid and its Role in the Activity of Receptors*. European Journal of Physiology 361, 279-285.

[59] Diamond, J., Gray, J.A.B., Inman D.R. (1958) *The relation between receptor potentials and the concentration of sodium ions.* Journal of Physiology 142(2), 382-394.1.

[60] Verrillo, R.T. (1963) *Effect of contactor area on the vibrotactile threshold*. J. Acoust. Soc. Amer. 35, 1962-1966.

[61] Verrillo, R.T, Fraioli, A.J., Smith, R.L. (1969) *Sensation magnitude of vibrotactile stimuli*. Perception & Psychophysics 6, 366-372.

[62] Bolanowski, S.J., Gescheider, G.A., Verrillo, R.T., Checkosky, C.M. (1988) *Four channels mediate the mechanical aspects of touch*. J. Acoust. Soc. Amer. 84, 1680-1694.

[63] Gescheider, G. A., Bolanowski, S.J., Verrillo, R.T. (2004) *Some characteristics of tactile channels*. Behavioural Brain Research 148, 35-40.

[64] Grandori, F., Pedotti, A. (1982) *A mathematical model of the Pacinian corpuscle*. Journal of Biological Cybernetics 46, 7-16.

[65] Benjamin, M., Redman, S., Milz, S., Buttner, A., Amin, A., Morrigl, B., Brennel, E., Emery, P., McGonagle, D., Bydder, G. (2004) *Adipose tissue at entheses: the rheumatological implication of its distribution*. Ann. Rheum. Dis. 63, 1549-1555.

[66] Sakada, S., Sasaki, T. (1984) *Blood-nerve barrier in the Vater-Pacini corpuscle of cat mesentery.* Anat. Embryol. (Berl.) 169(3), 237-247.

[67] Holmes, M.H., Bell, J. (1992) *Model of the dynamics of receptor potential in a mechanoreceptor.* Journal of Mathematical Bioscience 110(2),139-174.

[68] Sedy, J., Szeder, V., Walro, J.M. (2004) *Pacinian corpuscle development involves multiple Trk signaling pathways.* Journal of Developmental Dynamics 231(3), 551-563.

[69] Vega, J.A., Garcia-Suarez, O., Montano, J.A. (2009) *The Meissner and Pacinian sensory corpuscles revisited: new data from the last decade*. Journal of Microscopy Research and Technique 72(4), 299-309.

[70] Floyd, A.E., Mansmann, R.A. (2000) *Equine podiatry*, Elsevier, p.85.

[71] *All Natural Horse Care*, from www.all-natural-horse-care.com/barefoot-hoof-diagrams.html

[72] Carleton, H.M., Drury, R.A.B., Wallington, E.A. (1967) *Carleton`s Histological Technique*, Oxford University Press (USA)

[73] *Molecular Probes, Life Technologies*, from www. products.invitrogen.com/ivgn/product/D3167

[74] Zipfel, W.R., William, R.M., Watt, R.M.,Webb, W. (2002) *Nonlinear magic. Multiphoton microcopy in the biosciences.* Nature 21,1369-1377.

[75] Campagnola, P.J., Loew, L.M. (2003) *Second-harmonic imaging microscopy for visualizing biomolecular arrays in cells, tissue and organisms*. Nature Biotechnology 11, 1356-1360.

[76] Ustione, A., Piston, D.W. (2011) *A simple introduction to multiphoton microscopy*. Journal of Microscopy 243, 221-226.

[77] Zambusch, A., Holton, G.R., Xie, X.S. (1999) *Three-dimensional vibrational imaging by coherent anti-stokes raman scattering.* Physical Review Letters 82, 4142-4145

[78] http://emps.exeter.ac.uk/physics-astronomy/research/biomedical/multiphoton/mechanisms/

[79] Wiederhield, C.A., Woodbury, J.W., Kirk, E.S., Rushmer, R.F. (1964) *Pipette pressure in the microcirculation of frogs' mesentery*. J. Physiol. 207, 173-176.

[80] *All Natural Horse Care*, from www.all-natural-horse-care.com/barefoot-hoof-diagrams.html

[81] Bowker, R.M. (1998) *Hemodynamic Flow Hypothesis for Energy Dissipation in the Equine Foot,* Hoofcare & Lameness 70, 36-41.

[82] Mansfield, J., Moger, J., Green. E., Moger, C., Winlove, C.P. (2013) *Chemically specific imaging and in-situ chemical analysis of articular cartilage with stimulated Raman scattering.* Journal of Biophotonics 6(10), 803-814.

[83] Loewenstein, W.R. (1972) *Mechanic-electric transduction in the Pacinian corpuscle*. Nature 431, 397-404.

[84] Holmes, M.H., Bell, J. (1992) *Model of the dynamics of receptor potential in a mechanoreceptor,* Journal of Mathematical Bioscience,110(2), 139-174.

[85] Fanun, M. ed. (2010) Colloids in Drug Delivery, CTC Press, pp. 168-169.

[86] Crank. J., Nicolson. P.A. (1947) *Practical method for numerical evaluation of solutions of partial differential equations of the heat conduction type*. Proc. Camb. Phil. Soc. 43(1), 50–67.

[87] Hochmuth, R.M. (2000) *Micropipette aspiration of living cells*. Journal of Biomechanics 33(1), 15-22.

[88] Arkill, K.P. (2005) *Mass transport in articular cartilage*. PhD Thesis, University of Exeter.